Studies on Magnetic Properties in Porous Coordination Polymer

Ko Yoneda

2009

Preface

The study presented in this thesis has been carried out under the direction of Professor Susumu Kitagawa during April 2005 – March 2009 at the Department of Synthetic Chemistry and Biological Chemistry, Graduate School of Engineering, Kyoto University.

The author is greatly indebted to Professor Susumu Kitagawa for his significant guidance, continuous encouragement, valuable discussion and giving his a lot of invaluable opportunities which broaden his horizons. The author also wishes to express his sincere gratitude to Associate Professor Masaaki Ohba for his kind suggestion and discussion throughout this work. The author is grateful to Associate Professor Ho-Chol Chang (Hokkaido University), Research Associate Takashi Uemura, Research Associate Satoshi Horike, Dr. Ryotaro Matsuda, and Dr. Shuhei Furukawa for their hearty encouragements, and kind advices. The author is deeply grateful to Emeritus Professors Sumio Kaizaki (Osaka University) for his continuous support and hearty encouragement from the start of this work. The author deeply thanks to Professor Satoshi Kawata (Fukuoka University) for his continuous encouragement and advice throughout this work. The author is deeply grateful for Dr. Ana B. Gaspar, Professor M. Carmen Muñoz and Professor José A. Real (València University) for their corporation and discussion throughout the collaboration work. The author is thankful to Emeritus Professor Takashi Kawamura (Gifu University) for his kind suggestion, helpful advice for the syntheses and measurements. The author is grateful to Professor Hiroki Oshio (Tsukuba University) and Research Associate Takuya Shiga (Tsukuba University) for the instruction of magnetic measurements. The author wishes to thank Dr. Mikio Yamasaki (Rigaku Corporation) for his advice about the single crystal X-ray diffraction measurement. The author is grateful to Mr. Hideo Ando, Dr. Yoshihide Nakao and Professor Shigeyoshi Sakaki (Kyoto University) for valuable discussion from theoretical point of view.

The author also thanks to Dr. Daisuke Tanaka, Dr. Wakako Kaneko, Dr. Daisuke Kiriya, Mr. Nobuhiro Yanai, Mr. Takuya Miyagawa and Mr. Ryo Ohtani for their corporations and kind advices.

The author is thankful to Ms. Hiroko Hirohata, Ms. Kiyo Yamashita and Ms. Yoshiko Shimizu for their secretarial works and warm encouragement. Acknowlegements are to all other members of the group of Professor Kitagawa for their

hearty encouragement and friendship during her time in the laboratory.

The author is much indebted for the financial support of Research Fellowships of the Japan Society for the Promotion of Science for Young Scientists.

Finally, the author wishes to offer special thanks to his parents Michio Yoneda and Minori Yoneda, his brother Taku Yoneda, Yu Yoneda and So Yoneda for their all patience, constant financial supports and affectionate encouragements.

Ko Yoneda
Department of Synthetic Chemistry and Biological Chemistry
Graduate School of Engineering, Kyoto University
July, 2009

Contents

General Introduction

Coordination Polymers (CPs)

The research of coordination polymers (CPs) consisting of metal ions and organic or inorganic ligands has made substantial progress in recent years, and has opened a new area of chemistry. The concept of "coordination compounds", so-called "metal complexes", was established by Alfred Werner in the early 1900s. The structures and properties of coordination compounds vary according to the kinds of central metal ions and surrounding ligands. They have been systematically investigated and their various characteristics (structures, acidity and basicity, redox activity, optical property, magnetism, *etc.*) have been clarified. Then the coordination compounds have been developed from a discrete mononuclear system to an infinite polymer system through a polynuclear cluster system. The CPs essentially consist of alternate array of mono- or polynuclear metal sites and organic ligands as linkers. The structural diversity of CPs exceeds that of the parental coordination compounds, and CPs can inherit and merge the original characteristics of the constituent coordination compounds based on appropriate molecular design. CPs have potential to be versatile materials because of the following characteristics, (i) a designable regular framework based on the geometry of the constitutive metal ions and organic ligands, (ii) the chemical diversity in the basis of various combination of components, (iii) the easy preparation by the self-assembling method, (iv) a flexible framework responding to the external stimuli, and (v) appearances of physical phenomena such as bulk magnetic ordering and electric conductivity. Such CPs are promising compounds to be new solid-state materials with specific function, electronic structures and/or versatile physical properties. In particular, the coordination polymers providing uniform pores in the structure have been regarded as "porous coordination polymers (PCPs)" or "metal-organic frameworks (MOFs)", and attract much attention as a new class of porous material.[1–5] The PCPs possess zeoletic abilities as adsorbents based on a nano scaled open space inside the framework with unique characteristics; highly regular framework, high porosity, flexibility, and designability of pore surface, which can create highly functionalized pores. Compared with existing inorganic porous materials, PCPs provide significant enhancement in flexibility and in the dynamics of their frameworks. Such PCPs are expected to be applied not only as general-use porous solid, i.e. gas strage,[6–10] separation material,[11,12] ion exchange and hererogeneous catalyst,[13–17] but as new

multifunctional nanoporous materials incorporating magnetic,[18–20] electric,[21,22] optical[23] and chiral properties.[24,25] One of the recent research topics in the field of material chemistry is the functionalized PCPs. One of the representative functionalized PCPs is magnetic PCP showing magnetic ordering or spin crossover phenomena with porous properties, which is being conceived to switch magnetic properties through guest adsorption processes (Scheme 1).

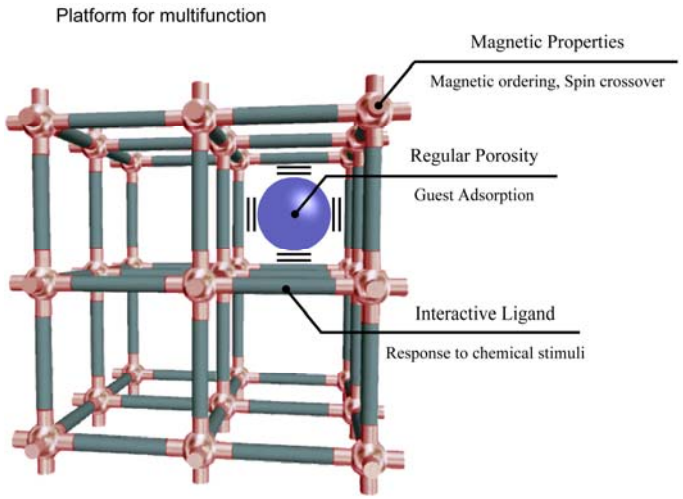

Scheme 1. Proposed functionalized porous framework incorporated magnetic properties

Coordination Polymer Magnets (CPMs)

Coordination polymers providing magnetic properties have been have been appeared substantially in the late 1980s as a new class of magnetic material, molecular magnets (MMs).[26–43] MMs are of magnetic materials consisting of paramagnetic molecules, *e.g.* organic radicals, metal complexes, and show a long-range magnetic ordering as well as general magnets. To achieve the magnetic ordering, it is necessary that highly-ordered-array structure of magnetic centers and long-range control of magnetic interaction. Most of MMs have 1D – 3D regular arrangements of paramagnetic metal complexes, and the basic molecular design to construct such magnetic framework has common senses with that of coordination polymers (CPs). Therefore, the MMs having polymeric framework are classified into the category of CPs as coordination polymer magnets (CPMs). Systematic studies on CPMs occurred at the end of the 1980's and three important magnetic systems were reported:

one-dimensional charge-transfer complex $[Fe(Me_5cp)_2][TCNE]$ (Me_5cp^- = pentamethylcyclopentadienyl and TCNE = tetracyanoethylene) by Miller *et al.*,[26–29] one-dimensional oxamato-bridged bimetallic complex $\{MnCu(pbaOH)(H_2O)_3\}x$ ($bpaOH^{4-}$ = 2-hydroxy-1,3-propylenedi(oxamate) anion) by Kahn *et al.*[30–36] and one-dimensional Mn-radical complex $\{M(hfa)_2(NITR)\}_x$ (hfa^- = hexafluoroacetylacetonateand NITR = 2-R-4,4,5,5-tetramethyl-4,5-dihydro-1-imidazolyl-1-oxy-3-oxide) by Gatteschi *et al.*[37–43] These pioneering works presented a significant concept for construction of magnetic framework based on paramagnetic building units (metal complexes and organic radicals). These results opened the way to the molecular magnetic materials providing well-designed structure, flexibility and versatility and developed it into a new active research area. Such magnets are advantageous for the systematic study based on elaborate molecular design compared with the conventional magnets (metal oxides, alloys, *etc.*). The studies started at a challenge to achieve the magnetic ordering with controlling the magnetic interaction and an infinite arrangement of magnetic centers. The efforts enable us to control the magnetic interaction by regulating bridging distances, angles and electronic configuration of magnetic centers resulting in changing the overlap integral between magnetic centers. Then research objectives of CPMs have been transited the early targets, "achievement of magnetic ordering" and "elucidation of magnetostructural relationship", and shifted to the advanced one, "achievement of multiple properties and functions". Some of CPs have presented coexistence and/or interlock of magnetism with other physical properties, *e.g.* $[BEDT\text{-}TTF]_3[MnCr(C_2O_4)_3]$ by Coronado *et al.* (ferromagnetism and conductivity),[44] $[Mn_3(HCOO)_6](EtOH)$ by Kobayashi *et al.* (ferrimagnetism and ferroelectric property),[45] $K_{0.2}Co_{1.4}[Fe(CN)_6]\cdot 6.9H_2O$ by Sato *et al.* (light-induced ferromagnetism)[46,47] and $K^{I}_{0.31}V^{II}_{0.49}V^{III}_{0.51}[Cr^{III}(CN)_6]_{0.94}\cdot 6.5H_2O$ by Ohkoshi *et al.* (magneto-optical properties).[48] However, such multi-functional CPMs are still limited, and new CPMs providing novel functions are under development still now. Preparing multi-functional CPMs with rational design and understanding the correlation among properties make fundamental basis for developing novel functional materials in the future.

Porous Coordination Polymer Magnets (PCPMs)

CPMs sensitively respond to structural changes with magnetic output, because the magnetic interactions are susceptible to changes of local bridging structure associated

with changes of overlap integral between magnetic orbitals.[49,50] With focusing the flexible CP's framework, the structural flexibility allows for responses to various external stimuli, in particular to guest molecules as chemical stimulus.[51–58] Kahn *et al*. have introduced a concept of "magnetic sponge'' which can reversibly release and reabsorb both noncoordinated and coordinated solvent molecules accompanied by a dramatic change of magnetic properties. A discrete paramagnetic compound $[CoCu(obbz)(H_2O)_4]\cdot 2H_2O$ ($obbz^{4-}$ = *N*,*N*'-bis(2-carboxyphenyl)oxamido) was changed to 1-D ferrimagnet $[CoCu(obbz)(H_2O)_3]$ (T_c < 2 K) and 2-D (or 3-D) ferrimagnet $[CoCu(obbz)(H_2O)]$ (T_c = 30 K) by heating. The conversion among 0-D paramagnet, 1-D ferrimagnet and 2-D ferrimagnet are completely reversible through a simple dehydration/rehydration accompanying generation and cleavage of Co – O bonds.[59,60] In line with this concept, several CPMs have accomplished reversible magnetic conversions by a solvation/desolvation process accompanied by structural transformation, *e.g.* a reversible single-crystalto-single-crystal transformation of $[Mn(HL)(H_2O)][Cr(CN)_6]\cdot H_2O$ (L = *N*,*N*-dimethylethylenediamine) between a 2-D ferrimagnet (T_c = 35.2 K) and a 3-D ferrimagnet (T_c = 60.4 K) through release and uptake of lattice and ligand water molecules, reported by Ohba and Kitagawa *et al*.[61] These structural changes are classified into two categories, (1) shrinkage and expansion of the intermolecular space by desolvation and resolvation, and (2) generation/cleavage of bridges through release and uptake of coordinated solvent molecules. From this aspect, PCPs exhibiting magnetic ordering, porous coordination polymer magnets (PCPMs), are promising compounds to switch the magnetic properties using chemical stimuli. The PCPMs are expected to perform "chemo-switching" of magnetic properties, however there is a structural issue to be solved. The magnetic ordering requires short bridging structures to mediate a strong magnetic interaction between magnetic centers, whereas the porous frameworks generally consist of relatively long bridging ligands to form large inner space. Several rational designs of PCPMS have been reported and the number of porous magnets has been increased in the past few years, *e.g.* a reversible magnetic conversion of a Prussian blue analog, $Co^{II}_3[Cr^{III}(CN)_6]_2\cdot nH_2O$, from a ferromagnet ($T_c$ = 28 K) to a ferrimagnet (T_c = 22 K) depending on himidity, reported by Ohkoshi *et al*.,[53] a reversible change of $\{[Cu_3(ptmtc)_2(py)_6(EtOH)_2(H_2O)]\}$ (ptmtc = polychlorinated triphenylmethyl tricarboxylic acid radical) between a 2-D ferrimagnet (T_c < 2 K) and an amorphous paramagnet by desolvation/resolvation, reported by Veciana *et al*.[51] These PCPMs could be potentially developed to guest-responsive switching sensory and memory devices, however there is a large gap in working temperature between the guest

adsorption/desorption processes and the magnetic events, and such chemical responses were detected not as real-time action but as structural changes of the resting forms stand this stage.

Porous Coordination Polymers Incorporating Spin-crossover Sites (SCO-PCPs)

As mentioned above, guest-responsive magnetic conversion of PCPMs has been reported so far, however there is a large gap in working temperature between the guest adsorption/desorption processes and the magnetic ordering because of the high melting point and the low T_c. The spin-crossover (SCO) phenomenon is one of the solutions to implement the combination of porous and magnetic properties while overcoming above-mentioned temperature gap. SCO is a well known phenomenon which electron configurations can be switched between high-spin (HS) and low-spin (LS) states in response to external stimuli (temperature, pressure and light irradiation), producing changes in magnetism, color and structure. In particular, Fe(II) compounds exhibit remarkable magnetic changes between the paramagnetic HS (S = 4/2) and the diamagnetic LS (S = 0) states.[18,50,62–69] A number of SCO compounds have been elaborated with control of their spin state in molecules and molecular assemblies, and some of them have successfully exhibited bistable states around room temperature.[70,71] When rigid linkers, communicating the SCO centers, propagate the SCO cooperatively to the whole framework, the first-order spin transition (ST) with hysteresis may occur with conferring a bistable character on the framework. Therefore, PCPs incorporated SCO centers (SCO-PCP) are expected to undergo a guest-responsive SCO (Schem 2).[72–76]

Two pioneering SCO-PCPs have been reported so far. The first example is $[Fe^{II}L_2(NCS)_2]\cdot n$S (L = 1,2-di-(4-pyridyl)ethylene (bpe), trans-4,4'-azopyridine (azpy); S = alcohol molecule) reported Real, Kepert and co-workers.[73] The compound (L = azpy and S = EtOH) exhibits reversible solvate-responsive magnetic change. The as-synthesized compound displays a broad half-SCO transition between 50 and 150 K, whereas the desolvated form shows no SCO. The initial half-SCO behavior is recovered when the desolvated sample is immersed in alcohol solvent. The second example, $\{Fe(pmd)(H_2O)[M^I(CN)_2]_2\}\cdot H_2O$ (M = Ag, Au; pmd = pyrimidine), was reported by Real *et al.*[74] As-synthesized samples display cooperative half-SCO with hysteresis (8 K wide) centered at T_c = 219 K for M = Ag and 167 K for M = Au, respectively. After removing the coordinated and lattice water molecules, large structural change was induced, in which the pmd ligands coordinate to the nearest Fe(II)

as a result of topochemical solid-state reaction. In the case of M = Ag, this structural transformation results in shifting the T_c to 132.5 K with a larger hysteresis (17 K wide). On the other hand, the isostructural Au completely loses the SCO behavior after dehydration. The initial half-SCO behavior is recovered by rehydration in the air. The above-described examples clearly display guest-responsive SCO, however the SCO and guest adsorption-desorption processes are still not simultaneous events. Therefore, it is an essential step in implementing the simultaneous guest adsorption/desorption and SCO, i.e. chemo-switching the spin state, to create new PCPs exhibiting SCO around room temperature.

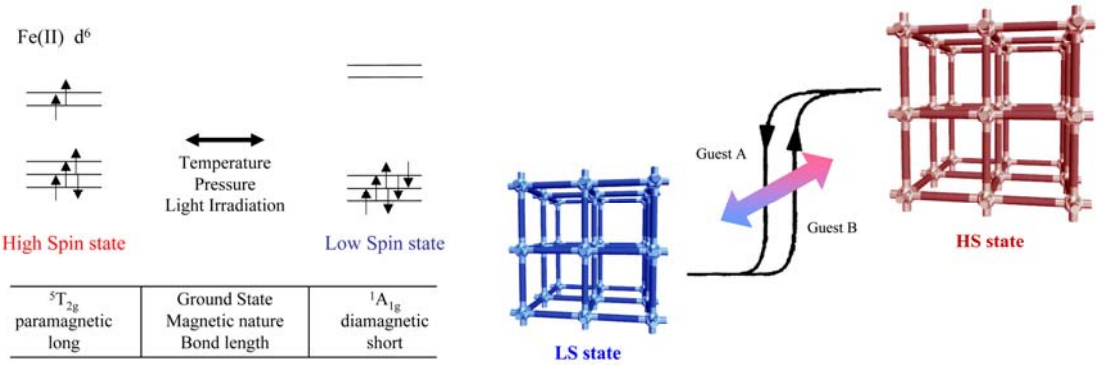

Scheme 2. Switching of magnetic and optical signals in spin crossover compounds using physical (left) and chemical (right) stimuli

Chemo-switching of Magnetism in Coordination Polymers

As mentioned above, CPs and PCPs potentially provide chemical responsivity. In particular, the magnetic frameworks would be controled their magnetic properties by the chemical stimuli through host-guest interactions and structural changes (Scheme 3). In such chemo-switching system, molecular information of chemicals (size, shape, affinity *etc*.) would work as key factors to control the magnetic output, which resembles a simplified form of the conversion process from chemical stimulus to information signal in the chemosensory organs for taste and smell. In line with the concept, we advanced quest for new CPMs and PCPMs exhibiting magnetic ordering or spin transition at first, then we systematically studied magnetic behavior with various guest molecules. To reveal the chemo-switching process, we carried out in situ observation of guest adsorption and magnetic change, and accurate quantum calculation of host-guest interaction.

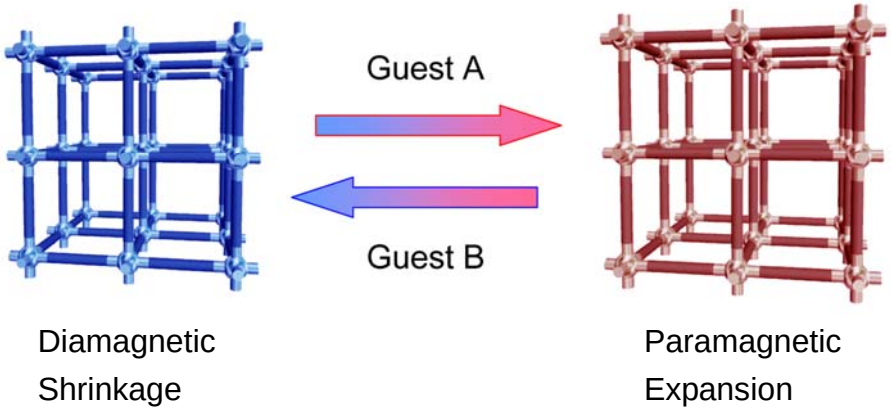

Scheme 3. Chemo-responsive porous framework changing its magnetic property, color and volume depending on information of guest molecules

Survey of this thesis

Chapter 1 described the synthesis and characterization of homometallic PCPMs with *E*,*E*-muconic acid having two carboxylate groups. Two novel coordination polymers, $[M(L)(MeOH)_2]_n$ (M^{II} = Ni (**1**), Co (**2**); H_2L = *E*,*E*-muconic acid) form 3-D pillared-layer-like structure based on 2-D grid sheet extended by *syn-anti* type carboxylate-bridges. The structure provides 1-D channels with *ca*. 4.9 × 4.9 $Å^2$ gate and the void space of 34.7% for **1** and 42.0% for **2** excepting for the coordinated MeOH. In both compounds, a ferromagnetic interaction operates between M^{II} ions through the the *syn-anti* type carboxylate bridges due to zero overlap of magnetic orbitals (accidental orthogonality) through orthogonalized p-orbitals of carboxylate. Compound **1** exhibits a ferromagnetic ordering at 1.7 K, whereas **2** shows no long-range ordering because of a weakened ferromagnetic interaction by antiferromagnetic contributions of dπ electrons and spin-orbit coupling. Both compounds are irreversively changed to amorphous paramagnets by desolvation. This synthesis using dicarboxylate with the rigid diene part proposes a new strategy for constructing porous magnetic frameworks.

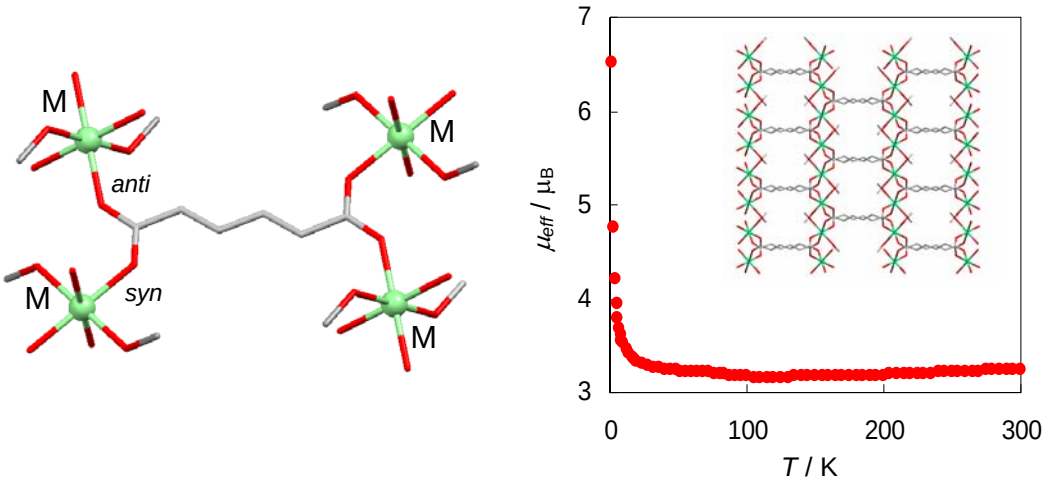

Chapter 1

Chapter 2 described the syntheses, structures, and magnetic properties of 2-D Cu^{II} CPs based on a tricopper core unit. Two novel coordination CPs, $\{Cu[Cu(L)(H_2O)(py)]_2\}_n$ (**1**) and $\{Cu[Cu(L)(MeOH)]_2 \cdot 2H_2O\}_n$ (**2**), were synthesized using 2-(oxalylamino)benzoic acid (H_3L). The ligand L provides oxamate and carboxylate groups, and different 2-D layer structures are formed based on oxamato-bridged tricopper units bridging via the carboxylate groups. In both compounds, an antiferromagnetic interaction operates in the tricopper core through the oxamato bridges. In the bulk, compound **1** shows very weak antiferromagnetic interaction between the tricopper cores through carboxylate bridging axial and equatorial positions of Cu^{II}. On the other hand, compound **2** exhibits a tendency for ferrimagnetic ordering at 2 K, resulting from ferromagnetic interaction through *syn-anti* type carboxylato bridges linking equatorial positions of neighboring Cu^{II} centers. This is a rare homometallic ferrimagnetic system based on an odd-numbered metal unit with mixed antiferromagnetic and ferromagnetic interactions. The synthetic method using multinuclear core unit would be available for constructing porous magnetic frameworks.

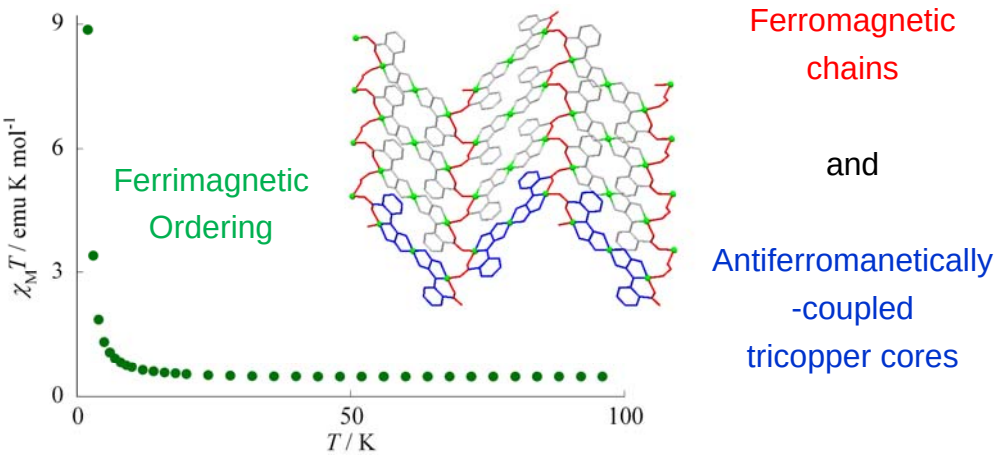

Chapter 2

Chapter 3 described a synthesis, a structure and spin crossover (SCO) behavior of a 1-D Fe^{II} CP. The 1-D Fe^{II} compounds, [{Fe(NCS)(μ-bpypz)}$_2$(μ-4,4'-bpy)]·MeOH (Hbpypz = 3,5-bis(2-pyridyl)pyrazole, 4,4'-bpy = 4,4'-bipyridine (**1**)), was prepared using diiron units, [{Fe(NCS)(μ-bpypz)}$_2$], sandwitched by two $bpypz^-$ ligands. The discrete diiron complex shows a two-step SCO through a mixture state of a fully high-spin and a fully low-spin diiron units. Compound **1** forms a 1-D chain structure linking the diiron units by 4,4'-bpy, and exhibits a steep SCO (T_c = 162.2 K) with a small thermal hysteresis of *ca.* 2 K wide. The sharp spin transition (ST) suggests that **1** shows cooperativity between the diiron units. The rigid 4,4'-bpy linker, communicating the Fe^{II} SCO centers, plays a significant role to propagate the SCO cooperatively to the whole framework, in which the first-order ST with hysteresis may occur with conferring a bistable character on the framework. This result demonstrates availability of incorporation of SCO centers in PCPs framework for chemo-switching of magnetism.

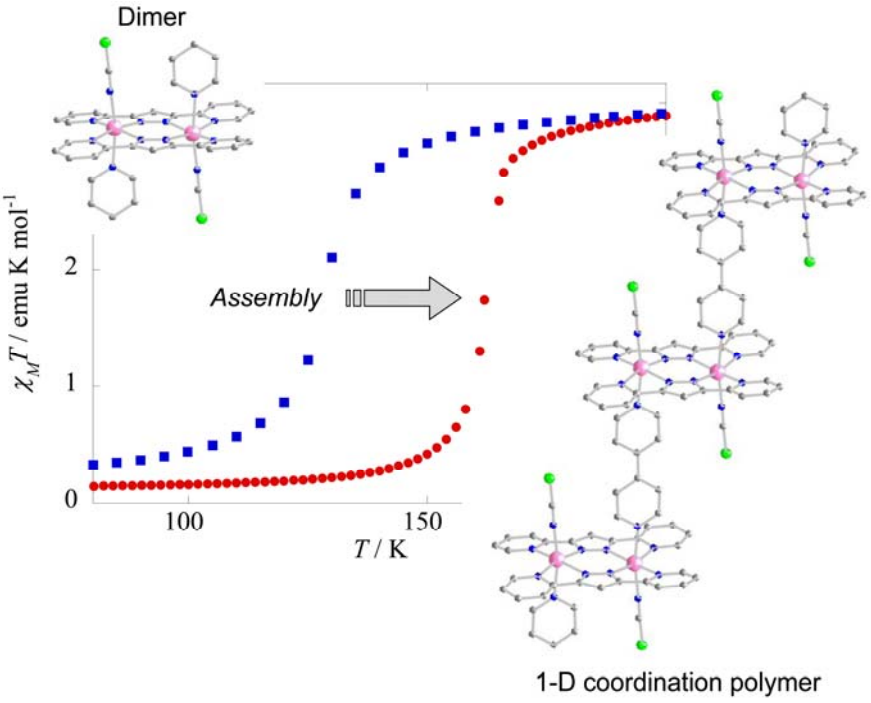

Chapter 3

Chapter 4 described a reversible structural and magnetic conversion of a novel 3D CPM, $[Ni(dipn)]_2[Ni(dipn)(H_2O)][Fe(CN)_6]_2 \cdot 11H_2O$ (dipn = *N*,*N*-di(3-aminopropyl)-amine). X-ray crystallographic results revealed that this compound forms a 3-D porous framework with honeycomb type channel structure consists of 2-D layers extended by alternate array of $[Ni(dipn)]^{2+}$ and $[Fe(CN)_6]^{3-}$, and $[Ni(dipn)(H_2O)]^{2+}$ units linking the 2-D layers. Lattice water molecules form hydrogen-bonds with a coordinated water on Ni^{II} and nonbridging cyano nitrogen atoms of $[Fe(CN)_6]^{3-}$. The compound exhibits a ferromagnetic ordering below 8.5 K due to a ferromagnetic interaction based on the strict orthogonality of magnetic orbitals of Ni^{II} and Fe^{III} ions. After vacuuming at room temperature, a dehydrated form $[Ni(dipn)]_2[Ni(dipn)(H_2O)]$-$[Fe(CN)_6]_2 \cdot H_2O$ is obtained and it shows an amorphous-like XRPD pattern and paramagnetic behavior. The dehydrated form adsorbs water at room temperature, and then recovers the initial crystallinity and ferromagnetic ordering completely. The compound demonstrates a reversible magnetic conversion associated with the crystal-to-amorphous-like phase transformation triggered by water desorption/adsorption. These results prove that the synthetic strategy based on cyanide-bridged bimetallic assemblies is advantageous for the formation of flexible CPMs providing interlocked guest-induced magnetic and structural conversion.

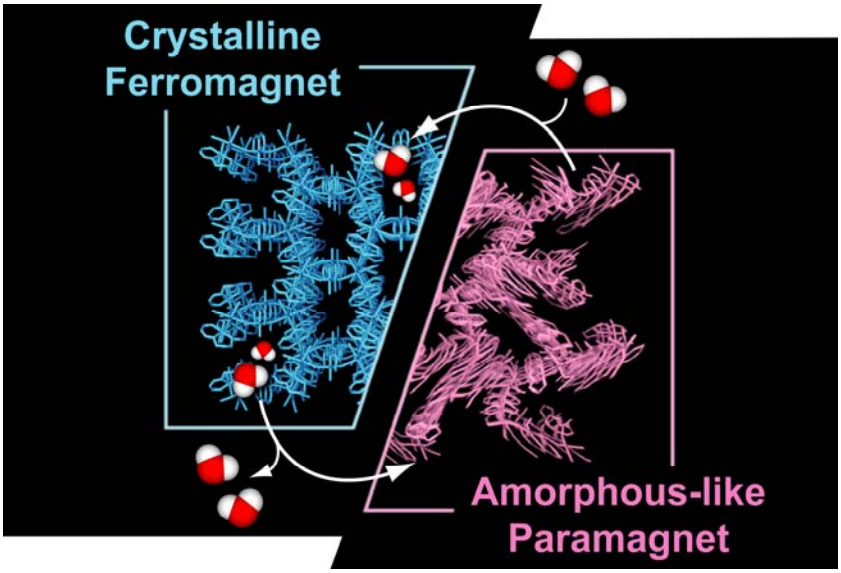

Chapter 4

Chapter 5 described a chemoresponsive bidirectional spin-state switching in a PCP, $\{Fe^{II}(pz)[Pt^{II}(CN)_4]\}$ (pz = pyrazine), incorporating SCO subunits. This compound forms a Hofman-type 3-D porous framework based on pz-bridged 2-D layers extended by Pt^{II} – CN – Fe^{II} linkages, and displays a first-order ST with ca. 25 K wide hysteresis centered at T_c = 297 K. The guest-free framework adsorbs various guest molecules in the gas phase or solution and forms their clathrates. Most of guest molecules transform the compound from the low-spin (LS) state to the high-spin (HS) state, whereas CS_2 exceptionally causes the reverse HS-to-LS transition. In situ magnetic measurements following guest vapor injection elucidated the simultaneous guest adsorption and bidirectional spin transition. X-ray crystallographic results of the guest clathrates reveal that the framework provides two guest-interactive sites, one between the pz-bridges (site A) and another between the four-coordinated Pt centers (site B). The highly accurate theoretical calculation highlight significant interaction CS_2 at sites A and B based on The van der Waals interactions. The systematic studies of guest effect on the spin state and the theoretical calculations point to three key factors as the origins of the relative stabilities of the HS and LS states: (1) the size and shape of G; (2) the G···pz interaction at site A; and (3) the G···Pt interaction at site B. The chemo-switching of magnetism in PCPs will open a route for evolving the PCPs to environmentally responsive materials and for new conceptual spintronics.

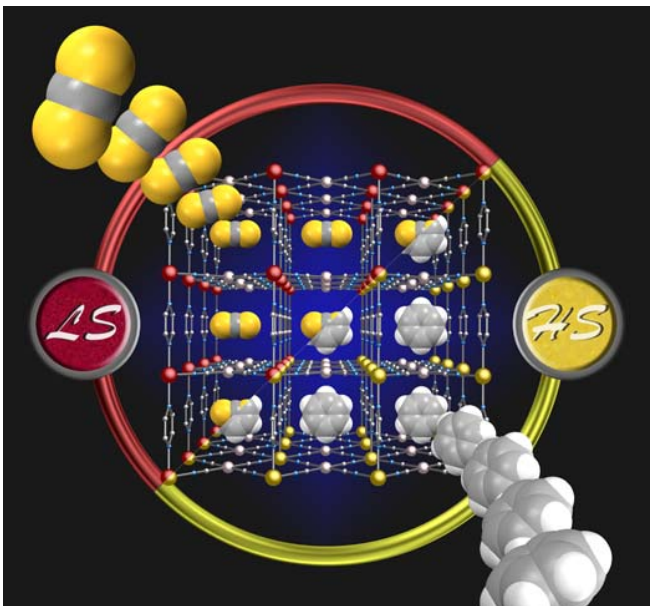

Chapter 5

Chapter 6 described three types of cyanide-bridged porous magnetic frameworks exhibited reversible guest-responsive magnetic conversion, i.e.: (1) reversible magnetic and structural conversion of $[Ni(dipn)]_2[Ni(dipn)(H_2O)][Fe(CN)_6]_2 \cdot 11H_2O$ (**1**: dipn = *N*,*N*-di(3-aminopropyl)amine) triggered by water desorption/adsorption; (2) reversible topochemical transformation of a ferrimagnet, $[Mn(HL)(H_2O)][Cr(CN)_6]H_2O$ (**2**: L = *N*,*N*-dimethylethylenediamine); and (3) bidirectional magnetic chemo-switching of $\{Fe(pz)[Pt(CN)_4] \cdot 2H_2O\}$ (**3**: pz = pyrazine).

In the case of **1**, flexible Fe – CN – Ni linkage and bidirectional hydrogen bonds between lattice water molecule and non-bridging cyano nitrogen atoms play crucial roles in the reversible crystalline-to-amorphous and ferromagnet-to-paramagnet conversion through dehydration and hydration processses. Compound **2** provides a flexible 2-D magnetic framework incorporating removable solvent co-ligands, which delivers reversible topochemical structural transformation and magnetic coversion in response to solvation/desolvation. The 3-D porous framework of **3** incorporating spin-crossover and guest-interactive sites successfully implements a desired magnetic switching responsive to guest molecules at room temperature. These results demonstrate availability of polycyanometallate for constracting guest-responsive magnetic frameworks.

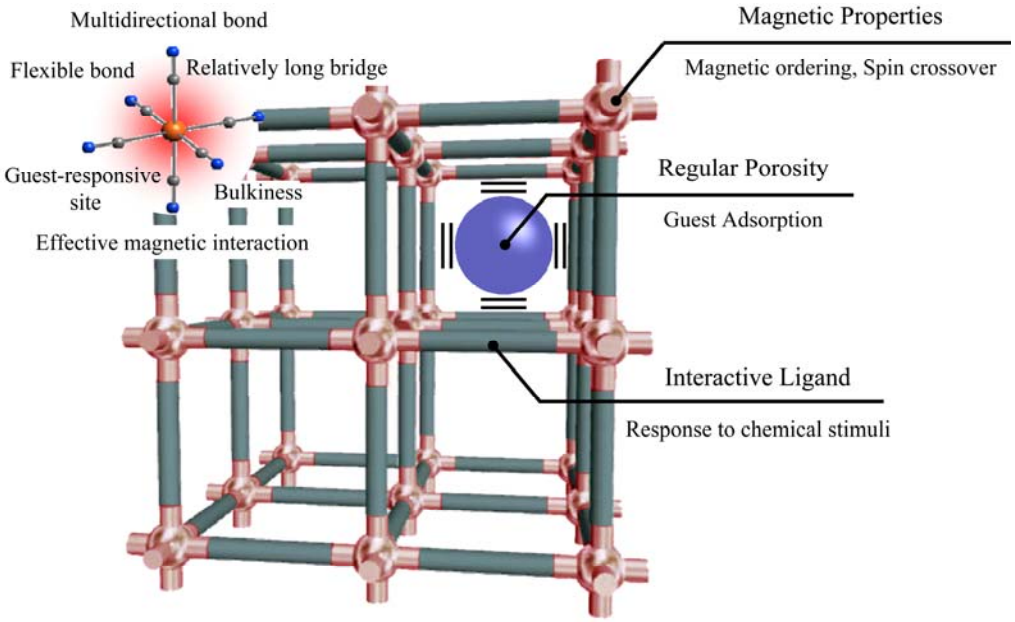

Chapter 6

References

1. B.Moulton, M. Zaworotko, *J. Chem. Rev.* **2001**, *101*, 1629.
2. S. Kitagawa, R. Kitaura, S. Noro, *Angew. Chem., Int. Ed.* **2004**, *43*, 2334.
3. O. M. Yaghi, M. O'Keeffe, N. W. Ockwig, H.K Chae, M. Eddaoudi, J. Kim, *Nature **2003**, 423*, 705.
4. G. Ferey, C. Mellot-Draznieks, C. Serre, F. Millange, *Acc. Chem. Res.* **2005**, *38*, 217.
5. O. M. Yaghi, J. Long, *Chem. Soc. Rev.* **2009**, *38*, 5.
6. R. Matsuda, R. Kitaura, S. Kitagawa,Y. Kubota, R. V. Belosludov,T. C. Kobayashi, H. Sakamoto, T. Chiba, M. Takata, Y. Kawazoe, Y. Mita, *Nature* **2005**, *436*, 238.
7. G. Ferey, C. Mellot-Draznieks, C. Serre, F. Millange, J. Dutour, S. Surble, I. Margiolaki, *Science* **2005**, *309*, 2040.
8. J. L. C. Rowsell, O. M. Yaghi, *Angew. Chem., Int. Ed.* **2005**, *44*, 4670.
9. R. E. Morris, P. S. Wheatley, *Angew. Chem. Int. Ed.* **2008**, *47*, 4966.
10. B. D. Chandler, G. D. Enright, K. A. Udachin, S. Pawsey, J. A. Ripmeester, D. T. Cramb, G. K. H. Shimizu, *Nat. Mater.* **2008**, *7*, 229.
11. O. M. Yaghi, G. M.Li, H. L. Li, *Nature* **1995**, *378*, 703.
12. B. L. Chen, C. D. Liang, J. Yang, D. S. Contreras, Y. L. Clancy, E. B. Lobkovsky, O. M. Yaghi, S. Dai, *Angew. Chem., Int. Ed.* **2006**, *45*, 1390.
13. M. Fujita, Y. J. Kwon, S. Washizu, K. Ogura, *J. Am. Chem. Soc.* **1994**, *116*, 1151.
14. J. S. Seo, D. Whang, H. Lee, S. I. Jun, J. Oh, Y. J. Jeon, K. Kim, *Nature* **2000**, *404*, 982.
15. C. -D.Wu, A. Hu, L. Zhang, W. Lin, *J. Am. Chem. Soc.* **2005**, *127*, 8940.
16. S. Hasegawa, S. Horike, R. Matsuda, S. Furukawa, K. Mochizuki, Y. Kinoshita, S. Kitagawa, *J. Am. Chem. Soc.* **2007**, *129*, 2607
17. S. Horike, M. Dinca, K. Tamaki, J. R. Long, *J. Am. Chem. Soc.* **2008**, *130*, 5854.
18. D. Maspoch, S. R. Molina, J. Veciana, *Chem. Soc. Rev.*, **2007**, *36*, 770.
19. O. Sato, J. Tao, Y. -Z. Zhang, *Angew. Chem. Int. Ed*. **2007**, *46*, 2152.
20. M. Kurmoo, *Chem. Soc. Rev.* **2009**, *38*, 1353.
21. H. Kitagawa, N. Onodera, T. Sonoyama, M. Yamamoto, T. Fukuwa, T. Mitani, M. Seto, Y. Maeda, *J. Am. Chem. Soc.* **1999**, *121*, 10068.
22. Y. Fuma, M. Ebihara, S. Kutsumizu, T. Kawamura, *J. Am. Chem. Soc.* **2004**, *126*, 12238.
23. Evans, W. B. Lin, *Acc. Chem. Res.* **2003**, *35*, 511
24. D. Bradshaw, T. J. Prior, E. J. Cussen, J. B. Claridge, M. J. Rosseinsky, *J. Am.*

Chem. Soc. **2004**, *126*, 6106.
25. S. -H. Cho, B. Ma, S. T. Nguyen, J. T. Hupp, T. E. Albrecht-Schmitt, *Chem. Commun*., **2006**, 2563.
26. J. S. Miller, J. C. Calabrace, H. Rommelmann, S. R. Chittipeddi, J. H. Zhang, W. M. Reiff, A. J. Epstein, *J. Am. Chem. Soc.* **1987**, *109*, 769.
27. J. S. Miller, A. J. Epstein, W. M. Reiff, *Chem. Rev.* **1988**, *88*, 201.
28. J. S. Miller, J. C. Calabrace, R. L. Harlow, D. A. Dixon, J. H. Zhang, W. M. Reiff, S. Chittipeddi, M. A. Selover, A. J. Epstein, *J. Am. Chem. Soc.* **1990**, *112*, 5496.
29. C. Kollmar, M. Couty, O. Kahn, *J. Am. Chem. Soc.* **1991**, *113*, 7994.
30. Y. Pei, M. Verdaguer, O. Kahn, J. Sletten, J. P. Renard, *Inorg. Chem.* **1987**, *26*, 138.
31. O. Kahn, Y. Pei, M. Verdaguer, J. P. Renard, J. Sletten, *J. Am. Chem. Soc.* **1988**, *110*, 782.
32. F. Lloret, K. Nakatani, Y. Journaux, O. Kahn, Y. Pei, J. P. Renard, *J. Chem. Soc., Chem. Commun.* **1988**, 642.
33. P. J. Koningsbruggen, O. Kahn, K. Nakatani, Y. Pei, J. P. Renard, M. Drillon, P. Legoll, *Inorg. Chem.* **1990**, *29*, 3325.
34. O. Guillou, O. Kahn, R. L. Oushoorn, *Inorg. Chim. Acta.* **1992**, *198*, 119.
35. V. Baron, B. Gillon, J. Sletten, C. Mathoniere, E. Codjovi, O. Kahn, *Inorg. Chim. Acta.* **1995**, *235*, 69.
36. S. Turner, O. Kahn, L. Rabardel, *J. Am. Chem. Soc.* **1996**, *118*, 6428.
37. A. Caneschi, D. Gatteschi, P. Rey, R. Sessoli *Inorg. Chem.* **1988**, *27*, 1756.
38. A. Caneschi, D. Gatteschi, R. Sessoli, P. Rey, *Acc. Chem. Res.* **1989**, *22*, 392.
39. A. Caneschi, D. Gatteschi, J. P. Renard, P. Rey, R. Sessoli, *Inorg. Chem.* **1989**, *28*, 1976.
40. A. Caneschi, D. Gatteschi, J. P. Renard, P. Rey, R. Sessoli, *Inorg. Chem.* **1989**, *28*, 2940.
41. A. Caneschi, D. Gatteschi, J. P. Renard, P. Rey, R. Sessoli, *Inorg. Chem.* **1989**, *28*, 3314.
42. A. Caneschi, D. Gatteschi, J. P. Renard, P. Rey, R. Sessoli, *J. Am. Chem. Soc.* **1989**, *111*, 785.
43. A. Caneschi, D. Gatteschi, P. Rey, R. Sessoli, *Chem. Mater.* **1992**, *4*, 204.
44. E. Coronado, J. R. Galán-Mascarós, C. J. Gómez-García, V. Laukhin, *Nature* **2000**, *408*, 447.
45. H. Cui, Z. Wang, K. Takahashi, Y. Okano, H. Kobayashi, A. Kobayashi, *J. Am. Chem. Soc.* **2006**, *128*, 15074.
46. O. Sato, T. Iyoda, A. Fujishima, K. Hashimoto, *Science* **1996**, *272*, 704.

47. O. Sato, T. Iyoda, A. Fujishima, K. Hashimoto, *Science* **1996**, *271*, 49.
48. S. Ohkoshi, M. Mizuno, G. Hung, K. Hashimoto, *J. Phys. Chem. B,* **2000**, *104*, 9365.
49. L. Néel, *Annals Phys.* **1948**, *3*, 137.
50. O. Kahn, *Molecular Magnetism,* VCH, Weinheim, **1993**.
51. D. Maspoch, D. Ruiz-Molina, K. Wurst, N. Domingo, M. Cavalliano, F. Biscarini, J. Tejada, C. Rovira, J. Veciana, *Nature Mater.* **2003**, *2*, 190.
52. G. Férey, *Nature Mater.* **2003**, *2*, 136.
53. S. Ohkoshi, K. Arai, Y. Sato, K. Hashimoto, *Nature Mater.* **2004**, *3*, 857.
54. Z. Wang, B. Zhang, H. Fujiwara, H. Kobayashi, M. Kurmoo, *Chem. Commun.* **2004**, 416.
55. M. Kurmoo, H. Kumagai, K. W. Chapman, C. J. Kepert *Chem. Commun.* **2005**, 3012.
56. S. Ohkoshi, Y. Tsunobuchi, H. Takahashi, T. Hozumi, M. Shiro, K. Hashimoto, *J. Am. Chem. Soc.* **2007**, *129*, 3084.
57. N. Yanai, W. Kaneko, K. Yoneda, M. Ohba, S. Kitagawa, *J. Am. Chem. Soc.* **2007**, *129*, 3496.
58. X. -N. Cheng, W. -X. Zhang, Y. -Y. Lin, Y. -Z. Zheng, X. -M. Chen, *Adv. Mater.* **2007**, *19*, 1494.
59. J. Larionova, S. A. Chavan, J. V. Yakhmi, A. G. Frøystein, J. Sletten, C. Sourisseau, O. Kahn, *Inorg. Chem.*, **1997** *36*, 6374.
60. O. Kahn, J. Larionova, J. V. Yakhmi, *Chem. -Eur. J.*, **1999** *5*, 3443.
61. W. Kaneko, M. Ohba, S. Kitagawa, *J. Am. Chem. Soc.* **2007**, *129*, 13706.
62. "Spin Crossover in Transition Metal Compounds" (Eds: P. Gütlich, H. A. Goodwin), *Top. Curr. Chem.*, **2004**, *233-235*.
63. O. Kahn, C. J. Martinez, *Science* **1998**, *279*, 44..
64. H. Spiering, T. Kohlhaas, H. Romstedt, A. Hauser, C. Bruns-Yilmaz, J. Kusz, P. Gütlich, *Coord. Chem. Rev.*, **1999**, *629*, 190.
65. P. Gütlich, A. Hauser, H. Spiering, *Angew. Chem. Int. Ed.*, **1994**, *33*, 2024.
66. P. Gütlich, Y. Garcia, T. Woike, *Coord. Chem. Rev.*, **2001**, *219*, 839.
67. J. A. Real, A. B. Gaspar, V. Niel, M. C. Muñoz, *Coord. Chem. Rev.*, **2003**, *236*, 121.
68. A. Hauser, J. Jeftic, H. Romstedt, R. Hinek, H. Spiering, *Coord. Chem. Rev.*, **1999**, *190-192*, 471.
69. B. Gaspar , M. Seredyuk, P. Gütlich, *J. Mol. Struct.*, **2009**, *924-926*, 9.
70. J. G. Haasnoot, *Coord. Chem. Rev.* **2000**, *200*, 131.
71. E. Coronado, J. R. Galán-Mascarós, M. Monrabal-Capilla, J. García-Martínez, P.

Pardo-Ibáñez, *Adv. Mater.* **2007**, *19*, 1359.
72. S. Ohkoshi, T. Matsuda, H. Tokoro, K. Hashimoto, *Chem. Mater.*, **2005**, *17*, 81.
73. G. J. Halder, C. J. Kepert, B. Moubaraki, K. S. Murray, J. D. Cashion, *Science* **2002**, *298*, 1762.
74. V. Niel, A. L. Thompson, M. C. Muñoz, A. Galet, A. E. Goeta, J. A. Real, *Angew. Chem. Int. Ed.* **2003**, *42*, 3760.
75. G. J. Halder, K. W. Chapman, S. M. Neville, B. Moubaraki, K. S. Murray, J. -F. Létard. C. J. Kepert, *J. Am. Chem. Soc.*, **2008**, *130*, 17552.
76. S. M. Neville, G. J. Halder, K. W. Chapman, M. B. Duriska, P. D. Southon, J. D. Cashion, J. -F. Létard, B. Moubaraki, K. S. Murray, C. J. Kepert, *J. Am. Chem. Soc.*, **2008**, *130*, 2869.

Chapter 1

Three-dimensional Ferromagnetic Frameworks of *Syn-Anti* Type Carboxylate-bridged Ni^{II} and Co^{II} Coordination Polymers

Abstract

Two novel coordination polymers, $[M(L)(MeOH)_2]_n$ (M^{II} = Ni (**1**), Co (**2**); H_2L = *E*,*E*-muconic acid) having 3-D pillared-layer structure based on 2-D grid sheet extended by *syn-anti* type carboxylate-bridges were prepared. In both compounds, a ferromagnetic interaction operates between M^{II} ions through the *syn-anti* type carboxylate bridges due to accidental orthogonality of magnetic orbitals through orthogonalized p-orbitals of carboxylate. Compound **1** exhibits a ferromagnetic ordering at 1.7 K, whereas **2** shows no long-range ordering because of weak ferromagnetic interaction diminished by antiferromagnetic contributions of dπ electrons and spin-orbit coupling.

Introduction

Many attempts to attain multi-functions by using coordination polymers (CPs) have been devoted in this decade. It is one of the rational strategies to mount physical properties, *e.g.* magnetism,[1–4] dielectric properties,[5–8] *etc*., on the framework to deliver multi-functions. From the magnetic aspects, porous coordination polymers (PCPs) providing a long-range magnetic ordering is a challenging target. The difficulties in controlling both structure and magnetic interaction are still remain, although the synthesis of homometallic PCPs has been proceeded especially by hydrothermal method. In addition, it is difficult to provide simultaneously the porous framework and the long-range magnetic ordering, because of a confliction of respective structural demands.[9–13]

Carboxylate derivatives are well known as good bridging ligands in coordination chemistry. Also they have been frequently applied to construct the framework of CPs and PCPs, as they have high capability to bridge metal ions and high stability in hydrothermal synthetic condition.[14,15] The carboxylate-bridge has many bridging modes, *e.g. syn-syn*, *anti-anti*, *syn-anti*, *etc*., and the *syn-anti* type provides a ferromagnetic interaction due to zero overlap of magnetic orbitals (accidental orthogonality) through orthogonalized p-orbitals of carboxylate.[16–18]

Here, we focused on utilizing of the *syn-anti* type carboxylate bridge to prepare ferromagnetic PCPs. To construct such frameworks, we selected *E*,*E*-muconic acid (H_2L) as a bridging ligand. H_2L has two carboxylate groups which form an angle of 120˚ with a spindle of the rigid diene part. In the arrangement of metal-binding sites, *syn-anti* type bridges are expected to form multi-dimensional frameworks based on a ladder motif (Scheme 1). In this paper, we report the synthesis, crystal structures and magnetic properties of carboxylate-bridged PCPs, $[M^{II}(L)(MeOH)_2]_n$ (M = Ni (**1**), Co (**2**)).

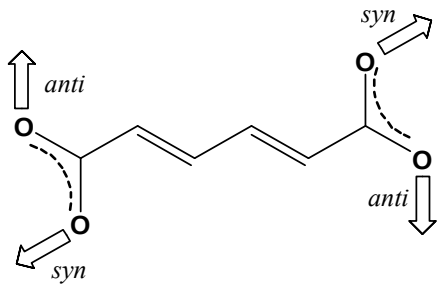

Scheme 1

Results and Discussions

Crystal structure

Crystal parameters are listed in Table 1. Representative structures are given in Figs. 1 – 4.

*$[M^{II}(L)(MeOH)_2]_n$ (M = Ni (**1**), Co (**2**))*

Single crystal X-ray diffraction analysis revealed that both compounds were isomorphous. In the asymmetric unit, the M(II) ions are located at the inversion center and are in a quasi octahedral environment with four oxygen atoms of L^{2-} and two methanol molecules. Both carboxylate groups of L^{2-} act as bidentate ligands (4.1111-mode in Harris notation[19]) where O1 and O2 coordinate to the adjacent metal ions in *syn* and *anti* mode, respectively, and form *syn-anti* type bridges (Fig. 2). The M – O1 and M – O2 bond distances are 2.086(4) and 2.041(4) Å for **1** and 2.115(1) and 2.070(1) Å for **2**, respectively. The M – O1 – C1 and $M^{\#1}$ – O2 – C1 bond angles are 136.3(3) and 132.3(3)° for **1** and 136.76(9) and 131.70(9)° for **2**, respectively. The dihedral angle between $MO1O1^{\#2}O2^{\#3}O2^{\#4}$ and $M^{\#1}O1^{\#1}O1^{\#6}O2O2^{\#7}$ planes is 86.02(9)° for **1** and 86.72(3)° for **2** (symmetry operations; #1: 1/2 – *x*, –1/2 + *y*, 1/2 – *z*, #2: 1/2 – *x*, 1/2 – *y*, – *z*, #3: *x*, – *y*, – 1/2 + *z*, #4: 1/2 – *x*, 1/2 + *y*, 1/2 – *z*, #5: – *x*, – *y*, – *z*, #6: *x*, – *y*, 1/2 + *z*, #7: 1/2 – *x*, –1/2 – *y*, 1 – *z*).

In the lattice, a 2-D grid sheet based on M_4 rhomboid is formed on the *bc* plane by the carboxylate bridges (Fig. 3). And the layers are linked by the diene parts of L^{2-} along the *a* axis affording a 3-D pillared-layer framework (Fig. 4). The nearest intra- and inter-sheet M···M distances are 5.362(7) and 9.290(2) Å for **1** and 5.409(1) and 9.310(2) Å for **2**, respectively. The structure potentially provides 1-D channels running along the *c* axis with 4.9 × 4.9 $Å^2$ gate (under consideration of VDW radii without coordinated MeOH molecules), the void space is 34.7 % for **1** and 42.0 % for **2**.[20] The photoactive diene parts of L were not polymerized by UV and *γ*-ray irradiation in this arrangement.

Table 1. Crystallographic parameters for $[M^{II}(L)(MeOH)_2]_n$ (M = Ni (**1**) and Co (**2**))

Compound	**1**	**2**
Formula	$C_8H_{12}O_6Ni$	$C_8H_{12}O_6Co$
Formula Weight	262.89	263.11
Temperature / K	223	223
Crystal Color	lime green	pink
Crystal System	monoclinic	monoclinic
Space Group	*C*2/c (#15)	*C*2/c (#15)
a / Å	19.70(4)	19.764(5)
b / Å	6.929(13)	7.0368(9)
c / Å	8.185(15)	8.216(2)
α / deg	90	90
β / deg	109.923(7)	110.067(3)
γ / deg	90	90
V / Å^3	1050(3)	1073.3(4)
Z value	4	4
D_{calc} / g·cm^{-3}	1.663	1.628
μ / mm^{-1}	1.853	1.604
R	0.0614	0.0227
Rw	0.1482	0.0622
Goodness of Fit	1.206	1.074

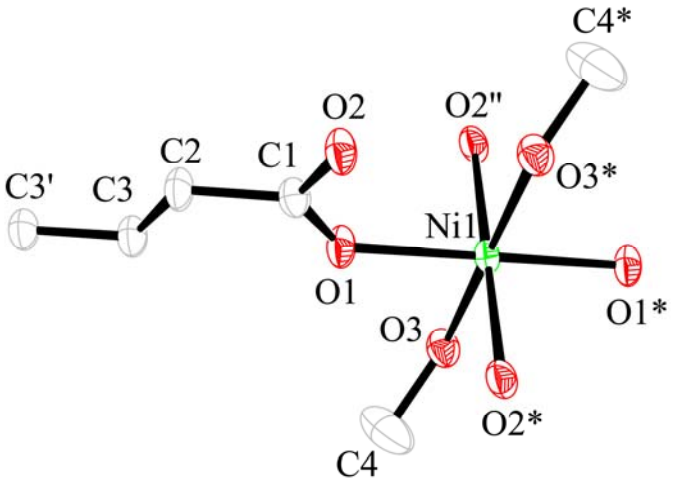

Fig. 1. ORTEP drawing of the asymmetric unit of **1** with the atom numbering scheme at 223 K. Displacement ellipsoids set at 50 % probability. Hydrogen atoms of the ligands omitted for clarity. Nickel, oxygen, and carbon atoms are denoted with green, red, and gray, respectively.

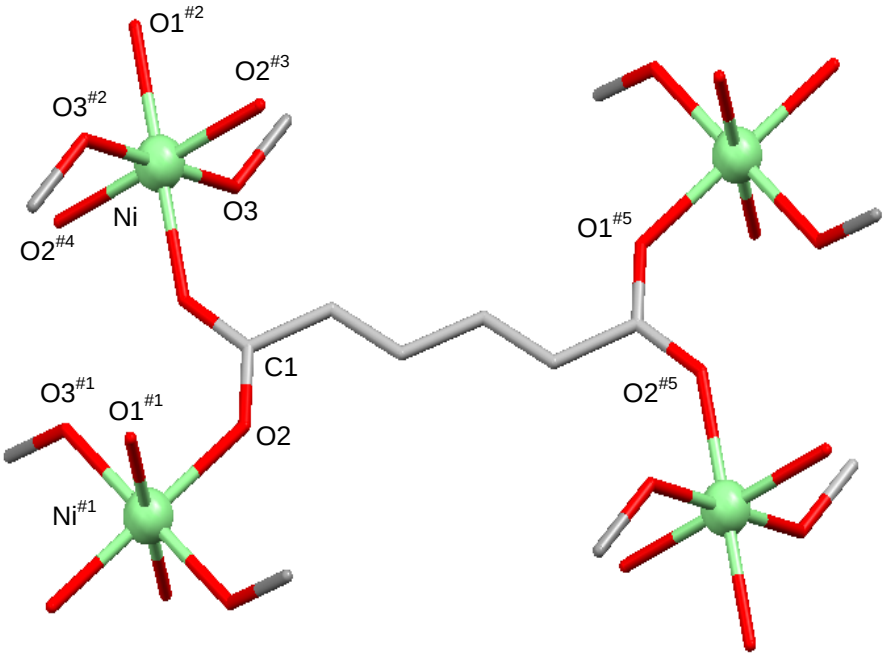

Fig. 2. Bridging structure of L^{2-}. Nickel, oxygen, and carbon atoms are denoted with green, red, and gray, respectively.

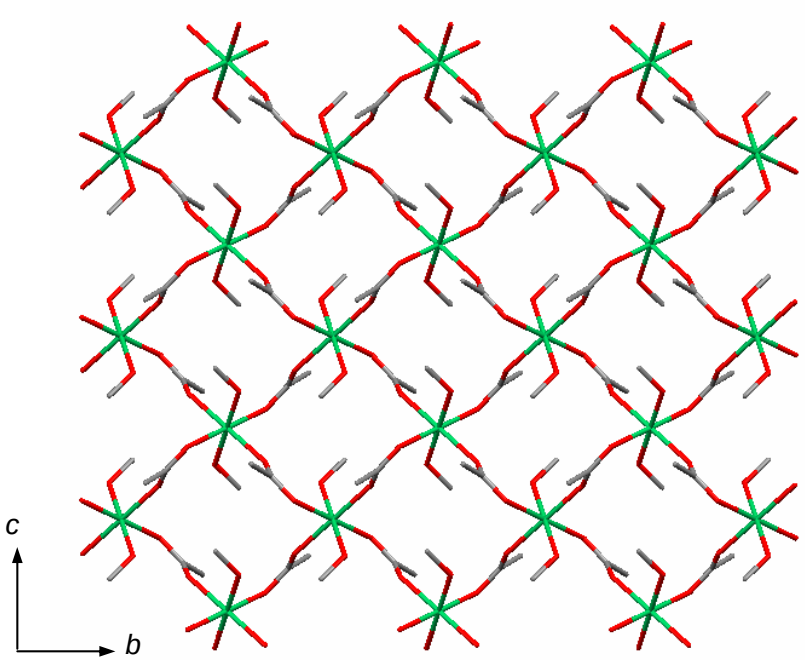

Fig. 3. Projection of the 2-D sheet onto the *bc* plane (omitted diene parts for clarify). Nickel, oxygen, and carbon atoms are denoted with green, red, and gray, respectively.

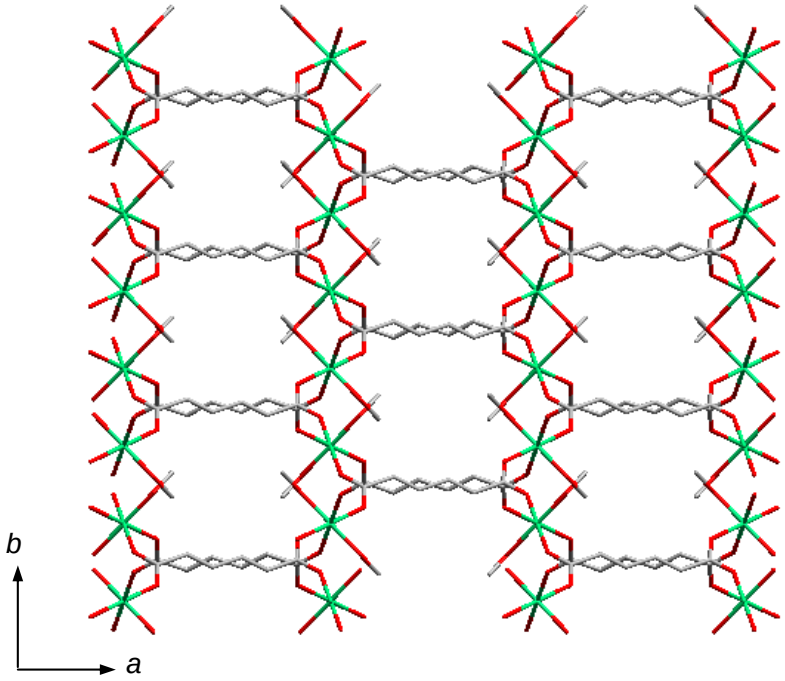

Fig. 4. Projection of the 3-D framework onto the *ab* plane. Nickel, oxygen, and carbon atoms are denoted with green, red, and gray, respectively.

Thermogravimetric analysis

The thermogravimetric analysis (TGA) results of both compounds indicated that the coordinated MeOH molecules were removed by 200 ˚C. Compound **2** also shows color change from pink to purple by the desolvation, however both compounds irreversibly lost crystallinity during the desolvation and decomposed over 340 ˚C (for **1**) and 400 ˚C (for **2**). The amorphization was confirmed by powder X-ray diffraction. Both compounds did not exhibit remarkable gas adsorption because of the fragile frameworks to desolvation.

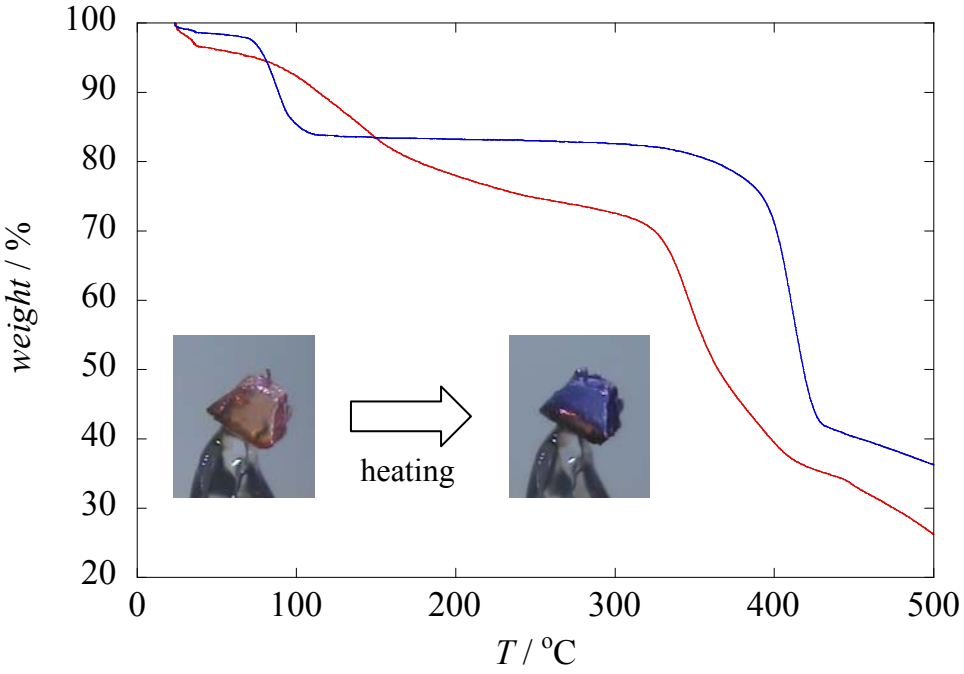

Fig. 5. TGA analysis of **1** (–) and **2** (–). The sample was heated from 30 to 500 °C under a nitrogen atmosphere at a heating rate of 5 °C min^{-1}. Insert is photos of **2** at −50 °C (left) and 85 °C (right), respectively.

Magnetic properties

The $\chi_M T$ *vs*. *T* plots and *M vs*. *H* plots of **1** and **2** were given in Figs. 6 and 7. Weak field magnetization of **1** under an applied field of 5 Oe was given in Fig. 8.

The $\chi_M T$ *vs. T* plot (2 – 300 K) of **1** under an applied field of 500 Oe are shown in Fig. 6. The $\chi_M T$ value is almost constant between 300 and 20 K (1.51 – 1.41 emu·K·mol^{-1} (3.48 – 3.35 μ_B)) and rapidly increases up to a maximum value of 5.32 emu·K·mol^{-1} (6.52 μ_B) at 2 K. The maximum value is much higher than expected one for non-interacting $S = 1$ spin. The Curie-Weiss plot in the temperature ranges of 300 – 20 K gives a Weiss constant θ of +7.0 K. The fast increase of $\chi_M T$ and the positive θ value suggest the operation of a ferromagnetic interaction between the Ni^{II} ions through the *syn-anti* type carboxylate bridges. In the dc and ac magnetic susceptibility measurements (1.8 – 20 K), zero-field-cooled magnetization curve (ZFCM), in-phase (χ_M') and out-of-phase (χ_M") signals show no peak down to 1.8 K. The magnetic phase transition temperature (T_c) of **1** was determined to be 1.7 K by low-temperature measurements with ^{3}He option for SQUID magnetometer. The *M vs. H* curve for **1** at 2 K shows a rapid increase to saturate at 50 kOe (2.04 $N\beta$). Also, magnetic hysteresis is observed at 0.5 K with very small coercive field of *ca.* 20 Oe. These results also support the ferromagnetic ordering of **1**. The low T_c is attributed to the weak intrasheet ferromagnetic interaction through the *syn-anti* type carboxylate bridges and very weak intersheet magnetic interaction. Whereas, compound **2** showed a decrease of $\chi_M T$ value with decreasing temperature because of the spin-orbit coupling of the ground state of high-spin Co(II) ($^4T_1$). Slight increase of $\chi_M T$ was observed around 2 K, however a long-range magnetic ordering was not observed. The weak ferromagnetic interaction would be caused by antiferromagnetic contributions between $(t_{2g})^5(e_g)^2$ electron configurations.

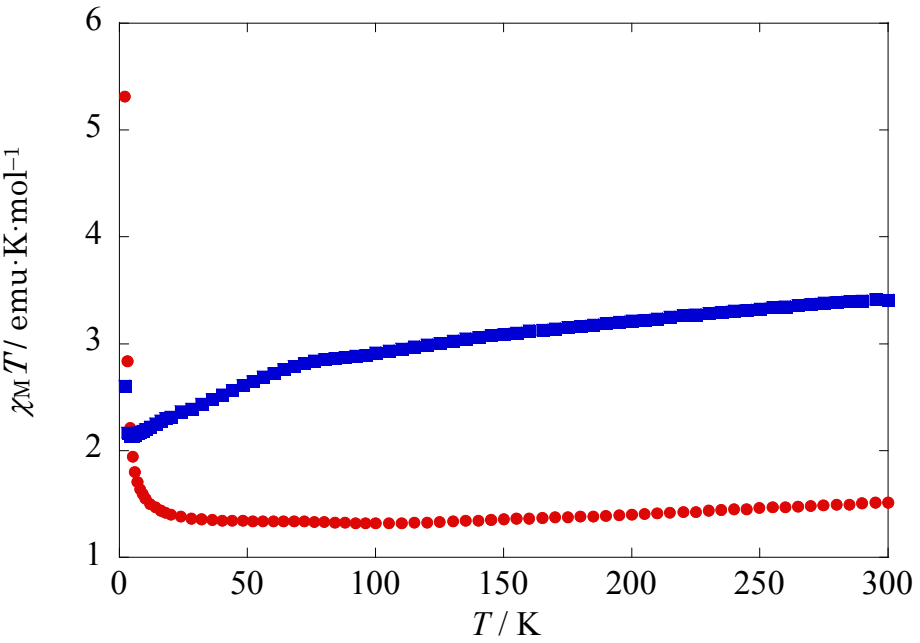

Fig. 6. $\chi_M T$ vs. T plots for **1** (●) and **2** (■) in an applied field of 500 Oe.

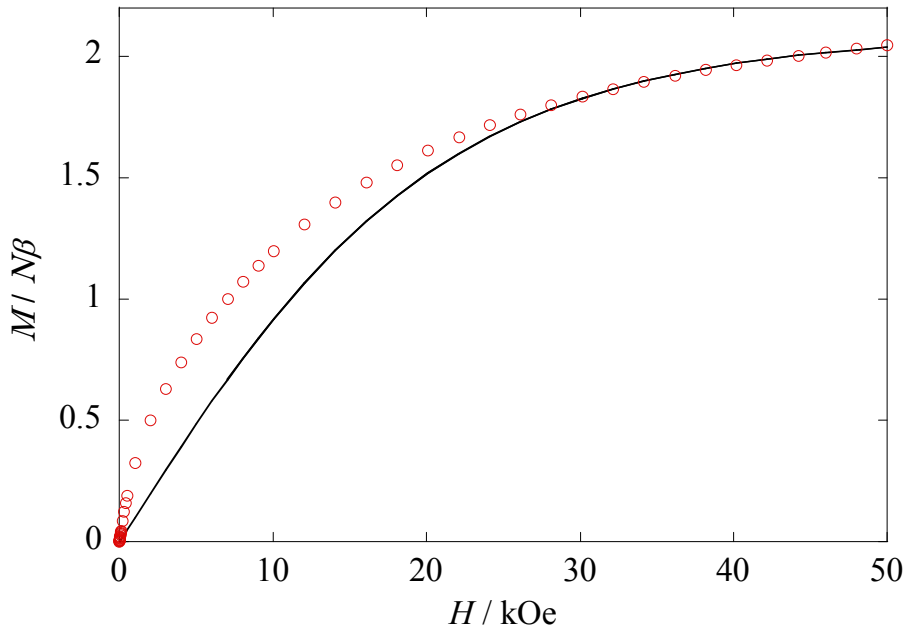

Fig. 7. Field dependences of magnetization at 2 K for **1**. The solid line is the calculated Brillouin curve for $S = 1$ with $g = 2.11$.

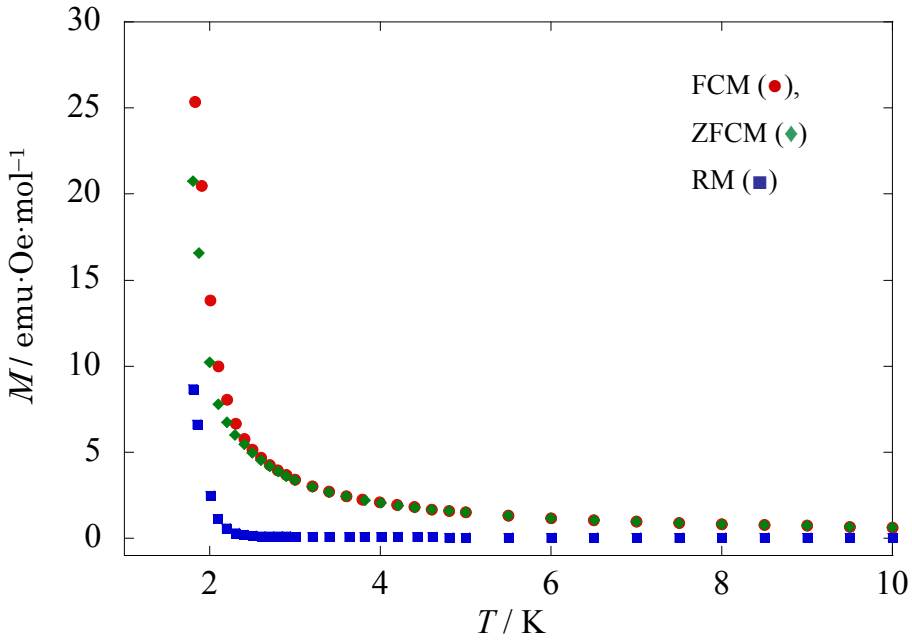

Fig. 8. Field-cooled magnetization (●), zero-field cooled magnetization (♦), and remnant magnetization (■) versus *T* plots of **1** in an applied field of 5 Oe.

Conclusion

The novel porous coordination polymers magnets, $[M(L)(MeOH)_2]_n$ (M(II) = Ni (**1**) Co (**2**)), were prepared using *E*,*E*-muconic acid. The *E*,*E*-muconic acid providing two carboxylate groups linked by rigid diene part derived three-dimensional pillared-layer frameworks based on *syn-anti* type carboxylate-bridged layers, and these compounds showed weak ferromagnetic interaction because of accidental orthogonality of magnetic orbitals through orthogonalized p-orbitals of carboxylate. Compound **1** exhibited a ferromagnetic ordering in the homometallic framework below 1.7 K. Although the pillared-layer-type porous framework based on the structural motif of *E*,*E*-muconic acid did not provide high thermal stability, the framework set out a new design of magnetic PCPs. Other dicarboxylate ligands providing longer rigid pillar part will give PCPs with larger permanent porosity, and such PCPs are expected to exhibit a specific guest responsive magnetic conversion.

Experimental

Materials

All chemicals and solvents, obtained from Tokyo Kasei Co., Ltd., and Wako Pure Chemical Industries, Ltd., were reagent grade. They were used without further purification.

Synthesis of [M(L)(MeOH)$_2$] (M = Ni (1), Co (2))

An aqueous solution (50ml) of $Ni(NO_3)_2 \cdot 6H_2O$ (0.14 g, 0.35 mmol) was put into a glass tube, and then a methanolic solution (50ml) of H_2L (0.05 g, 0.35 mmol) with a 10% methanol solution of tetra-*n*-butylammonium hydroxide (n-Bu)$_4$NOH was poured into the glass tube without mixing the solutions. After several days, Ni(L)(MeOH)$_2$ (**1**) was obtained as lime green platelet crystals.

Anal. Calcd. for $C_8H_{12}O_6Ni$: C, 36.55; H, 4.60 %. Found: C, 36.42; H, 4.18 %.

Compound **2** was also obtained as pink platelet crystals in a similar way to that of **1** using $Co(NO_3)_2 \cdot 6H_2O$ instead of $Ni(NO_3)_2 \cdot 6H_2O$.

Anal. Calcd. for $C_8H_{12}O_6Co$: C, 36.52; H, 4.60 %. Found: C, 36.10; H, 4.20 %.

Crystallographic Data Collection and Refinement of the Structure

Data collections of complexes **1** and **2** were carried out at 223 K, by a Rigaku Mercury CCD system with graphite-monochromated Mo-Kα radiation. The structure was solved by a standard direct method (Crystal Clear 1.3.7 crystallographic software package of the Molecular Structure Corp. and Rigaku). Full-matrix least-squares refinements were carried out using SHELXL 97[21] with anisotropic thermal parameters for all non-hydrogen atoms. All the hydrogen atoms were placed in the calculated positions and refined using a riding model.

Physical Measurements

Magnetic susceptibilities of polycrystalline **1** and **2** were measured on a Quantum Design MPMS-XL5R SQUID susceptometer in the temperature range of 1.8 – 300 K with an applied field of 500 Oe. Field-dependences of magnetization were measured in the field range of 0 − 50 kOe at 2 K. Samples were put into a gelatin capsule, mounted inside straw, and then fixed to the end of the sample transport rod. Diamagnetic correction was made with the Pascal's constants. Diamagnetic correction was made with the Pascal's constants. The molar magnetic susceptibility, χ_M, was

corrected for the diamagnetism of the constituent atoms. Magnetization data down to 0.5 K were collected with the same magnetometer equipped with a self-build ^{3}He cryostat (i-Quantum). All data were plotted in arbitrary scale, because the background data in this measurement was not corrected completely. Infrared spectra (4000 – 400 cm^{-1}) were taken using a Perkin-Elmer system 2000 Ft-IR, where KBr was used as the dispersal medium. Thermogravimetric analyses were recorded on a Rigaku Thermo plus TG 8120 apparatus in the temperature range between 30 and 500 °C under a nitrogen atmosphere at a heating rate of 5 °C min^{-1}.

References

1. C. J. Kepert, *Chem. Commun.* **2006**, *695*.
2. E. Coronado, J. R. G. -Mascaros, C. J. G. -Garcia, A. M.-Martinez, *Chem. -Eur. J.*, **2006**, *12*, 3484.
3. Z. Wang, B. Zhang, H. Fujiwara, H. Kobayashi, M. Kurmoo, *Chem. Comm.*, **2004**, 416.
4. V. Niel, A. L. Thompson, M. C. Muñoz, A. Galet, A. S. E. Goeta, J. A. Real, *Angew. Chem., Int. Ed.*, **2003**, *42*, 3760.
5. H. -B. Cui, Z. Wang, K. Takahashi, Y. Okano, H. Kobayashi, A. Kobayashi, *J. Am. Chem. Soc.* **2006**, *128*, 15074.
6. Y. -Z. Tang, X. -F. Huang, Y. -M. Song, P. W. H. Chan, R. -G. Xiong, *Inorg. Chem.*, **2006**, *45*, 4868.
7. T. Okubo, R. Kawajiri, T. Mitani, T.; Shimoda, *J. Am. Chem. Soc.* **2005**, *127*, 17598.
8. H. -B. Cui, K. Takahashi, Y. Okano, H. Kobayashi, Z. Wang, A. Kobayashi, *Angew. Chem. Int. Ed.*, **2005**, *44*, 6508.
9. N. Yanai, W. Kaneko, K. Yoneda, M. Ohba, S. Kitagawa, *J. Am. Chem. Soc*. **2007**, *129*, 3496.
10. S. Ohkoshi, S. Ikeda, T. Hozumi, T. Kashiwagi, K. Hashimoto, *J. Am. Chem. Soc*. **2007**, *129*, 3084.
11. M. Kurmoo, H. Kumagai; K. W. Chapman; C. J. Kepert, *Chem. Commun.* **2005**, 3012.
12. D. Maspoch, D. Ruiz-Molina, K. Wurst, N. Domingo, M. Cavallini, F. Biscarini, J. Tejada, C. Rovira, J. Veciana, *Nat. Mater.*, **2003**, *2*, 190.
13. M. Ohba, H. Ōkawa, *Coord. Chem. Rev*., **2000**, *198*, 313.
14. S. Kitagawa, R. Kitaura, S. Noro, *Angew. Chem., Int. Ed.*, **2004**, *43*, 2334.
15. M. Yaghi, M. O'Keeffe, N. W. Ockwig, H. K. Chae, M. Eddaoudi J. Kim, *Nature*, **2003**, *423*, 705.
16. X. -Y. Wang, Z. -M. Wang, S. Gao, *Chem. Commun.*, **2007**, 1127.
17. J. Pasán, J. Sanchiz, C. Ruiz-Pérez, F. Lloret, M. Julve, *Inorg. Chem.* **2005**, *44*, 7794.
18. B. Li, X. Wang, Y. Zhang, S. Gao, Y. Zhang, *Inorganica Chimica Acta*, **2005**, *358*, 3519.
19. R. A. Coxall, S. G. Harris, D. K. Henderson, S. Parsons, P. A. Tasker, R. E. P. Winpenny, *J. Chem. Soc. Dalton Trans*. **2000**, 2349.

20. L. Spek, *PLATON, A Multipurpose Crystallographic Tool*, Utrecht University, Utrecht, The Netherlands, **2005**.
21. G. M. Sheldrick, *SHELXL97*, University of Göttingen, Germany, **1997**.

Chapter 2

A Homometallic Ferrimagnet Based on Mixed Antiferromagnetic and Ferromagnetic Interactions through Oxamato and Carboxylato Bridges

Abstract

Two novel coordination polymers (CPs), $\{Cu[Cu(L)(H_2O)(py)]_2\}_n$ (**1**) and $\{Cu[Cu(L)(MeOH)]_2 \cdot 2H_2O\}_n$ (**2**), were synthesized using 2-(oxaloamino) benzoic acid (H_3L) providing oxamate and carboxylate groups, and magnetically characterized. Different 2-D layer structures were formed based on oxamato-bridged tricopper units bridging via the carboxylate group. In both compounds, an antiferromagnetic interaction operated through the oxamato-bridge in the tricopper core. Magnetic interaction between the tricopper units was negligible in compound **1** due to bridging between axial and equatorial positions of Cu^{II} centers. In contrast, **2** showed a tendency of ferrimagnetic ordering at 2 K, resulting from ferromagnetic interactions between the tricopper cores through *syn-anti* type carboxylato bridges linking equatorial positions of neighboring Cu^{II} centers.

Introduction

Coordination polymers have attracted much attention in the past decade because of their unique structures and properties. The CPs' frameworks show a rich diversity due to the combination of various components (metal ion, bridging ligand, coligand, *etc*.), which makes it possible to tune the CPs' frameworks and properties.[1–9] Consequently, CPs are expected to be a platform to deliver multiple functions. From this aspect, it is one of the rational strategies to incorporate physical properties, *e.g.*, magnetic,[3–7] dielectric properties,[8,9] *etc*., in the CPs' frameworks. Here, the design and construction of sensible frameworks providing target properties are the principal significant challenges. To construct a new magnetic framework, we selected a bridging ligand, 2-(oxaloamino)benzoic acid (H_3L; Chart 1), having oxamate and carboxylate groups. H_3L can form an oxamato-bridged trinuclear complex, $M^{II}[M^{II}(L)]_2$, which contains mononuclear complexes, $[M^{II}(L)]^-$. Furthermore, the trinuclear complex provides coordinatable sites and can form a self-assembled structure because of the terminal carboxylate groups. Because the carboxylate groups bridge the terminal M^{II} ions in a *syn-anti* style, which mediates a ferromagnetic interaction[10–12] due to steric demand, the coexistence of oxamato and carboxylato bridges is expected to exhibit a unique magnetic behavior resulting from the mixed antiferromagnetic and ferromagnetic interactions. Here, we report the synthesis, crystal structures, and magnetic properties of new CPs, $\{Cu[Cu(L)(H_2O)(py)]_2\}_n$ (**1**) and $\{Cu[Cu(L)(MeOH)]_2 \cdot 2H_2O\}_n$ (**2**), which consist of a tricopper core with L^{3-}.

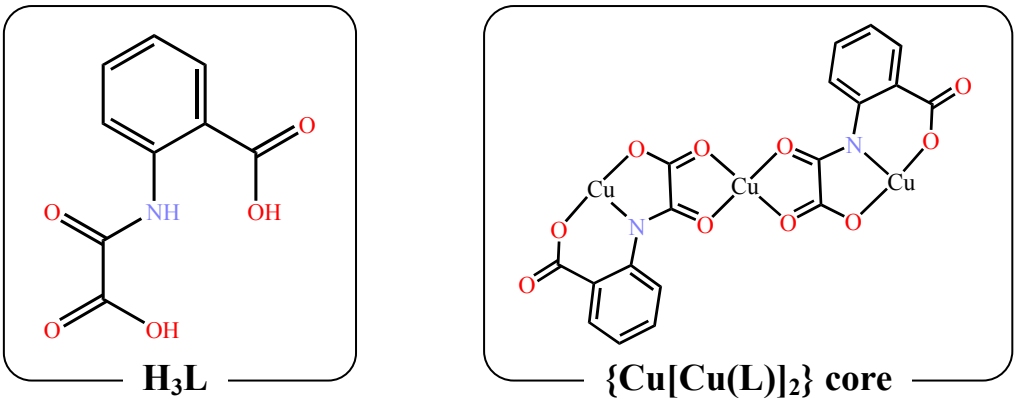

H_3L **$\{Cu[Cu(L)]_2\}$ core**

Chart 1

Results and Discussions

Crystal structure

Crystal parameters are listed in Table 1. ORTEP drawings of **1** and **2** are shown in Figs. 1 and 3 together with the atom numbering scheme. Packing structures are shown in Figs. 2 and 4.

*{Cu[Cu(L)(H_2O)(py)]$_2$}$_n$ (**1**)*

In both compounds, single crystal X-ray diffraction analysis revealed that the ligand L^{3-} coordinates to Cu1 with the tridentate NO_2 site to afford a $[Cu1(L)]^-$ unit, and two $[Cu1(L)]^-$ units coordinate to Cu2 affording an oxamato-bridged tricopper core. In the case of **1**, pyridine coordinates to the equatorial position of Cu1 as a terminal ligand. The geometry about Cu1 is square pyramidal with the NO_2 site of L^{3-} and nitrogen of pyridine in the equatorial plane, and an axial water. Cu2 atom is located on the inversion center and has an elongated octahedral geometry consisting of two oxamato groups of L^{3-} (O3, O5, $O3^{\#1}$, $O5^{\#1}$) and two axial carboxylate oxygen atoms of the adjacent tricopper cores ($O2^{\#2}$ and $O2^{\#3}$) with bond distance of 2.491(4) Å. In the lattice, **1** forms a 2-D sheet structure on the *bc* plane through the carboxylato bridges between the equatorial position of the terminal Cu1 and the adjacent axial position of the central Cu2. The 2-D sheets are linked through complementary hydrogen bonds between the carboxylate oxygen O2 and the axial water on Cu1 ($O6^{\#4}$) with a distance of 2.805 Å, the nearest intersheet Cu···Cu distance being Cu1···$Cu1^{\#4}$ with a value of 5.707 Å.

*{Cu[Cu(L)(MeOH)]$_2$·2H_2O}$_n$ (**2**)*

The asymmetric unit consists of three Cu(II) ions, two ligands, L^{3-}, two coordinated methanol molecules and two lattice water molecules. The geometry about Cu1 is square pyramidal with the NO_2 site of L^{3-} and carboxylate oxygen atoms of the adjacent Tricopper cores ($O2^{\#6}$) in the equatorial plane, and an axial MeOH. The apical methanol shows structural disorder. The Cu2 atom is in a square planar environment with two oxamate groups (O3, O5, $O3^{\#5}$, $O5^{\#5}$). In the lattice, this compound forms a 2-D structure extended on (1,0,1) plane, where the trinuclear core units are connected to each other by the *syn-anti* type carboxylato bridge between terminal Cu1 atoms, complementary hydrogen bonds between oxamate oxygen O5 and the axial MeOH on Cu1 ($O6^{\#8}$), and π···π contacts (*e.g.*, C8···$C6^{\#9}$ = 3.440 Å , C9···$C1^{\#9}$ = 3.473 Å), and forms a 1-D 2_1 helical arrangement of Cu1 atoms along the *b* axis. The helical chains

are linked by oxamato bridges forming a 2-D sheet structure. The nearest intersheet Cu···Cu distance is Cu1···Cu1$^{\#7}$ with a value of 7.316 Å. Symmetry operations: #1: $-x + 3/2, -y + 1/2, -z + 1$; #2: $x, -y, z - 1/2$; #3: $-x + 3/2, y + 1/2, -z + 1/2$; #4: $-x + 2, -y, -z + 2$; #5: $-x, -y, -z$; #6: $-x - 1/2, y - 1/2, -z + 1/2$; #7: $-x - 1, -y + 1, -z$; #8: x, $y - 1, z$; #9: $-x, 1 - y, -z$.

Table 1. Crystallographic parameters for $\{Cu[Cu(L)(H_2O)(py)]_2\}_n$ (**1**) and $\{Cu[Cu(L)(MeOH)]_2 \cdot 2H_2O\}_n$ (**2**)

Complex	**1**	**2**
Formula	$C_{28}H_{22}N_4O_{12}Cu_3$	$C_{20}H_{20}N_2O_{14}Cu_3$
Formula Weight	797.15	703.02
Temperature / K	223	183
Crystal Color	greenish blue	green
Crystal System	monoclinic	monoclinic
Space Group	*C*2/c (#15)	$P2_1/n$ (#14)
a / Å	19.294(2)	10.8891(7)
b / Å	10.2228(9)	6.1482(8)
c / Å	15.446(1)	17.437(2)
α / deg	90	90
β / deg	112.785(1)	98.640(2)
γ / deg	90	90
V / Å^3	2808.9(5)	1154.1(2)
Z value	4	2
D_{calc} / g·cm^{-3}	1.885	2.006
μ / mm^{-1}	2.328	2.820
R	0.0660	0.0461
Rw	0.1670	0.1430
Goodness of Fit	1.115	1.001

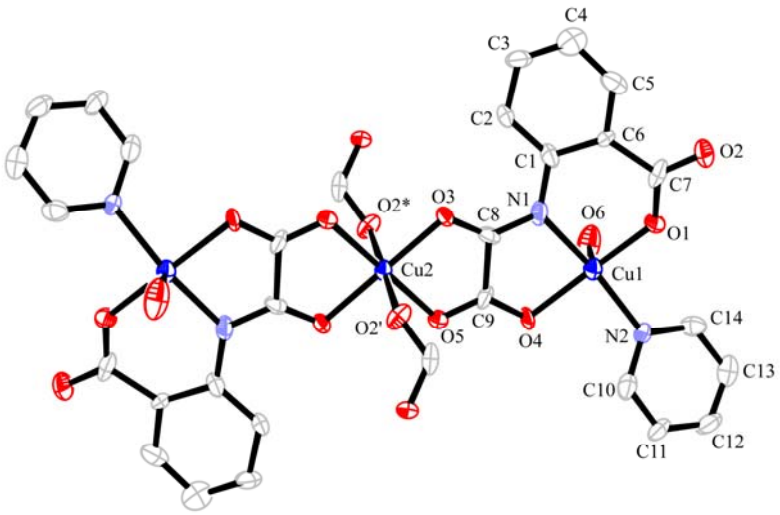

Fig. 1. ORTEP drawing of the asymmetric unit of **1** with the atom numbering scheme at 223 K. Displacement ellipsoids set at 50% probability. Hydrogen atoms of the ligands omitted for clarity. Copper, oxygen, nitrogen, and carbon atoms are denoted with blue, red, light blue, and gray, respectively.

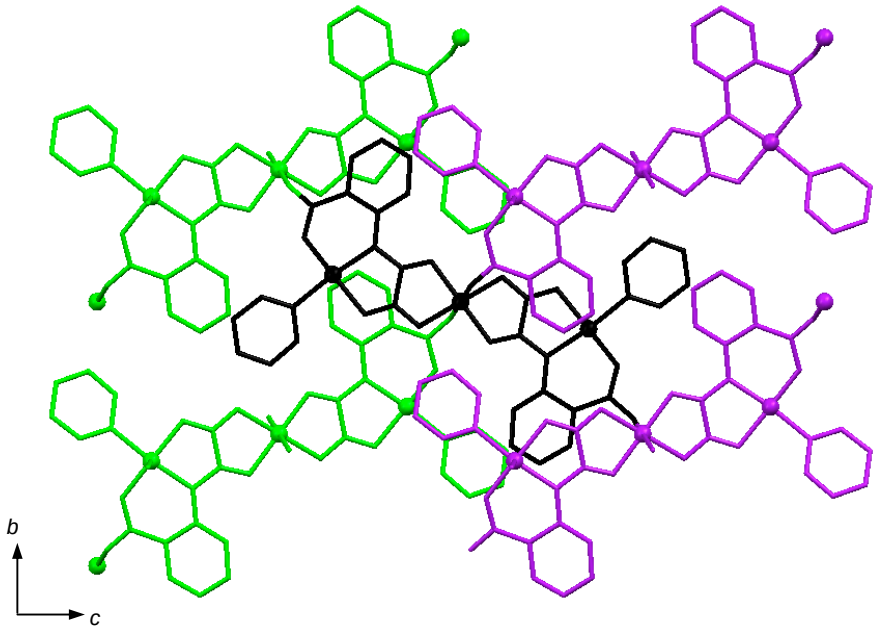

Fig. 2. Projections of the 2D sheet structures of **1** onto the *bc* plane.

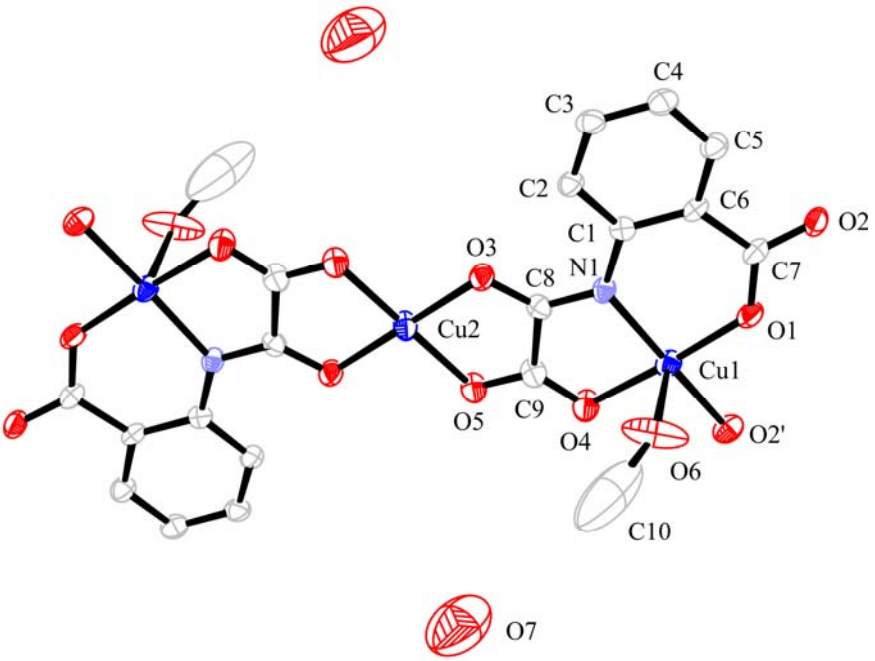

Fig. 3. ORTEP drawing of the asymmetric unit of **2** with the atom numbering scheme at 183 K. Displacement ellipsoids set at 50% probability. Hydrogen atoms of the ligands omitted for clarity. Copper, oxygen, nitrogen, and carbon atoms are denoted with blue, red, light blue, and gray, respectively.

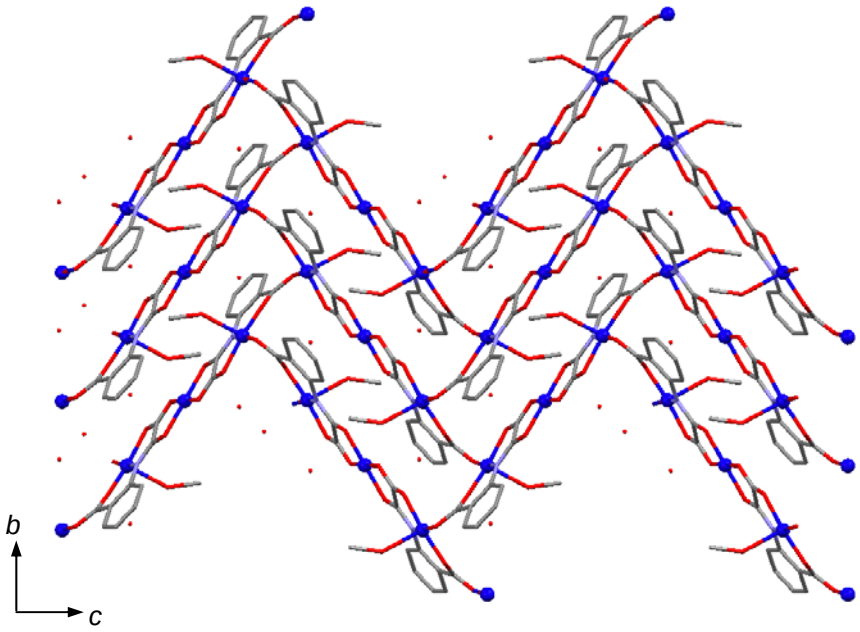

Fig. 4. Projections of the 2D sheet structures of **2** onto the *bc* plane.

Magnetic properties

The $\chi_M T$ *vs*. *T* plots and *M vs*. *H* plots of **1** and **2** were given in Figs. 5 and 6. Weak field magnetization of **1** under an applied field of 5 Oe was given in Fig. 7.

In the case of complex **1**, the value of $\chi_M T$ at 300K was 0.719 emu·K·mol^{-1} (2.40 μ_B), decreased with decreasing temperature and reached a plateau (0.333 emu·K·mol^{-1}, 1.63 μ_B), which is a characteristic behavior of a discrete antiferromagnetically coupled tricopper complex.[13,14] A least-squares fitting of the magnetic behavior based on the equation for S = 1/2 + 1/2 + 1/2 system with Heisenberg Hamiltonian ($H = -2J(S_{Cu1}\cdot S_{Cu2} + S_{Cu1'}\cdot S_{Cu2}) - 2J'(S_{Cu1}\cdot S_{Cu1'})$) was performed, where the magnetic interaction between Cu2 and Cu1$^{\#2}$ in the next tricopper unit through the carboxylato bridge was treated as an overall intermolecular interaction θ. The best-fit parameters obtained for **1** were J = – 142 cm^{-1}, J' = 0.0 cm^{-1}, g = 2.00, and θ = – 0.56 K, which suggests that an antiferromagnetic interaction through the oxamato bridge dominantly operated, and the interaction between Cu2 and Cu1$^{\#2}$ was negligible because of a low overlap integral of the magnetic orbitals between the equatorial and axial planes of Cu^{II}.[13] The saturation magnetization value is 0.93 $N\beta$ at 50 kOe. This indicates that one magnetic spin remains per the tricopper core.

The magnetic behavior of **2** was notably different from that of **1**. The value of $\chi_M T$ gradually decreased with decreasing temperature from 0.839 emu·K·mol^{-1} (2.59 μ_B) at R.T. to 0.490 emu·K·mol^{-1} (1.98 μ_B) at 44 K. Upon further cooling, the $\chi_M T$ sharply increased to a maximum value of 8.87 emu·K·mol^{-1} (8.42 μ_B) at 2 K, which suggests a tendency to magnetic ordering. The temperature dependences of the ac magnetic susceptibility and weak-field magnetization also support an onset of magnetic ordering. The *M vs*. *H* curve of **2** showed a sharp increase with a value for the saturation magnetization (M_s) of 1.10 $N\beta$ at 50 kOe. The value of M_s means that one spin remains in the tricopper core. The observation that saturation occurs faster than the theoretical curve based on the Brillouin function for S = 1/2 confirms the magnetic ordering. In the light of these magnetic data of **2**, its magnetic behavior is classified to "ferrimagnetic" based on antiferromagnetic coupling between ferromagnetic chain bridged by the *syn-anti* type carboxylate and the central Cu2 through the oxamato bridges. Because cusps were not observed in the ac magnetic response down to 2K, a complete ferrimagnetic ordering is expected below 2K.

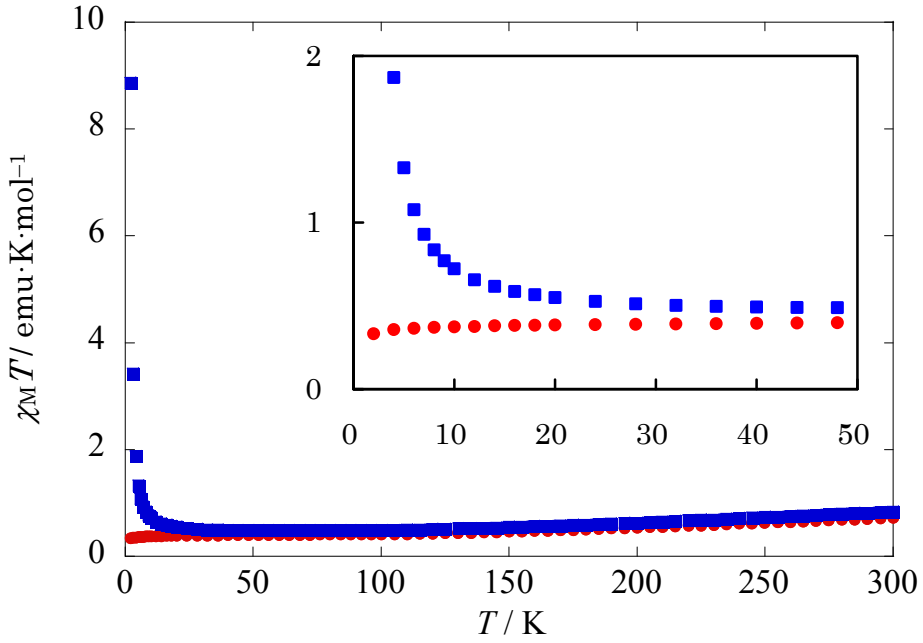

Fig. 5. $\chi_M T$ vs. T plots for **1** (●) and **2** (■) in an applied field of 500 Oe. The inset is an expansion in the range of 1.8 ~ 50 K.

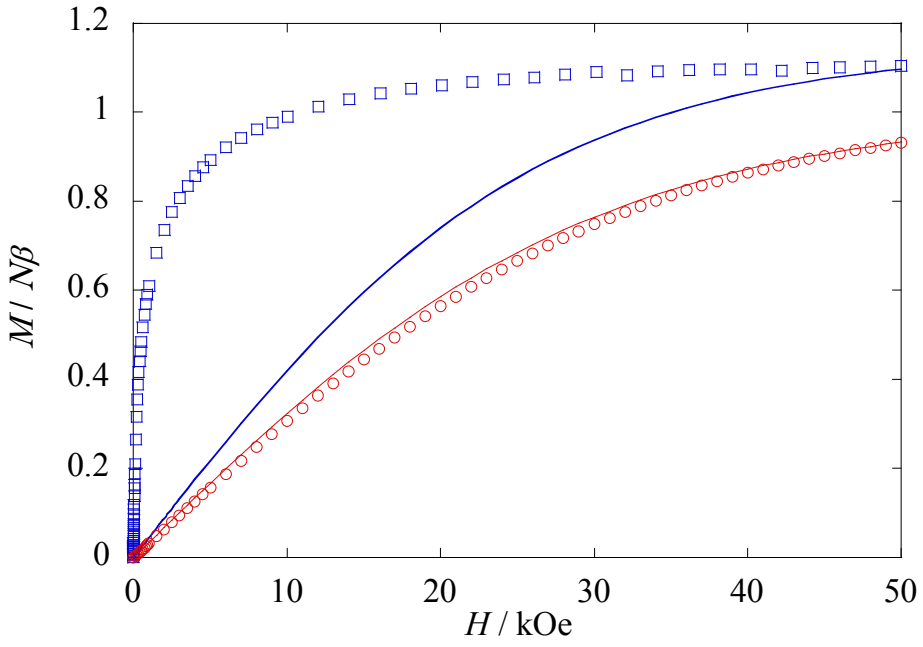

Fig. 6. Field dependences of magnetization of **1** (○) and **2** (□) at 2 K. The solid lines are the Brillouin function for $S = 1/2$ with $g = 2.00$ (**1**) and $g = 2.11$ (**2**).

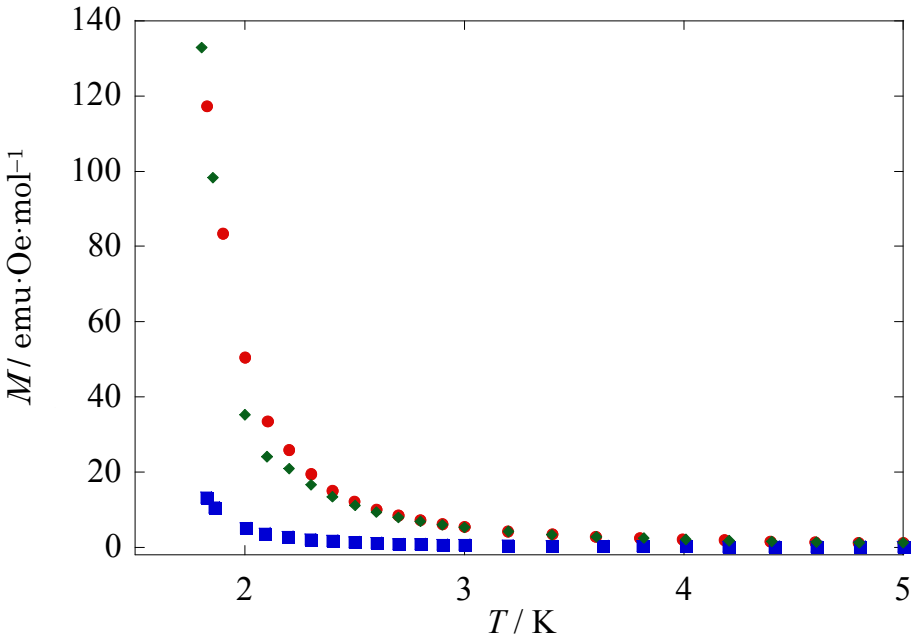

Fig. 7. Field-cooled magnetization (●), zero-field cooled magnetization (♦), and remnant magnetization (■) versus *T* plots of **2** in an applied field of 5 Oe.

Conclusion

Two new CPs based on tricopper units were successfully prepared using 2-(oxaloamino)benzoic acid as a bridging unit. Compounds **1** and **2** formed different types of 2-D layer structures consisting of oxamato-bridged tricopper cores. In the case of **1**, the central Cu^{II} in the tricopper core was linked with the terminal Cu^{II} in the nearest tricopper core through carboxylato bridges, whereas, the 2-D layer structure of **2** was constructed by linking the terminal Cu^{II} through *syn-anti* type carboxylato bridges. Compound **1** showed a relatively strong antiferromagnetic interaction ($J = -142$ cm^{-1}) through the oxamato bridge as a magnetically isolated tricopper core. On the other hand, **2** demonstrated a tendency of ferrimagnetic ordering around 2K, in which the residual spin in the antiferromagnetically coupled tricopper core was aligned by a weak ferromagnetic interaction through the *syn-anti* type carboxylato bridge. This is a rare homometallic ferromagnetic system[15,16] based on an odd-numbered metal unit with mixed antiferromagnetic and ferromagnetic interactions. The molecular design and synthetic strategy based on multinuclear core unit would be available for constructing porous ferrimagnetic frameworks.

Experimental

Materials

All chemicals and solvents, obtained from Tokyo Kasei Co., Ltd., and Wako Pure Chemical Industries, Ltd., were reagent grade. They were used without further purification.

2-(oxalylamino)benzoic acid ethyl ester (H_3L')

An ethanolic solution (80 cm^3) of anthranilic acid (4.988 g, 36.7 mmol) was added dropwise to an ethanolic solution (80 cm^3) of diethyl oxalate (16.233 g, 111 mmol) with stirring and heating. The mixture was stirred with adding triethylamine (10 cm^3) for four hours. The reaction mixture was concentrated and added dilute hydrochloric acid. Several days later at room temperature, the colorless precipitate obtained recrystallized from ethanol to obtain 2-(oxalylamino)benzoic acid ethyl ester (H_3L') as colorless plates. Yield: 3.228 g (37.1 %). Anal. Calcd. for $C_{11}H_{11}NO_5 \cdot H_2O$: C, 55.70; H, 4.67; N, 5.91 %. Found: C, 55.70; H, 4.67; N, 5.91 %.

Synthesis of $\{Cu[Cu(L)(H_2O)(py)]_2\}_n$ (1)

An aqueous solution (2ml) of $Cu(CH_3COO)_2 \cdot H_2O$ (0.0025 g, 0.013 mmol) was transferred to a glass tube, and then a ethanolic solution (2ml) of H_3L' (0.002 g, 0.008 mmol) and pyridine (1 drop) was poured into the glass tube without mixing the solutions. After several days, $\{Cu[Cu(L^3)(H_2O)(py)]_2\}_n$ were obtained as greenish blue platelet crystals.

Anal. Calcd. for $C_{28}H_{22}N_4O_{12}Cu_3$: C, 42.19; H, 2.78; N, 7.03 %. Found: C, 42.18 H, 2.83; N, 6.93 %.

Synthesis of $\{Cu[Cu(L)(MeOH)]_2 \cdot 2H_2O\}_n$ (2)

An aqueous solution (2ml) of $Cu(CH_3COO)_2 \cdot H_2O$ (0.0025 g, 0.013 mmol) was transferred to a glass tube, and then a ethanolic solution (2ml) of H_3L' (0.002 g, 0.008 mmol) was poured into the glass tube without mixing the solutions. After several days, $\{Cu[Cu(L)(MeOH)]_2 \cdot 2H_2O\}_n$ were obtained as green platelet crystals.

Anal. Calcd. for $C_{18}H_{12}N_2O_{12}Cu_3$: C, 33.84; H, 1.89; N, 4.38 %. Found: C, 33.00; H, 2.05; N, 4.26 %.

Crystallographic Data Collection and Refinement of the Structure

Data collections of complexes **1** and **2** were carried out at 223K and 183 K, respectively, by a Rigaku Mercury CCD system with graphite-monochromated Mo-Kα radiation. The structure was solved by a standard direct method (Crystal Clear 1.3.7 crystallographic software package of the Molecular Structure Corp. and Rigaku). Full-matrix least-squares refinements were carried out using SHELXL 97[17] with anisotropic thermal parameters for all non-hydrogen atoms. All the hydrogen atoms were placed in the calculated positions and refined using a riding model.

Physical Measurements

Magnetic susceptibilities of polycrystalline **1** and **2** were measured on a Quantum Design MPMS-XL5R SQUID susceptometer in the temperature range of 1.8 – 300 K with an applied field of 500 Oe. Field-dependences of magnetization were measured in the field range of 0 − 50 kOe at 2 K. Samples were put into a gelatin capsule, mounted inside straw, and then fixed to the end of the sample transport rod. Diamagnetic correction was made with the Pascal's constants. Diamagnetic correction was made with the Pascal's constants. The molar magnetic susceptibility, χ_M, was corrected for the diamagnetism of the constituent atoms.

References

1. D. Maspoch, D. R. Molina, J. Veciana, *Chem. Soc. Rev.* **2007**, *36*, 770.
2. S. Kitagawa, R. Kitaura, S. Noro, *Angew. Chem., Int. Ed.* **2004**, *43*, 2334.
3. W. Kaneko, M. Ohba, S. Kitagawa, *J. Am. Chem. Soc.* **2007**, *129*, 13706.
4. N. Yanai, W. Kaneko, K. Yoneda, M. Ohba, S. Kitagawa, *J. Am. Chem. Soc.* **2007**, *129*, 3496.
5. S. Ohkoshi, S. Ikeda, T. Hozumi, T. Kashiwagi, K. Hashimoto, *J. Am. Chem. Soc.* **2007**, *129*, 3084.
6. V. Niel, A. L. Thompson, M. C. Muñoz, A. Galet, A. S. E. Goeta, J. A. Real, *Angew. Chem., Int. Ed.* **2003**, *42*, 3760.
7. M. Ohba, H. Ōkawa, *Coord. Chem. Rev.* **2000**, *198*, 313.
8. H. -B. Cui, Z. Wang, K. Takahashi, Y. Okano, H. Kobayashi, A. Kobayashi, *J. Am. Chem. Soc.* **2006**, *128*, 15074.
9. T. Okubo, R. Kawajiri, T. Mitani, T. Shimoda, *J. Am. Chem. Soc.* **2005**, *127*, 17598.
10. K. Yoneda, M. Ohba, T. Shiga, H. Oshio, S. Kitagawa, *Chem. Lett.* **2007**, *36*, 1184.
11. X. Y. Wang, Z. M. Wang, S. Gao, *Chem. Commun.* **2007**, 1127.
12. J. Pasán, J. Sanchiz, C. Ruiz-Pérez, F. Lloret, M. Julve, *Inorg. Chem.* **2005**, *44*, 7794.
13. O. Kahn, *Molecular Magnetism,* VCH, Weinheim, **1993**.
14. N. Matsumoto, K. Inoue, M. Ohba, H. Ōkawa, S. Kida, *Bull. Chem. Soc. Jpn.* **1992**, *65*, 2283.
15. M. -H. Zeng, M. -C. Wu, H. Liang, Y. -L. Zhou, X. -M. Chen, S. -W. Ng, *Inorg. Chem.* **2007**, *46*, 7241.
16. S. Konar, P. S. Mukherjee, E. Zangrando, F. Lloret, N. R. Chaudhuri, *Angew. Chem., Int. Ed.* **2002**, *41*, 1561.
17. G. M. Sheldrick, *SHELXL97*, University of Göttingen, Germany, **1997**.

Chapter 3

Spin Transition in a 4,4'-bipyridine-bridged One-dimensional Coordination Polymer Constructed from a Pyrazolato-bridged Fe(II) Dimer

Abstract

Dinuclear Fe(II) complexes [{Fe^{II}(NCE)(μ-bpypz)(4-phpy)}$_2$] (E = S (**1**), BH_3 (**2**); 4-phpy = 4-phenylpyridine) and dinuclear-complex-based one-dimensional coordination polymers [{Fe^{II}(NCE)(μ-bpypz)}$_2$(μ-4,4'-bpy)]·MeOH (E = S (**3**), BH_3 (**4**); 4,4'-bpy = 4,4'-bipyridine) were prepared using 3,5-bis(2-pyridyl)pyrazole (Hbpypz) providing two metal-binding sites. These complexes demonstrated that substituent groups on the pyridine ligands and S/BH_3 substitution on NCE^- greatly influence their spin crossover behavior, presumably arising from the ligand-field strength. In addition the dinuclear complex **2** exhibits two step SCO where the plateau is found to be [HS–HS]···[LS–LS], but not [HS–LS] by the temperature variable X-ray analysis, IR and Raman spectra. The one-dimensional CPs **3** and **4** are found to form the extended three-dimensional polymeric structures through interchain $\pi - \pi$ stackings by the X-ray analysis. Mgnetic and Mössbauer measurements reveal that the CPs show steep single [HS–HS] to [LS–LS] transition and/or LIESST or light-induced excited pair spin state.

Introduction

Spin-crossover (SCO) metal complexes exhibit intriguing molecular bistability driven by external stimuli. Among them, SCO in Fe(II) complexes with a d^6 electron configuration are expected to lead to promising functional molecular devices such as molecular memory or switches.[1–4] The fundamental origin of the spin-crossover phenomenon is molecular, but the magnetic behavior strongly depends on intermolecular interaction. Up to now, the major source of information on spin transition systems comes from mononuclear iron(II) compounds. However, controlling both intra- and inter-molecular interactions if polynuclear compounds are employed would enhance the cooperativity in the systems. Thus, the cooperativity can be achieved by using suitable bridging ligands. Integration of an intramolecular magnetic interaction and SCO in polynuclear Fe(II) complexes could provide auxiliary functionality, whereas much attention has been paid to two-step SCO in mono- or dinuclear Fe(II) complexes where cooperativity is associated with inter- and intramolecular (short- and long-range) interactions.[5–7] However, only a limited number of two-step SCO dinuclear complexes are known. There have been extensive studies of a family of bpym (2,2'-bipyrimidine) bridged complexes,[8–17] following the latest report on the phdia (4,7-phenanthroline-5,6-diamine) bridged complex.[18] These complexes exhibit two-step SCO through the mixed spin intermediate [HS–LS] in the plateau which was directly monitored unambiguously by Mössbauer spectroscopy.[14,18] However, few X-ray structure of the SCO dinuclear diiron(II) complex have been reported so far. Murray *et al.* reported the structure of $[\{Fe(NCSe)(\mu\text{-pzpy})(pzpyH)\}_2]$ (pzpyH = 2-pyrazolylpyridine) very recently.[19] Also, we studied the X-ray structure of $[\{Fe^{II}(NCBH_3)(\mu\text{-bpypz})(py)\}_2]$ (py = pyridine, Hbpypz = 3,5-bis(2-pyridyl)pyrazole),[20] which was followed by the direct light induced SCO in terms of Raman spectra.[21] The bpypz bridged dinuclear complex with a replaceable axial pyridine is expected to lead to two-step SCO processes by controlling the intermolecular interactions. In addition, these dinuclear units are robust and can be used as a building block of assemblies. These results prompt us to construct polymetallic compounds, which consist of the dinuclear cluster unit and an additional linking ligand, for a fundamental understanding of cooperatibity between clusters and the synergy between the SCO phenomenon and intra- or inter- cluster magnetic exchange interaction. Here, we report structure and magnetic dinuclear complexes, $[\{Fe^{II}(NCE)(\mu\text{-bpypz})(4\text{-phpy})\}_2]$ (E = S (**1**), BH_3, (**2**); 4-phpy = 4-phenylepyridine) and one-dimensional coordination polymers, $[\{Fe^{II}(NCE)\text{-}(\mu\text{-bpypz})\}_2(\mu\text{-4,4'-bpy})]\cdot MeOH$ (E = S (**3**) or BH_3 (**4**); 4,4'-bpy = 4,4'-bipyridine).

Results and Discussions

Crystal structure

Crystal parameters and selected bond distances are listed in Tables 1 – 4. Representative structures are given in Figs. 1 – 6.

*[{Fe^{II}(NCS)(μ-bpypz)(4-phpy)}$_2$] (**1**)*

Despite many efforts, we did not succeed in growing single crystals of **1** suitable for single crystal X-ray analysis and we used powder diffraction pattern to determine the structure. The diffractograms of compounds **1** and **2** accompanied with the simulated pattern obtained from the crystal structure of **2**. The X-ray diffraction patterns show **1** and **2** to be isomorphous at room temperature, and thus, the dinuclear iron(II) structure is confirmed to be formed.

*[{Fe^{II}($NCBH_3$)(μ-bpypz)(4-phpy)}$_2$] (**2**)*

The X-ray analysis of **2** demonstrates that the space group at 296 K is identical to that at 200 K and 100 K. The geometrical configurations around the iron ions (Fig. 1) at 296 and 100 K are fundamentally the same as those of the corresponding py complex.[20] The iron atoms coordinated to two $bpypz^-$ to form the centrosymmetric dimer with only one kind of Fe(II) atom and the ligands in a distorted octahedral environment belonging to a pseudo C_{2h} point group. Each Fe atom is bound to the four nitrogen atoms of two pyridyl and two pyrazolate moieties in $bpypz^-$ in the basal plane and two nitrogen atoms of 4-phpy and $NCBH_3^-$ anion at the axial positions forming a distorted octahedral environment as clearly seen from the top and side views of the molecule. Average of Fe – N bond length at 296 K shows value typical of HS Fe(II) centers. The corresponding value at 100 K is 1.980 Å. The changes in Fe – N distances by *ca*. 0.19 Å suggest that all Fe(II) ions are in the LS state at 100 K. The unit cell volume decreases sharply from 1205.11(9) $Å^3$ at 296 K to 1105.17(14) $Å^3$ at 100 K: an 8.3% decrease upon SCO.

At 200 K, the X-ray analysis shows the existence of each one of the high-spin [HS–HS] and low-spin [LS–LS] dinuclear complexes in the asymmetric unit doubled in size from 296 and 100 K. That is, the bond lengths around the Fe1 and Fe2 at 200 K correspond to those around Fe1 at 100 and 296 K, respectively; average Fe – N = 2.0005 Å (Fe1) and 2.116 Å (Fe2) at 200 K; 1.9795 Å (Fe1) at 100 K and 2.1667 Å (Fe1) at 296 K; Fe1···$Fe1^{\#3}$ = 4.0605(8) Å and Fe2···$Fe2^{\#2}$ = 4.2000(8) Å at 200 K; Fe1···$Fe1^{\#1}$ = 4.0434(6) Å at 100 K and 4.2147(8) Å at 296 K (Symmetry operations:

#1: $-x+1, -y+1, -z+1$, #2: $-x+1, -y+2, -z+1$, #3: $-x, -y+1, -z$). There are π – π stacking interactions between the adjacent bpypz, by which a layer and a chain are formed as found for the py complex.[20] At 200 K, the [HS–HS] and [LS–LS] complexes are arranged in alternate chains through the π – π stackings not only between the 4-phpy, but also between the pyridyls of the bpypz. The π – π stackings between the bpypz exist for the pz···py between [HS–HS] and [HS–HS] as well as [LS–LS] and [LS–LS] and for the pyridyl (HS)···pyridyl (LS) as the py complex. For a given 4-phpy in [HS–HS] or [LS–LS] at 200 K, strong π – π stackings of the pyridyl and phenyl on one side are made, respectively, with the phenyl and pyridyl for the 4-phpy in the adjacent [LS–LS] or [HS–HS], and on the other back side weak phenyl···phenyl π – π stackings with the other neighboring 4-phpy in the [LS–LS] or [HS–HS] (Figs. 2 and 3). There are significant voids in the crystals, but no electron density is found. All these crystallographic characteristics support the occurrence of a direct two-step spin transition from [HS–HS] to [LS–LS] through a mixture of [HS–HS]···[LS–LS] intermediates.

*[{Fe^{II}(NCE)(μ-bpypz)}$_2$(μ-4,4'-bpy)]·MeOH (E = S (**3**), BH_3 (**4**))*

An ORTEP drawing of the structures at 200 K and 150 K around the iron ions in **3** are shown in Fig. 4. Both structures are isomorphous with each other. The structure at 200 K shows that the desired coordination has been achieved with the iron atoms being coordinated to two $bpypz^-$ to form a dinuclear complex. The dinuclear unit is centrosymmetric, thus, the only one kind of iron and ligands exist in the molecule. Each iron atom is bound to the four nitrogen atoms of two pyridyl and two pyrazolate moieties in $bpypz^-$ in the basal plane and two nitrogen atoms of 4,4'-bpy and NCS^- anion at the axial positions forming a distorted octahedral environment. Neighbor dimers connect by the 4,4'-bpy bridges through axial coordination of the Fe(II) ions, defining a 1-D chain. The chain forms a three dimensional structure by two types of π – π stacking interactions between the $bpypz^-$ ligands of the adjacent dimers on the neighbor chains (Fig. 5); (1) between pyridyl rings and (2) between pyridyl and pyrazole rings of the adjacent complexes. There are voids between the chains. Interstitial MeOH molecules are introduced in the void and disordered in two positions. Further, they have OH – π interaction with the bridged 4,4'-bpy (nearest neighbor O – C distance: 3.60 Å (150 K) and 3.66 Å (200 K)). Average of Fe – N bond length at 200 K is 2.17 Å, the value of which is typical of high spin (HS) Fe(II) centers while the corresponding value at 150 K is 2.00 Å. The changes in Fe – N distances by *ca*. 0.17 Å suggest that all Fe(II) ions are in the low spin (LS) state at 150 K. Fe···Fe distances

in the chain at HS state (200 K) and LS state (150 K) are 4.217(1) and 4.047(1) Å, respectively. Furthermore, the inter dimer Fe···Fe distance across the 4,4'-bpy bridge in the chain also becomes shortened 0.53 Å under the spin transition (11.558(1) Å (HS) to 11.020(1) Å (LS)) while the nearest neighbor inter-chain Fe···Fe distance extends from 6.336(4) Å (HS) to 6.473 Å (LS). The unit cell volume decreases sharply from 949.6(6) $Å^3$ at 200 K to 877.9(3) $Å^3$ at 150 K: a 7.6% decrease upon SCO.

The complex **4** is isomorphous with complex **3**, having 3-D network with 1-D bpy bridged chain. So only the distance is shown here. Average of Fe – N bond length at 350 K is 2.17 Å showing value typical of HS Fe(II) centers.

Table 1. Crystallographic parameters for [{Fe(NCBH$_3$)(μ-bpypz)(4-phpy)}$_2$] (**2**)

Compound	**2**	**2**	**2**
Formula	$C_{50}H_{42}N_{12}B_2Fe_2$	$C_{50}H_{42}N_{12}B_2Fe_2$	$C_{50}H_{42}N_{12}B_2Fe_2$
Formula Weight	944.28	944.28	944.28
Temperature / K	296	200	100
Crystal Color	red	red	black
Crystal System	triclinic	triclinic	triclinic
Space Group	$P\bar{1}$ (#2)	$P\bar{1}$ (#2)	$P\bar{1}$ (#2)
a / Å	9.4567(2)	9.3509(2)	9.0589(3)
b / Å	10.7576(6)	14.91240(10)	10.6824(11)
c / Å	13.1355(5)	17.1648(4)	12.6458(8)
α / deg	92.519(6)	99.612(1)	93.521(8)
β / deg	108.793(9)	94.551(1)	109.122(12)
γ / deg	105.710(5)	98.174(1)	104.560(8)
V / Å^3	1205.11(9)	2322.89(8)	1105.17(14)
Z value	1	2	1
D_{calc} / g·cm^{-3}	1.301	1.350	1.419
μ / mm^{-1}	0.650	0.674	0.708
R	0.0560	0.0739	0.0574
Rw	0.1638	0.1755	0.1745
Goodness of Fit	1.000	0.997	1.009

Table 2. Selected bond length for [{Fe(NCBH$_3$)(μ-bpypz)(4-phpy)}$_2$] (**2**)

T / K	296	200	100
Fe1 – N1 / Å	2.222(3)	2.051(4)	2.034(3)
Fe1 – N2 / Å	2.098(2)	1.936(3)	1.927(3)
Fe1 – N3$^{\#3}$ / Å	2.067(2)	1.936(3)	1.923(3)
Fe1 – N4$^{\#3}$ / Å	2.262(3)	2.060(4)	2.050(3)
Fe1 – N5 / Å	2.202(3)	2.005(4)	1.984(3)
Fe1 – N6 / Å	2.222(3)	2.002(5)	2.034(3)
Fe2 – N7 / Å	–	2.161(4)	–
Fe2 – N8 / Å	–	2.048(4)	–
Fe2 – N9$^{\#2}$ / Å	–	2.038(4)	–
Fe2 – N10$^{\#2}$ / Å	–	2.195(5)	–
Fe2 – N11 / Å	–	2.162(4)	–
Fe2 – N12 / Å	–	2.092(5)	–

Table 3. Crystallographic parameters for [{Fe(NCS)(μ-bpypz)}$_2$(μ-4,4'-bpy)]·MeOH (**3**) and [{Fe(NCBH$_3$)(μ-bpypz)}$_2$(μ-4,4'-bpy)]·MeOH (**4**)

Compound	**3**	**3**	**4**
Formula	$C_{39}H_{30}N_{12}OS_2Fe_2$	$C_{39}H_{30}N_{12}OS_2Fe_2$	$C_{39}H_{36}N_{12}OB_2Fe_2$
Formula Weight	858.56	858.56	822.11
Temperature / K	200	150	350
Crystal Color	orange	brown	orange
Crystal System	triclinic	triclinic	triclinic
Space Group	$P\bar{1}$ (#2)	$P\bar{1}$ (#2)	$P\bar{1}$ (#2)
a / Å	9.529(3)	9.2371(9)	9.5926(5)
b / Å	10.386(4)	10.2730(2)	10.6430
c / Å	10.680(4)	10.2499(1)	10.748(1)
α / deg	78.50(6)	78.43(4)	77.71(5)
β / deg	73.16(5)	73.91(4)	73.29(5)
γ / deg	70.91(5)	71.16(4)	71.69(4)
V / Å^3	949.6(6)	877.9(3)	988.7(1)
Z value	1	1	1
D_{calc} / g·cm^{-3}	1.501	1.624	1.327
μ / mm^{-1}	0.924	0.999	0.777
R	0.0475	0.0661	0.091
Rw	0.1069	0.153	0.27
Goodness of Fit	1.038	1.073	0.993

Table 4. Selected bond length for [{Fe(NCS)(μ-bpypz)}$_2$(μ-4,4'-bpy)]·MeOH (**3**) and [{Fe(NCBH$_3$)(μ-bpypz)}$_2$(μ-4,4'-bpy)]·MeOH (**4**)

Compound	**3**	**3**	**4**
T / K	200	150	350
Fe1 – N1 / Å	2.261(3)	2.065(3)	2.262(14)
Fe1 – N2 / Å	2.090(2)	1.944(4)	2.079(15)
Fe1 – N3$^{\#1}$ / Å	2.109(2)	1.957(2)	2.087(14)
Fe1 – N4$^{\#1}$ / Å	2.233(2)	2.059(4)	2.221(15)
Fe1 – N5 / Å	2.240(1)	1.986(2)	2.216(11)
Fe1 – N6 / Å	2.106(2)	1.958(3)	2.145(13)

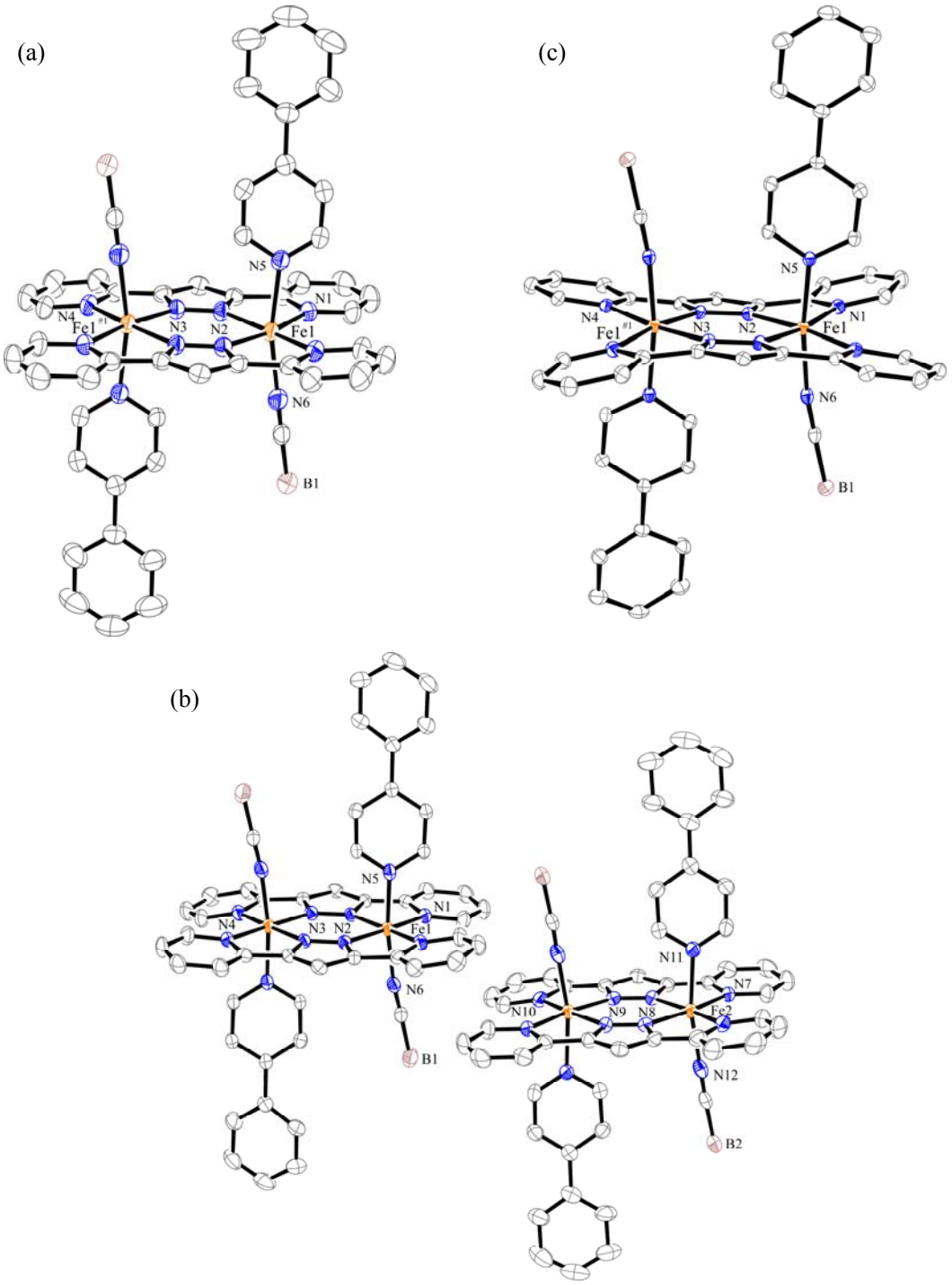

Fig. 1. ORTEP drawing of the asymmetric unit of [{Fe(NCBH$_3$)(μ-bpypz)(4-phpy)}$_2$] (**2**) with the atom numbering scheme at 296 K (a), 200 K (b) and 100 K (c). Displacement ellipsoids set at 30 % probability. Hydrogen atoms of the ligands omitted for clarity. Iron, nitrogen, carbon, and boron atoms are denoted with orange, blue, gray, and brown, respectively.

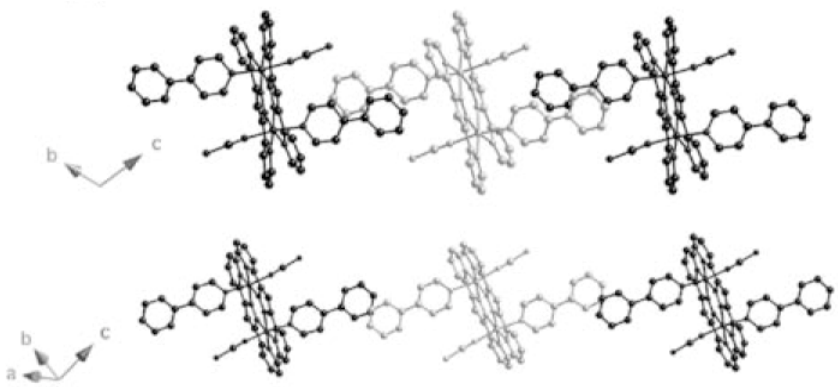

Fig. 2. Perspective views of dinuclear complex **2**: views nearly from the negative and positive side of the *a* axis, respectively.

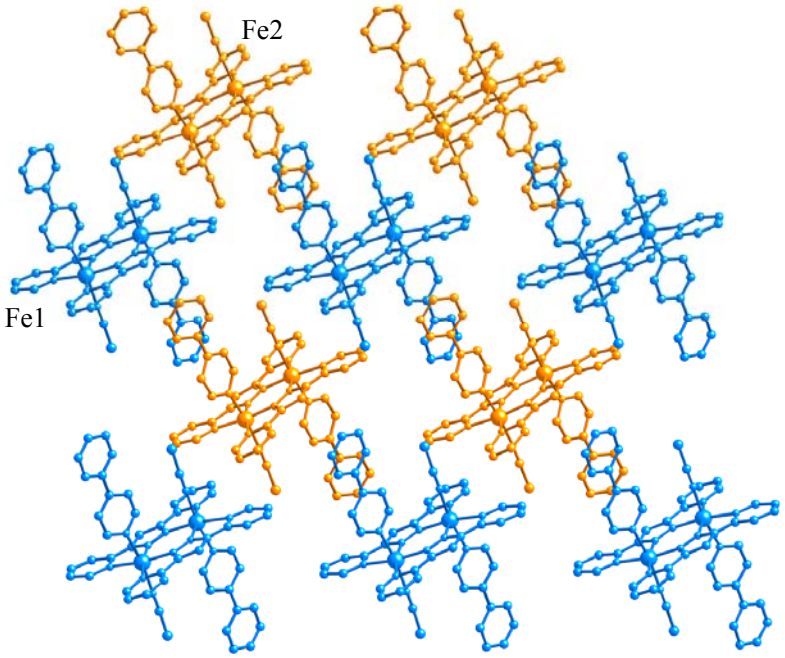

Fig. 3. Crystal structure of dinuclear complex **2** at 200 K; Fe1 [LS–LS] and Fe2 [HS–HS] dinuclear units are colored in sky blue and orange, respectively.

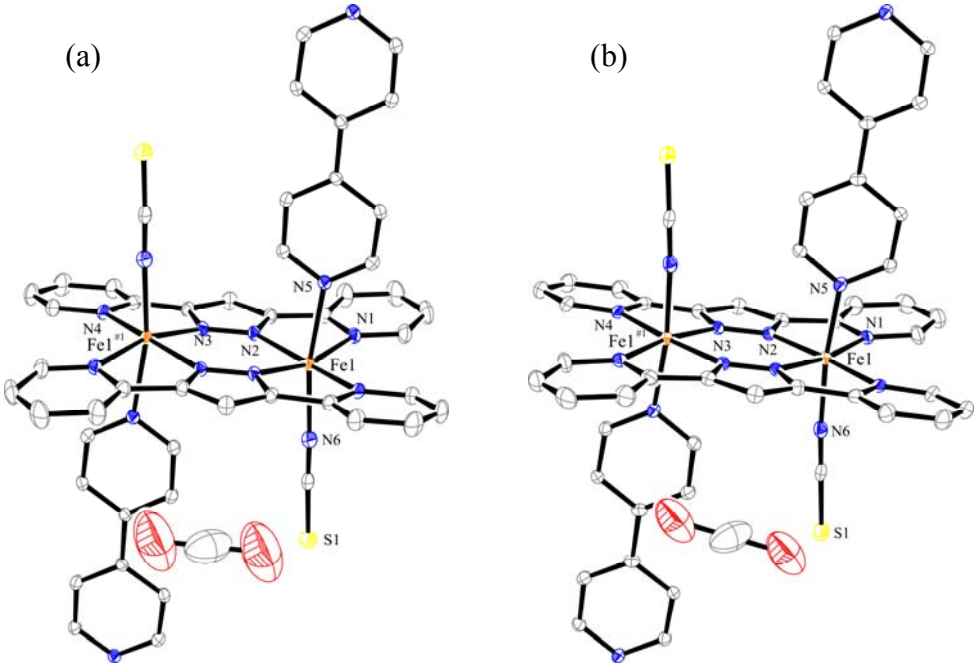

Fig. 4. ORTEP drawing of the asymmetric unit of [{Fe(NCS)(μ-bpypz)}$_2$-(μ-4,4'-bpy)]·MeOH (**3**) with the atom numbering scheme at 200 K (a) and 150 K (b). Displacement ellipsoids set at 30% probability. Hydrogen atoms of the ligands omitted for clarity. Iron, oxygen, nitrogen, carbon, and sulfur atoms are denoted with orange, red, blue, gray, and yellow, respectively.

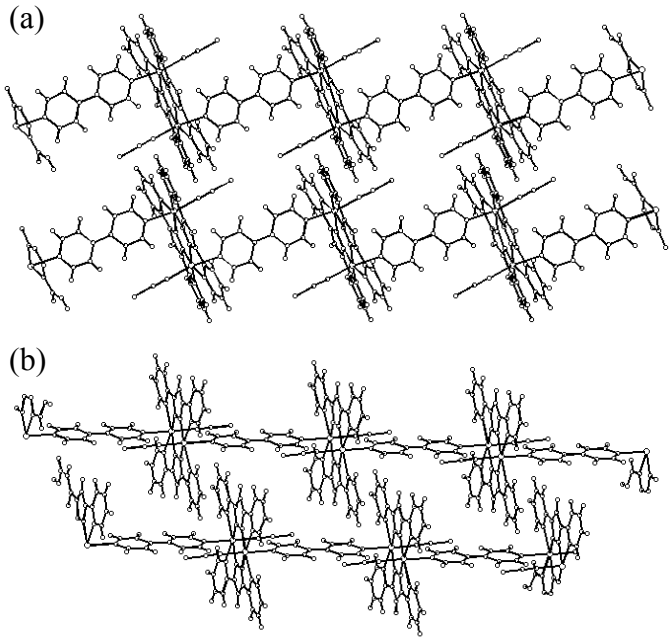

Fig. 5. Perspective views one-dimensional compound **3** representing the π – π stacking interactions between the bpypz$^-$ ligands of the adjacent dimers on the neighbor chains between pyridyl rings (a) and between pyridyl and pyrazole rings (b).

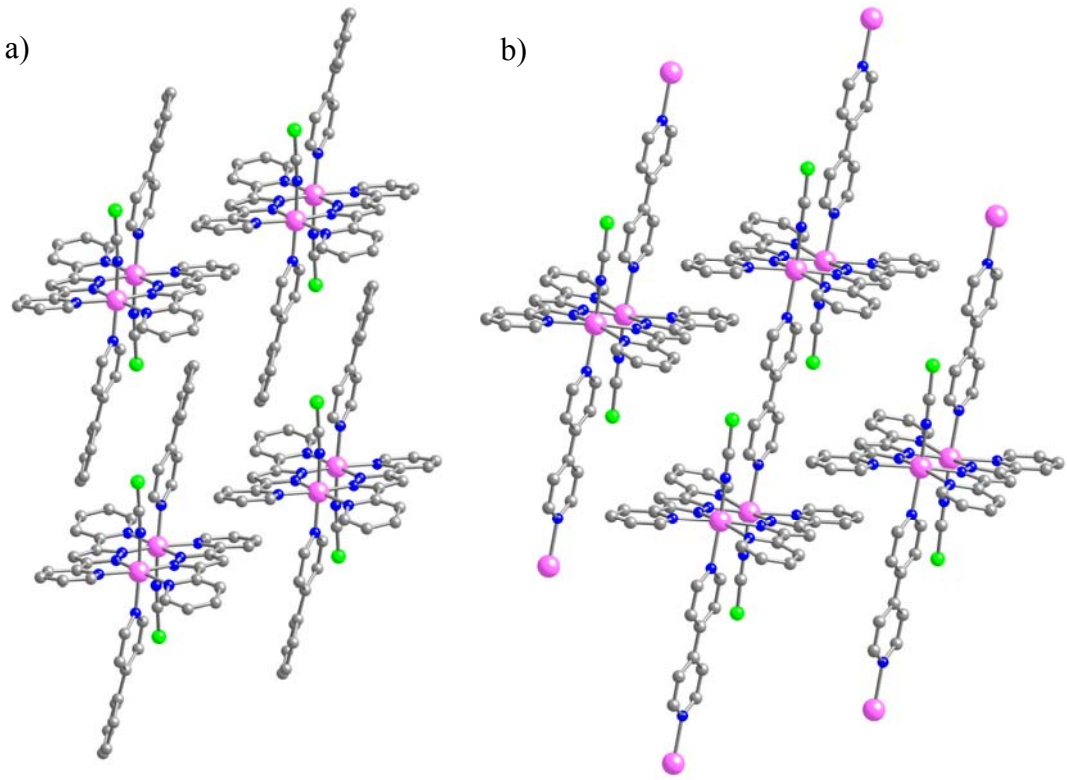

Fig. 6. Molecular structures of dinuclear compound **2** (a) and one-dimensional coordination polymer **3** (b).

Magnetic Properties

The $\chi_M T$ *vs*. T plots of 1 – 4 and [{Fe(NCE)(μ-bpypz)(py)}$_2$] (E = S, BH_3)[20] are given in Figs. 7 and 8. Fig. 9 shows temperature dependence of $\chi_M T$ (circle), Raman spectral intensity (lozenge), and LIESST (triangle) of **3**.

Every compounds show a spin-crossover phenomenon. The temperature dependence of the $\chi_M T$ value of **1** is reversible in both the cooling and warming mode with no hysteresis. The $\chi_M T$ value decreases on lowering the temperature, and then it remains nearly constant at 0.6 emu·K·mol^{-1}, the value of which corresponds to a mixture of low spin and high spin ions, with the molar fractions 0.17 and 0.83, respectively. Below 40 K, the $\chi_M T$ value slightly decreases, reaching a value of 0.2 emu·K·mol^{-1} at 2 K. This decrease in the low temperature range may be attributed to the antiferromagnetic coupling of the residual HS sites.

The variable temperature behavior of **2** of magnetic susceptibility $\chi_M T$ and T shows the overall SCO from the quintet ($\chi_M T$ = *ca*. 3.3 emu·K·mol^{-1}) fully high spin [HS–HS] to the singlet (0.2 – 0.1 emu·K·mol^{-1}) fully low spin [LS–LS] state, associated with the plateau of *ca*. 1.5 emu·K·mol^{-1} at 200 K, showing the approximately to 50 % spin conversion. The differential scanning calorimetry gives two exo- and endothermic peaks, respectively, in the cooling and warming modes. The temperatures at the maxima are fairly close to those estimated from the magnetic susceptibility measurements, supporting the two-step SCO.

Temperature dependence of the magnetic susceptibility of **3** shows the steep spin crossover from the quintet ($\chi_M T$ = 3.50 emu·K·mol^{-1} at 300 K) high spin [HS–HS] state to the singlet low spin (0.15 emu·K·mol^{-1} at 100 K) [LS–LS] state around 162 K. The behavior below the crossover transition arises from the dinuclear units being in the [LS–LS] form, with the non zero $\chi_M T$ 'plateau' originating from a combination of 2nd order Zeeman contributions to the LS Fe(II) susceptibilities plus a small Curie-like contribution from any trapped [HS–HS] form. The magnetic behavior in the heating and cooling modes indicate the occurrence of a small thermal hysteresis ($\Delta T \sim 2$ K). The differential scanning calorimetry gives one exo- (160.4 K) and endothermic (164 K) peaks, in the cooling and heating modes, respectively and thus, the spin-crossover temperature (T_c) is 162.2K, the value of which is higher than those of the related dinuclear complexes, [{Fe(NCS)(μ-bpypz)(X-py)}$_2$].[20,22]

In comparison with NCS^- and $NCBH_3^-$ compound which are structurally isomorphs, T_c is higher than latter compounds. The behavior is also observed in related systems in which the anionic groups have been replaced, most commonly by the cyanohydroborete

ion. The somewhat stronger field of this ligand, relative to that of NCS^-, usually results in a displacement of the transition to higher temperatures.

Mössbauer spectra

Mössbauer spectra of compound **2, 3** and **4** recorded at several temperatures are shown in Figs. 10 and 11, and values of the Mössbauer parameters obtained by least-squares fitting of the spectra are gathered in Table 6.

The Mössbauer spectrum recorded at 200 K for **2** was best fitted as two quadrupole doublets due to coexisting LS sites (δ = 0.480 mm·s^{-1}, ΔE_Q = 0.435 mm·s^{-1}) and HS sites (δ = 1.042 mm·s^{-1}, ΔE_Q = 1.985 mm·s^{-1}). The Mössbauer spectra confirm that the sample consists of a single phase structure exhibiting the two-step SCO, because only two pairs of the doublets corresponding to the HS and LS species are observed at the halfway point of the SCO. Therefore, there is no intermediate magnetic phase, [HS–LS] unlike the cases of $[Fe_2(PMAT)_2](BF_4)_4$·DMF[23] and [{Fe(bpym)-$(NCSe)_2$}$_2$(μ-bpym)].[3] In the case of complex **3** at 79.5 K, a pure low-spin state doublet is presents, with isomer shift values δ = 0.505 mm·s^{-1} and quadrupole splittings ΔE_Q = 0.573 mm·s^{-1}. Interestingly, two distinct quadrupole doublets, the parameters of which coincide with those of two temperature phases mentioned above, are observed at 168 K. At this temperature, two distinct quadrupole doublets are observed. These doublets are typical of the HS and LS contributions. The spectrum at 297 K shows a symmetrical doublet with δ = 1.00 mm·s^{-1} and ΔE_Q = 2.45 mm·s^{-1} values typical of HS Fe(II) centers. These features indicate the spin conversion occurs around 168 K and there is only one phase in each temperature range, that is, the dimer unit exhibits fully [HS–HS] and [LS–LS] states in the high and low temperature ranges, respectively. In the case of complex **4,** at 149.8 K, a pure low-spin state doublet is presents, with isomer shift values δ = 0.509 mm·s^{-1} and quadrupole splittings ΔE_Q = 0.552 mm·s^{-1}. As temperature is increased, a high-spin doublet of weak intensity is visible. At 249.3 K two distinct quadrupole doublets is observed. These doublets are typical of the HS and LS contributions. The spectrum at 297 K shows an asymmetrical doublet with δ = 0.986 mm·s^{-1} and ΔE_Q = 1.57 mm·s^{-1} values typical of HS Fe(II) centers. At the latter temperature, the spin crossover is almost complete. The distribution of HS and LS species found at the measured temperatures is in agreement with the magnetic measurements.

Cooperativity

The cooperativity of the thermal spin transition has been discussed by estimating the thermodynamic parameters by using the regular solution model of the Slichter and Drickamer treatment for solid-state phase transitions and by calculating the C factor for each complex.[24] The C values reported in Table 5. The detailed comparison in spin-crossover behavior between these complexes could be made by the least-squares fitting of the magnetic susceptibility using the regular solution model through Eq. (1).

$$\ln [(1 - \gamma_{HS}) / \gamma_{HS}] = \Delta H_{HL} + \Gamma(1 - 2\gamma_{HS}) / RT - \Delta S_{HL} / R$$
$$= \Delta H_{HL} + \Gamma(1 - 2\gamma_{HS}) / RT - \Delta H_{HL} / T_c / R \qquad (1)$$

where γ_{HS} is the high spin fraction, Γ is an interaction parameter, and ΔH_{HL} and ΔS_{HL} are the enthalpy and entropy changes associated with the spin transitions. The cooperative factor of the spin transition is defined by $C = \Gamma / 2RT_c$. A good simulations of the magnetic susceptibility are achieved with ΔH_{HL} = 7.92 kJ·mol^{-1}, ΔS_{HL} = 48.8 J·K^{-1}·mol^{-1}, and C = 1.06 for the heating mode and ΔH_{HL} = 7.42 kJ·mol^{-1}, ΔS_{HL} = 45.7 J·K^{-1}·mol^{-1}, and C = 1.06 for the cooling mode. The average values of ΔH_{HL} and ΔS_{HL} are in good agreement with those obtained from the DSC measurement (ΔH_{HL} = 7.77 kJ·mol^{-1}, ΔS_{HL} = 47.9 J·K^{-1}·mol^{-1}). Interestingly, C for **3** is larger than those for [{Fe(NCS)(μ-bpypz)(X-py)}$_2$][22] whereas ΔS_{HL} values are similar to each other. Moreover, ΔH_{HL} and T_c of **3** are close to those of **1** while C of **3** is much larger than that of **1** (C = 0.4). These features suggest that the coordination bonding interaction between the dimers in **3** enhances the cooperativity of the spin transition.

Light-Induced Excited Spin-State Trapping (LIESST) effect

Photogeneration of the metastable HS state at low temperatures, the so-called Light-Induced Excited Spin-State Trapping (LIESST) experiment, was carried out on a microcrystalline sample of **3**. The results are displayed in Fig. 9 (triangles). At 4.2 K, the sample was irradiated with green light (530 nm) for 5 h to reach a value of $\chi_M T$ = 0.44 emu·K·mol^{-1}, which is very much lower than the high spin value. However, $\chi_M T$ increases dramatically up to a value of 2.64 emu·K·mol^{-1} then drops rapidly in the temperature region 2 – 44 K as the light irradiation was switched off, and the temperature was increased. The temperature dependence of $\chi_M T$ after the light irradiation is totally different from what is observed in LIESST experiments performed on mononuclear species, and it resembles the magnetic behavior of [{Fe^{II}(NCS)(μ-bpypz)(DMSO)}$_2$].[20] The increase of $\chi_M T$ represents the change in thermal populations of the different microstates arising from a weak iron(II) – iron(II)

antiferromagnetic interaction,[9,14,17] which is expected to occur in the bpypz-bridged $\{Fe(bpypz)\}_2$ dimer unit due to the inefficient exchange ability of the bridging 4,4'-bipyridine.[25,26] This magnetic behavior, therefore, is attributed to the synergy between magnetic interaction and spin transition under light irradiation. At temperatures higher than 45 K, $\chi_M T$ drops rapidly to reach a value close to 0.15 emu·K·mol^{-1} at 65 K (the critical LIESST temperature, determined as the extreme of the derivative $\partial\chi_M T/\partial T$ was found as 54 K), representative the occurrence of a complete HS to LS relaxation at relatively lower temperature range. These features indicate that the rigidity and weak magnetic exchange ability of the bridged 4,4'-bipyridine improve the cooperativity of SCO. To confirm the LIESST phenomenon of **3**, we have also measured Raman spectra as an accessible probe of vibrations that are most affected by the geometric and electronic changes around the metal ion. The LIESST can qualitatively be followed by monitoring a change in intensity of the CN stretching of the SCN^- ligand (observed at 2071 and 2104 cm^{-1} for HS and LS, respectively) by irradiation of the light (632.8 nm) for Raman spectroscopy.[21] At 10 K, the intensity of the HS CN vibration is twenty times bigger than that of the LS signal and the intensity of the signal decreases on heating and reaches zero at 100 K (Fig. 9). This observation of the spin transition from HS to LS demonstrates the LIESST. Moreover, the steep decrease in intensity is a mirror image of the SCO suggestive of the high cooperativity of **3**.

Table 5. Spin-crossover temperature T_c, least-squared fitted thermodynamic parameters (ΔH_{HL} and ΔS_{HL}) and cooperativity factor C

Complex	T_c / K	ΔH_{HL} / kJ·mol^{-1}	ΔS_{HL} / J·K^{-1}·mol^{-1}	C
[{Fe(NCS)(μ-bpypz)(py)}$_2$]	129	5.96	46.6	0.87
1	150	7.18	47.8	0.43
3	158	7.92	48.8	1.06
[{Fe(NCBH$_3$)(μ-bpypz)(py)}$_2$]	207	12.9	62.6	0.46
4	247	10.5	40.2	0.70

Table 6. Temperature dependences of isomer shift (δ) and quadrupole splitting (ΔE_Q) values

Complex	T / K	δ / mm·s^{-1}	ΔE_Q / mm·s^{-1}
2	100	0.485	0.565
	200	0.480, 1.042	0.435, 1.985
	300	0.979	1.701
3	79.5	0.505	0.573
	167.5	0.477, 1.09	0.530, 2.88
	297	1.00	2.45
4	149.8	0.509	0.552
	249.3	0.468, 1.04	0.507, 1.66
	297	0.986	1.57

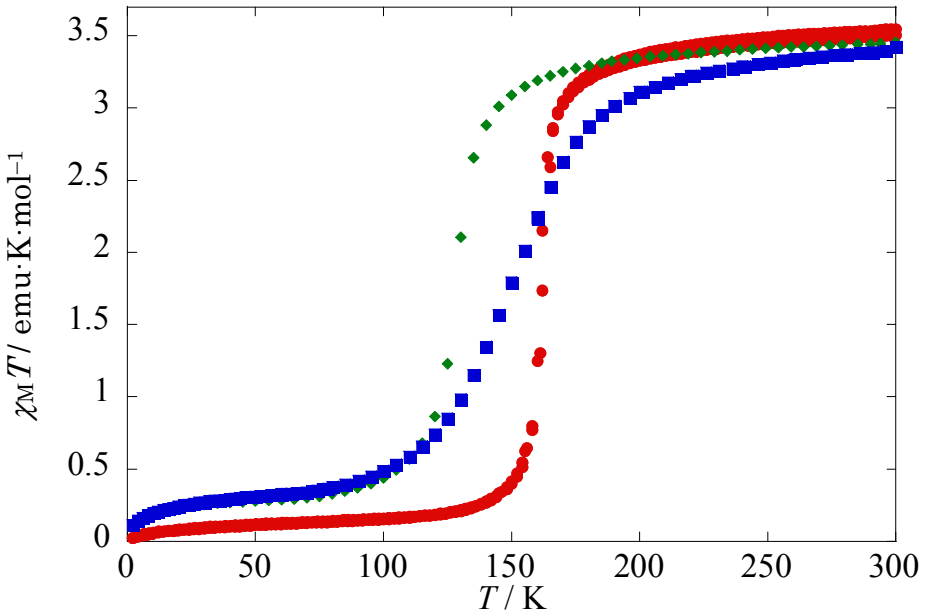

Fig. 7. Temperature dependences of $\chi_M T$ for **1** (■), **3** (●) and [{Fe(NCS)(μ-bpypz)(py)}$_2$][20] (♦) under an applied dc field of 500 Oe.

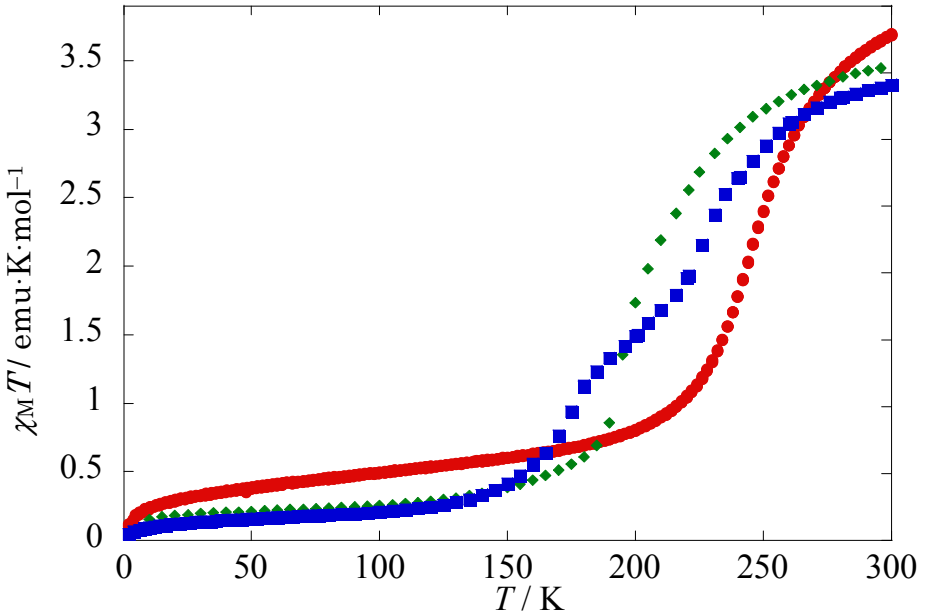

Fig. 8. Temperature dependences of $\chi_M T$ for **2** (■), **4** (●) and [{Fe(NCBH$_3$)(μ-bpypz)(py)}$_2$][20] (♦) under an applied dc field of 500 Oe.

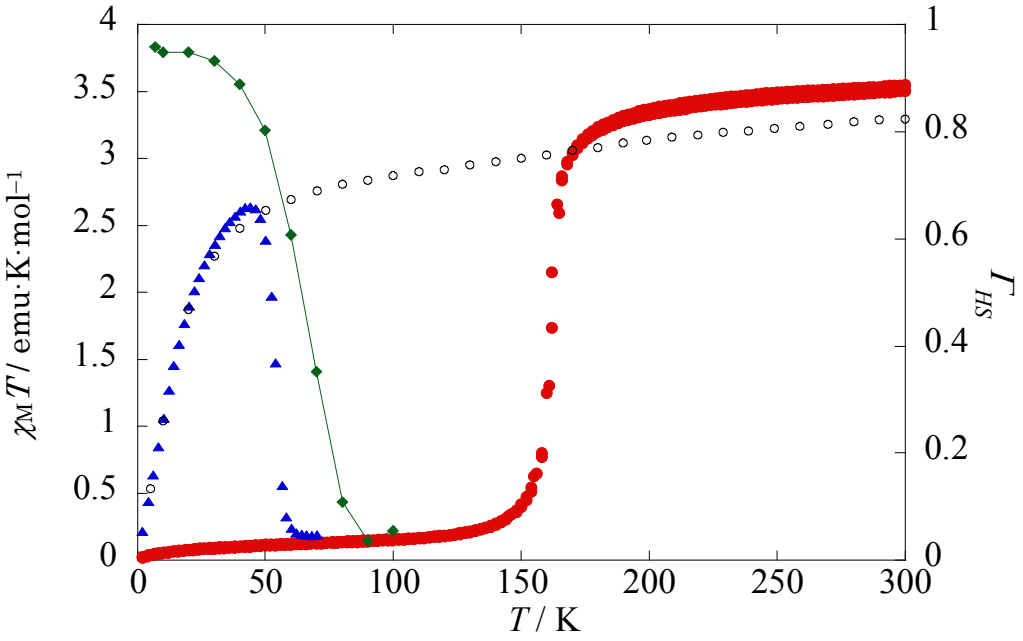

Fig. 9. Temperature dependences of $\chi_M T$ (●), Raman spectral intensity (♦) and LIESST (▲) of **3**. The open circle (○) is temperature dependences of $\chi_M T$ for [{Fe^{II}(NCS)(μ-bpypz)(DMSO)}$_2$].[20]

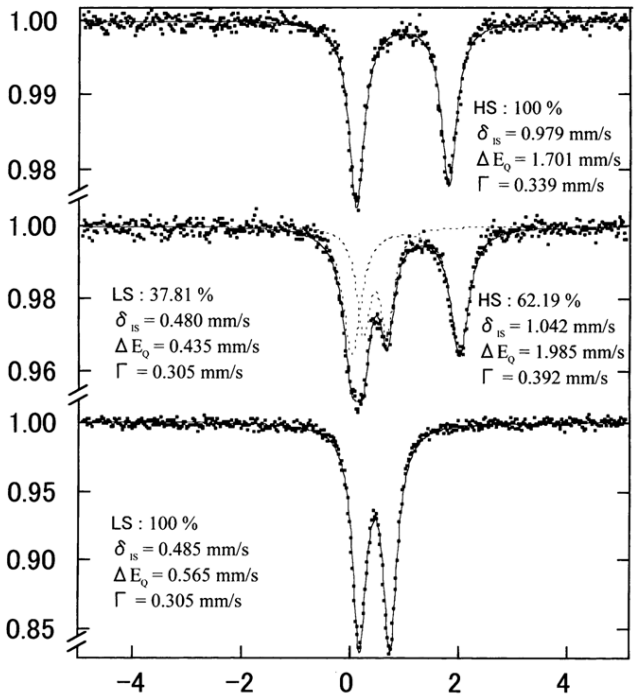

Fig. 10. Representative Mössbauer spectra of the dinuclear complex **2** in the temperature range 300 – 100 K.

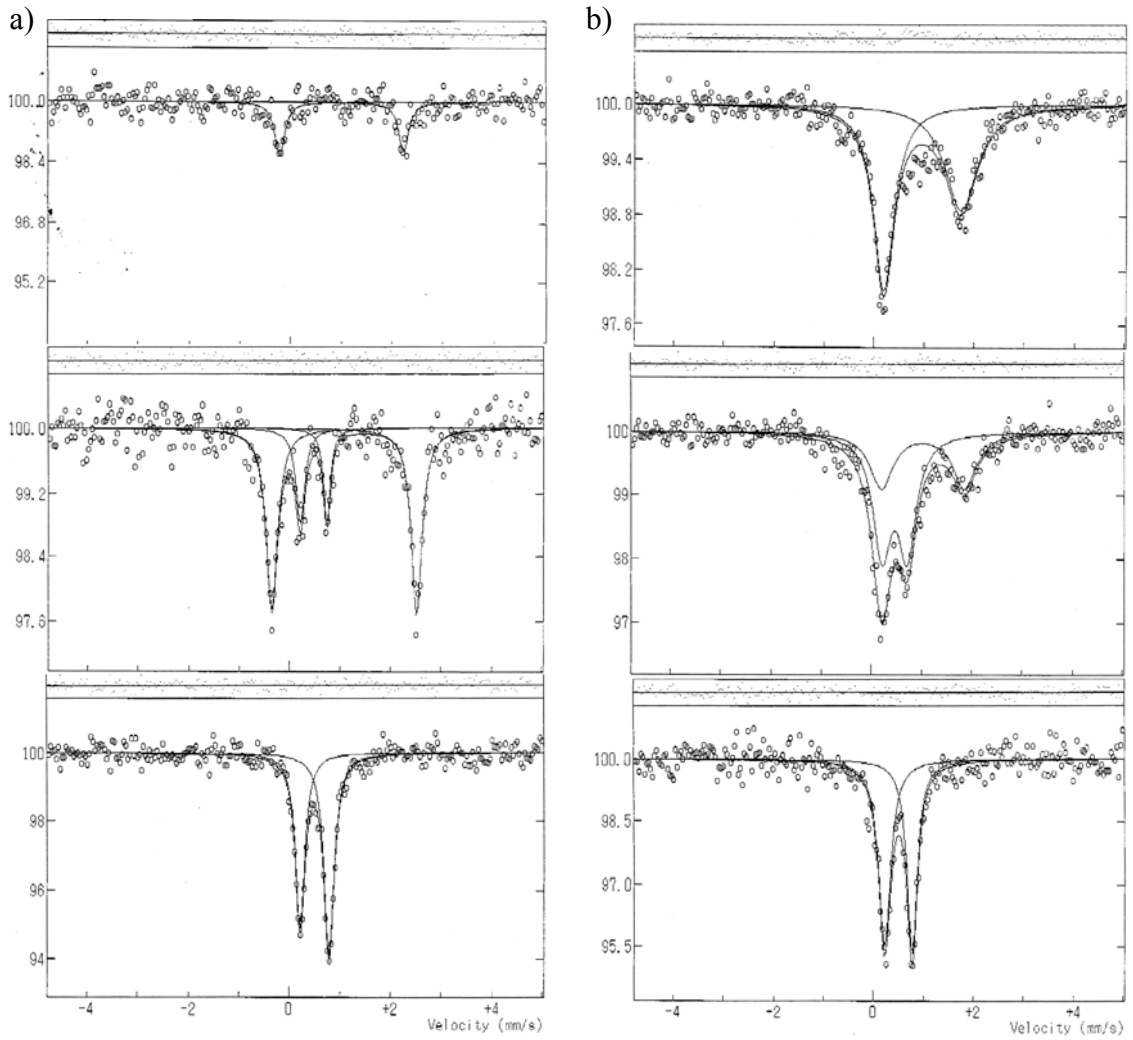

Fig. 11. Representative Mössbauer spectra of the one-dimensional compounds **3** in the temperature range 79.5 – 300 K (a), and **4** in the temperature range 149.8 – 297 K (b).

Conclusion

In conclusion, the two-step SCO of complex **2** is found to proceed through a mixture of [HS–HS] and [LS–LS] at the plateau which behaves like a mononuclear type in contrast to the step-wise two-step SCO through a mixed spin state [HS–LS] for the bpym and phdia complexes. Such a two-step SCO process may result from the difference in intra- and inter-molecular interactions. The intramolecular interactions in complex **2** are characteristic of the rigid bridging site comprising two tetradentate bpypz ligands as compared with the flexible bidentate bridging moiety in the μ-bpym and μ-phdia Fe(II) complexes. As for the intermolecular interactions in complex **2**, there are additional $\pi - \pi$ stackings between the pyridyl and phenyl of the 4-phpy other than those between the bpypz ligands as for the pyridine complex. Since the synergy between the inter- and intra-molecular interactions is considered to be responsible for two-step SCO, the strong intermolecular interactions in complex **2** are likely to favor the like-spin pair ([HS–HS]···[LS–LS]) rather than the mixed spin one ([HS–LS]). The two-step SCO occurrence for the present 4-phpy complex along with the preliminary observation for the corresponding isoquinoline complex could give a clue to deeper understanding of two-step SCO phenomena in dinuclear complexes. The complexes **3** provides the first dinuclear iron(II) complex-based one-dimensional polymer compound in which the spin transition from high- to low-spin states has been followed by crystal structural analyses and in which no step in $\chi_M T$ due to [HS–LS] states is observed. The magnetic transition is sharp, with a hysteresis, indicating effective cooperativity is occurring between the Fe(II) dinuclear units through the bridged bipyridine. Further dinuclear iron(II)-based polynuclear examples of the present and related types are being required.

Experimental

Materials

All chemicals and solvents, obtained from Tokyo Kasei Co., Ltd., and Wako Pure Chemical Industries, Ltd., were reagent grade. They were used without further purification.

trans-[Fe(NCS)$_2$(py)$_4$] and *trans*-[Fe(NCBH$_3$)$_2$(py)$_4$]

The starting complex *trans*-[Fe(NCS)$_2$(py)$_4$] was obtained by a method given in the literature.[21] *trans*-[Fe(NCBH$_3$)$_2$(py)$_4$] was obtained by the analogous method to trans-[Fe(NCS)$_2$(py)$_4$]; to an aqueous solution (125 mL) containing 6.93 g of Fe(NH$_4$)$_2$SO$_4$·6H$_2$O and 10 mg of ascorbic acid was slowly added an aqueous solution (200 mL) containing 1.65 g of NaNCBH$_3$ and pyridine (5 mL) under a nitrogen atmosphere. The pale yellow precipitate obtained was filtered off and washed with 10 mL portions of water-ethanol-pyridine (1 : 17 : 2). After drying in vacuo, a brown powder was obtained.

Though many attempts to crystallize the complexes were made, complex **1** could not be crystallized, though for the complex **2**, **3** and **4** crystals suitable for X-ray analysis were obtained successfully. Single crystals were grown from a layered solution as follows.

[{Fe(NCS)(μ-bpypz)(4-phpy)}$_2$] (1)

Hbpypz (0.074 g, 0.033 mmol) was dissolved in 36 mL of a methanol solution of excess 4-phpy after deprotonating with a 10% methanol solution of tetra-*n*-butylammonium hydroxide (*n*-Bu)$_4$NOH (0.87 g, 0.34 mmol). To this solution was added 15 mL of a methanol solution of *trans*-[Fe(NCS)$_2$(py)$_4$] (0.16 g, 0.33 mmol) under an N_2 stream. A yellow precipitate was obtained and after stirring this reaction mixture for 2 h, the precipitate was filtered off and washed with methanol. The solid was then dried in vacuo.

Yield 71%. Anal. Calc. for $C_{50}H_{36}N_{12}S_2Fe_2$: C, 61.23; H, 3.70; N, 17.14 %. Found: C, 60.10; H, 3.52; N, 16.72%.

[{Fe(NCBH$_3$)(μ-bpypz)(4-phpy)}$_2$] (2)

Complex **2** was prepared by a similar method to the corresponding NCS complex **1**.

Yield 36%. Anal. Calc. for $C_{50}H_{42}N_{12}B_2Fe_2$: C, 63.60; H, 4.48; N, 17.80 %. Found: C, 63.06; H, 4.31; N, 17.28 %.

[{Fe(NCS)(μ-bpypz)}$_2$(μ-4,4'-bpy)]·MeOH (3)

A methanolic solution (2 mL) of *trans*-[Fe(NCS)$_2$(py)$_4$] (3.7 mmol·L^{-1}) was transferred to a glass tube, and then a methanolic solution of 2 mL of Hbpypz (3.7 mmol·L^{-1}) and 4,4'-bpy (1.8 mmol·L^{-1}) with a 10 % methanol solution of tetra-*n*-butylammonium hydroxide (*n*-Bu)$_4$NOH (3.7 mmol·L^{-1}) was poured into the glass tube without mixing the solutions under an N_2 stream. Brown crystals began to form at ambient temperature in 1 month. One of these crystals was used for X-ray crystallography. Physical measurements were conducted on a polycrystalline powder that was synthesized as follows; Hbpypz (0.05 g, 0.22 mmol) was dissolved in 80 mL of a methanol solution of 4,4'-bpy (0.018 g, 0.11 mmol) with a 10% methanol solution of (*n*-Bu)$_4$NOH (0.34 g, 0.22 mmol). To this solution was added 80 mL of a methanol solution of *trans*-[Fe(NCS)$_2$(py)$_4$] (0.11 g, 0.22 mmol) under an N_2 stream. A brown precipitate was obtained and after stirring this reaction mixture for 2 h, the precipitate was filtered off and washed with methanol. The solids were then dried in vacuo.

Yield 80 %. Calcd. (%) for $C_{39}H_{30}N_{12}OS_2Fe_2$: C, 54.56; H, 3.52; N, 19.58. Found (%): C, 54.43; H, 3.27; N, 19.80.

The homogeneity of the powder sample was confirmed by comparison of the observed with that powder diffraction patterns obtained calculated from the single-crystal data.

[{Fe(NCBH$_3$)(μ-bpypz)}$_2$(μ-4,4'-bpy)]·MeOH (4)

Complex **4** was prepared by a similar method to the corresponding NCS complex **3**.

Yield 70 %. Calcd. (%) for $C_{39}H_{36}N_{12}B_2OFe_2$: C, 56.98; H, 4.41; N, 20.45. Found (%): C, 55.60; H, 4.06; N, 20.89.

Crystallographic Data Collection and Refinement of the Structure

Data collection of **2** was carried out at 100, 200, and 296 K by a Rigaku Raxis-rapid imaging plate (IP) system with graphite-monochromated Mo Kα radiation. Data collection of **3** was carried out at 150 and 200 K, by a Rigaku Mercury charge coupled device (CCD) system with graphite-monochromated Mo Kα radiation. Data collection of **4** was carried out at 350 K, by a Rigaku Mercury charge coupled device (CCD) system with graphite-monochromated Mo Kα radiation. Crystallographic data are given in Tables 1 – 4. The structure was solved by a standard direct method (Crystal Clear 1.3.7 crystallographic software package of the Molecular Structure Corp. and Rigaku). Full-matrix least-squares refinements were carried out with anisotropic thermal parameters for all non-hydrogen atoms. All the hydrogen atoms were placed

in the calculated positions and refined using a riding model.

Physical Measurements

Magnetic susceptibility data were recorded over the temperature range from 2 to 350 K in the presence of a magnetic field at 5000 Oe with a SQUID susceptometer (Quantum Design, San Diego, CA). All data were corrected for diamagnetism, which was calculated from Pascal's tables. For the LIESST experiments, a xenon arc lamp was used as the light sources. The interference filtered light of a xenon arc lamp was guided via an optical fiber into the SQUID magnetometer. The sample was placed at the edge of the optical fiber. The measurements were performed on a very thin layer of powdered sample. The weight was estimated by comparing the thermal SCO curve with that for a heavier and accurately weighted sample. X-ray powder diffraction data were collected on a Rigaku MultiFlex diffractometer by using Cu Kα radiation. Calorimetric measurements were performed using a differential scanning calorimeter Seiko Instrument Inc. DSC 220C. The Mössbauer spectra were recorded using a Wissel 1200 spectrometer and a proportional counter. ^{57}Co(Rh) moving in a constant acceleration mode was used as radioactive source. The hyperfine parameters were obtained by least-squares fitting to Lorentzian peaks. The isomer shifts are reported relative to metal Fe foil at 293 K.

References

1. P. Gütlich, Y. Garcia, H. A.Goodwin, *Chem*. *Soc*. *Rev*., **2000**, *29*, 419.
2. O. Kahn, C. J. Martinez, *Science*, **1998**, *279*, 44.
3. J. A. Real, A. B. Gaspar, V. Niel, M. C. Muñoz, *Coord*. *Chem*. *Rev*., **2003**, *236*, 121.
4. G. J. Halder, C. J.Kepert, B. Moubaraki, K. S. Murray, J. D. Cashion, *Science*, **2002**, *298*, 1762.
5. D. Chernyshov, M. Hostettler, K.W. Törnroos, H. -B. Bürgi, *Angew*. *Chem*., *Int*. *Ed*., **2003**, *42*, 3825.
6. H. Toflund, in *Magnetism*: *A Function*, ed. O. Kahn, Kluwer Academic, The Netherlands, **1996**, 323.
7. R. Boca, *Theoretical Foundations of Molecular Magnetism*, Elsevier, Amsterdam, **1999**.
8. J. A. Real, J. Zaremhowitch, O. Kahn, X. Solans, *Inorg*. *Chem*., **1987**, *26*, 2939.
9. G. Chastanet, A. B. Gaspar, J. A. Real, J. -F. Létard, *Chem*. *Commun*., **2001**, 819.
10. E. Andrés, G. De Munno, M. Julve, J. A. Real, F. Lloret, *J*. *Chem*. *Soc*., *Dalton Trans*., **1993**, 2169.
11. G. DeMunno, M. Julve, J. A. Real, F.Lloret, *Inorg*. *Chim*. *Acta*, **1996**, *250*, 81.
12. J. A. Real, H. Bolvin, A. Bousseksou, A. Dworkin, O. Kahn, F. Varret, J. Zarembowitch, *J*. *Am*. *Chem*. *Soc*., **1992**, *114*, 4650.
13. J. A. Real, I. Castro, A. Boussenksou, M. Verdaguer, R. Burriel, M. Castro, J. Linares, F. Varret, *Inorg*. *Chem*., **1997**, *36*, 455.
14. J. -F. Létard, J. A. Real, N. Moliner, A. B. Gasper, L. Capes, O. Cador, O. Kahn, *J*. *Am*. *Chem*. *Soc*., **1999**, *121*, 10630.
15. V. Ksenofontov, H. Spiering, S. Reiman, Y. Garcia, A. B. Gaspar, N. Moliner, J.A. Real, P. Gütlich, *Chem*. *Phys*. *Lett*., **2001**, *348*, 381.
16. V. Ksenofontov, A. B. Gaspar, J. A. Real, P. Gütlich, *J*. *Phys*. *Chem*. *B*, **2001**, *105*, 12266.
17. B. Gaspar, V. Ksenofontov, J. A. Real, P. Gütlich, *Chem*. *Phys*. *Lett*., **2003**, *373*, 385.
18. V. Ksenofontov, A. B. Gaspar, V. Niel, S. Reimen, J. A. Real, P. Gütlich, *Chem*.*-Eur*. *J*., **2004**, *10*, 1291.
19. B. A. Leita, B. Moubaraki, K. S. Murray, J. P. Smith, J. D. Cashion, *Chem*. *Commun*., **2004**, 156.
20. K. Nakano, N. Suemura, S. Kawata, A. Fuyuhiro, T. Yagi, S. Nasu, S. Morimoto, S. Kaizaki, *Dalton Trans*., **2004**, 982.

21. N. Suemura, M. Ohama, S. Kaizaki, *Chem*. *Commun*., **2001**, 1538.
22. K. Nakano, N. Suemura, K. Yoneda, S. Kawata, S. Kaizaki, *Dalton Trans.*, **2005**, 740.
23. M. H. Klingele, B. Moubaraki, J. D. Cashion, K. S. Murray, S. Brooker, *Chem. Commun.*, **2005**, 987.
24. O. Kahn, *Molecular Magnetism*, VCH, New York, **1993**.
25. N. Moliner, M. C. Muñoz, S. Létard, L. Salmon, J. -P. Tuchagues, A. Bousseksou, J. A. Real, *Inorg. Chem.*, **2002**, *41*, 6997.
26. P. Jensen, S. R. Batten, B. Moubaraki, K. S. Murray, *J. Chem. Soc., Dalton Trans*., **2002**, 3712.

Chapter 4

Reversible Water-Induced Magnetic and Structural Conversion of a Flexible Microporous Ni(II)Fe(III) Ferromagnet

Abstract

A cyanide-bridged bimetallic ferromagnet, $[Ni(dipn)]_2[Ni(dipn)(H_2O)][Fe(CN)_6]_2 \cdot 11H_2O$ (dipn = *N*,*N*-di(3-aminopropyl)amine) was prepared using $[Fe(CN)_6]^{3-}$ building unit and dipn coligand. The compound formed a 3-D microporous framework, and exhibited a ferromagnetic ordering based on the strict orthogonality of magnetic orbitals of Ni^{II} and low-spin Fe^{III} at 8.5 K. The crystalline compound was changed to amorphous by dehydration, and the crystallinity was recovered by rehydration. The reversible gaseous water-induced crystal-to-amorphous-like phase transformation accompanied a ferromagnet/paramagnet conversion.

Introduction

Flexible and dynamic porous coordination polymers attract much attention as promising functional materials compared with robust polymers.[1–9] They are regarded as being structurally bistable frameworks, and expected to show not only structural changes but also modulation of their physical properties to achieve multiple functions.[10–26] As for magnetic properties, several magnetic coordination polymers providing an open framework have succeeded in exhibiting reversible guest-induced magnetic conversions by transformation of 0-D,[18] 1-D[17] and 2-D[16] frameworks or changes of local coordination environments.[15] Their characterization has been mainly focused on their responses to guest molecules; however, their gas-adsorption abilities have been scarcely evaluated yet. As a next target, we focused on the inherent structural flexibility of 3-D porous magnets, which are expected to show remarkable magnetic and structural conversions in response to gas adsorption/desorption. Such flexibility and porosity are not features inherent in general magnets. These so-called "flexible porous magnets" will exhibit selective accommodation or separation of guest molecules complying with their sizes and shapes, and also specific orientation, alignment and reaction of the guest molecules in the pores under a strong spontaneous internal magnetic field.

On the other hand, the practical synthesis of porous magnets remains a current issue, because structural demands for high spin density to achieve long-range magnetic ordering conflict with those for porosity.[15–26] One of the rational strategies for porous magnets is based on a framework providing paramagnetic centers located in the sides and corners of the inner pore, where the side and the corner correspond to a connector and a linker for the framework, respectively.[16] From this viewpoint, the hexacyanometallate anion, $[M(CN)_6]^{n-}$, is a suitable linker, because it gives a relatively long side (*ca.* 10 Å) for the inner pore and forms monodentate cyano bridges for effective magnetic interaction[27] and structural flexibility. Here, we prepared a 3-D porous ferromagnet, $[Ni(dipn)]_2[Ni(dipn)(H_2O)][Fe(CN)_6]_2\cdot 11H_2O$ (**1A**)[28] (dipn = *N*,*N*-di(3-aminopropyl)amine), which shows significant magnetic conversion associated with a reversible gaseous water-induced crystal-to-amorphous-like phase transformation.

Results and Discussions

Crystal structure

The asymmetric unit of **1A** consists of one $[Fe(CN)_6]^{3-}$ anion, one $[Ni(1)(dipn)]^{2+}$ and one half $[Ni(2)(dipn)(H_2O)]^{2+}$ cations and 11 water molecules (Fig. 1). Three equatorial cyano nitrogen atoms of $[Fe(CN)_6]^{3-}$ (N(1), N(3) and N(6)) coordinate to three adjacent $[Ni(1)(dipn)]^{2+}$ cations, and one axial cyano nitrogen atom (N(2)) coordinates to the axial position of the adjacent $[Ni(2)(dipn)(H_2O)]^{2+}$ cation. In the lattice, the Fe – CN – Ni(1) linkages form a 2-D sheet expanding on the *bc* plane (Figure S2) and the Fe – CN(2) – Ni(2) linkages connect the 2-D sheets along the *a* axis and construct a 3-D porous framework (Fig. 2). The coordinated water in the equatorial position of Ni(2) faces the pore and is incorporated in the inner wall. Only one lattice water that forms bidirectional hydrogen bonds with cyano nitrogen atoms N(4)* and N(5), has a clearly determined position (O(2)···N(4)* = 2.890 Å, O(2)···N(5) = 3.007 Å, *: symmetry operation $(1/2 - x, -1/2 + y, 1 - z)$). The other lattice water molecules reside in a disorderly manner in the pore. Rectangular channels are constructed along the [001] direction with estimated gate size of 3.5×4.3 Å^2 with the coordinated water or 3.5×8.7 Å^2 without water. The solvent-accessible void in the framework is estimated to be 29.0 % by PLATON[29] in the absence of all water molecules.

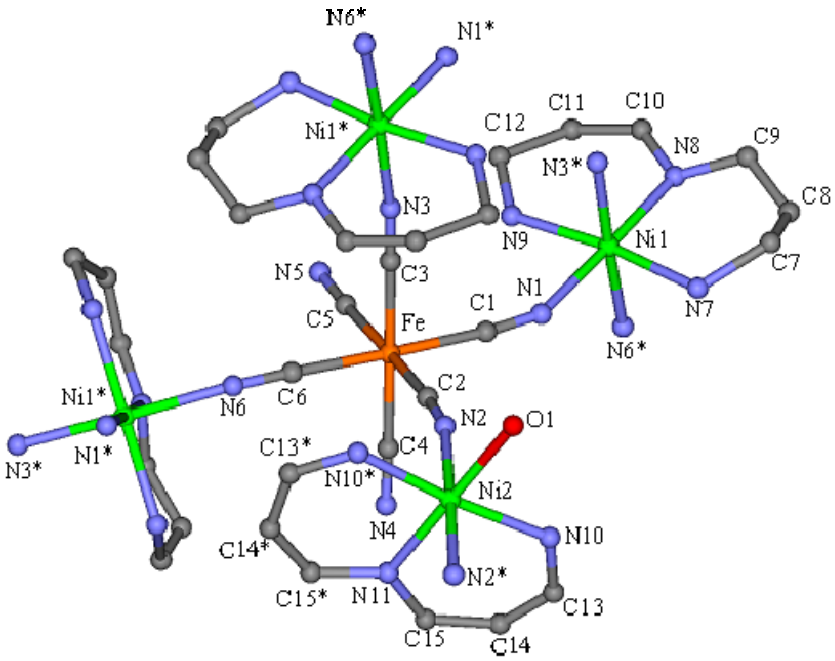

Fig. 1. Asymmetric unit of $[Ni(dipn)]_2[Ni(dipn)(H_2O)][Fe(CN)_6]_2 \cdot 11H_2O$ (**1A**) with the atom numbering scheme (lattice water molecules are omitted). Atoms: Ni (green), Fe (orange), N (blue), C (gray), O (red).

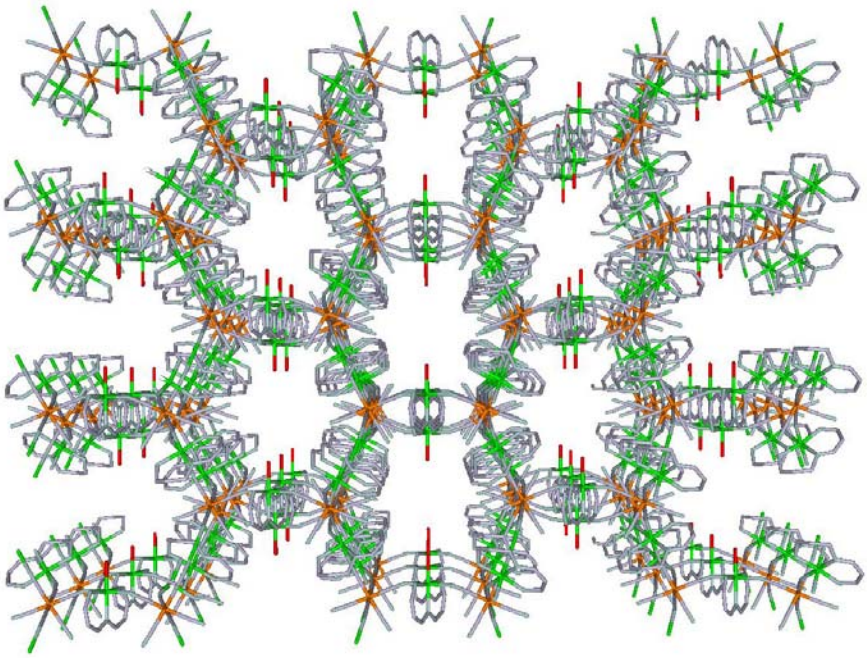

Fig. 2. 1D channel structure of **1A** along the *c* axis. Lattice water molecules are omitted. Atoms: Ni (green), Fe (orange), O (red).

Water adsorption/desorption

TG-DTA results of **1A** indicated that all the water molecules were removed by 423 K and the framework decomposed above 453 K (Fig. 3). Under vacuum at 298 K, **1A** lost 10 water molecules per formula unit, converting to **1B** (Fig. 4). Two residual water molecules of **1B** can be assigned to coordinated and hydrogen-bonded ones by structural and TG-DTA results.

The dehydrated form, $[Ni(dipn)]_2[Ni(dipn)(H_2O)][Fe(CN)_6]_2 \cdot H_2O$ (**1B**), and anhydrous form, $[Ni(dipn)]_3[Fe(CN)_6]_2$ (**1C**), were prepared in vacuum at 298 K and 373 K, respectively. Compounds **1A** and **1B** showed two sharp ν_{CN} bands at 2142 and 2120 cm^{-1}, indicating the existence of bridging and terminal cyano groups in the lattice, whereas, ν_{CN} stretching of **1C** gave a broad band around 2050 cm^{-1}, reflecting a disorder of the cyano bridges by dehydration.

A temperature-dependent XRPD investigation under N_2 of **1A** showed that the crystallinity was immediately lost above 313 K, which suggests that the arrangement of the framework was disordered by dehydration (Fig. 5). Both the dehydrated form **1B** and the anhydrous form **1C** gave amorphous-like XRPD patterns. Remarkably, the amorphous-like **1B** recovered its crystallinity smoothly on being exposed to gaseous water (100% relative humidity, Fig. 6). The rehydrated form was denoted as **1B'**. TGA results indicated that **1B'** contains 12 water molecules per formula unit, the same as **1A** (Fig. 7). On the other hand, **1C** did not recover its crystallinity on being exposed to gaseous water or immersed in water, which suggests the residual lattice water forming bidirectional hydrogen bonds with cyano groups and the coordinated water of Ni(2) play a significant role in the structural recovery. The adsorption isotherms of water on **1B** were measured at 298 K (Fig. 8). Compound **1B** gradually adsorbed water as the relative pressure increased and showed a high uptake of 236 ml/g (9.93 mol/mol) at 21.5 mmHg, indicating that the amorphous-like form **1B** can adsorb water and reconstruct the initial framework without undergoing the dissolution and reprecipitation processes that are often discussed with solution-mediated structural transformations.[5]

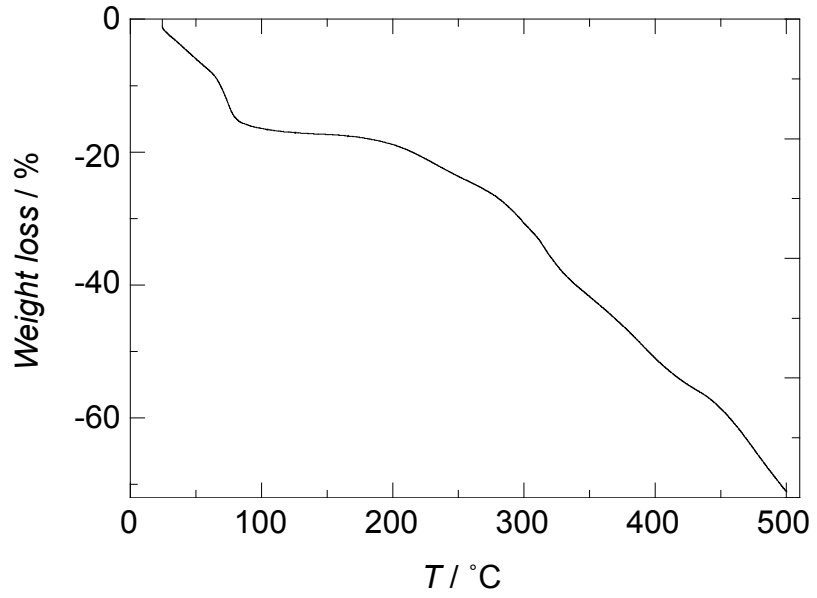

Fig. 3. Thermogravimetric analysis (TGA) under N_2 of $[Ni(dipn)]_2[Ni(dipn)(H_2O)][Fe(CN)_6]_2 \cdot 11H_2O$ (**1A**). The weight loss of 17.4 % until 150 ˚C agrees with the calculated value of 17.8 % for twelve water molecules per formula unit. The framework began to decompose at 180 ˚C.

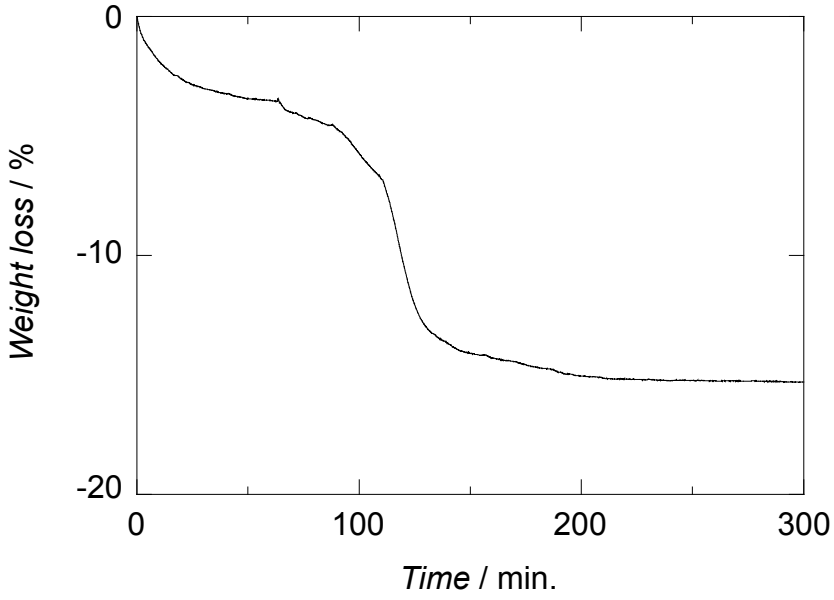

Fig. 4. Time-dependent TGA traces of **1A** under vacuum at R.T. The weight loss of 15.2 % agrees with the calculated value of 14.9 % for ten water molecules per formula unit. **1A** liberated 10 lattice water molecules per formula unit at R.T., converting to dehydrated form $[Ni(dipn)]_2[Ni(dipn)(H_2O)][Fe(CN)_6]_2 \cdot H_2O$ (**1B**).

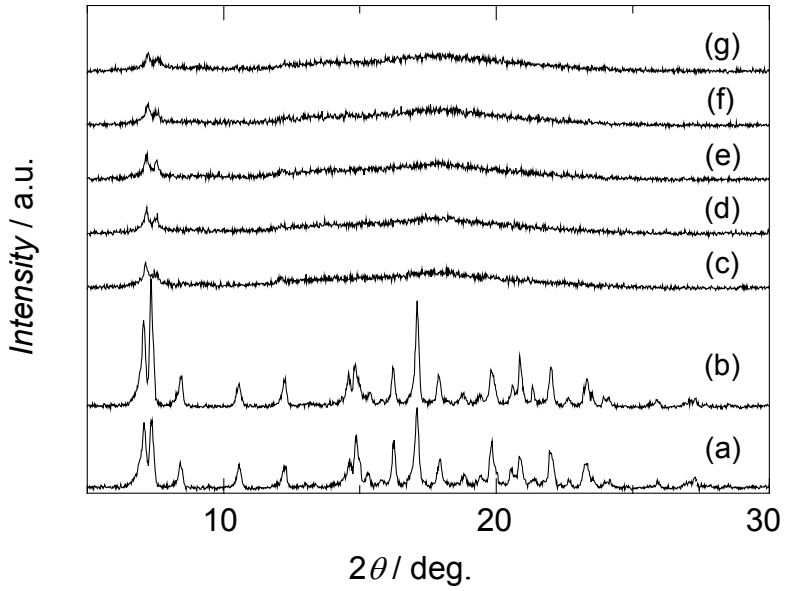

Fig. 5. Temperature dependences of XRPD patterns of **1A** under N_2 at (a) R.T.; (b) 30 ˚C; (c) 40 ˚C; (d) 50 ˚C; (e) 60 ˚C; (f) 80 ˚C; (g) 100 ˚C (anhydrous form **1C**). The crystallinity was drastically lost above 40 ˚C by releasing of the lattice water molecules.

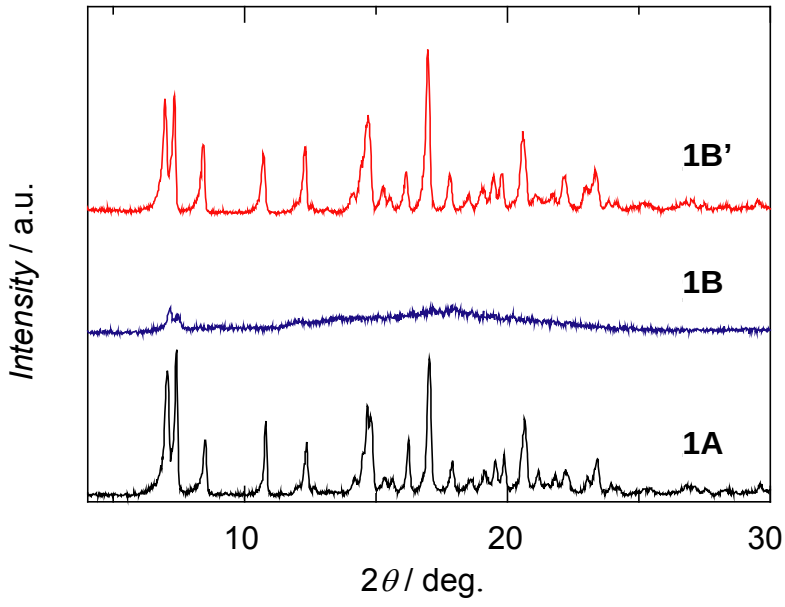

Fig. 6. The XRPD patterns of the original form **1A**, the dehydrated form **1B** and the rehydrated form **1B'**.

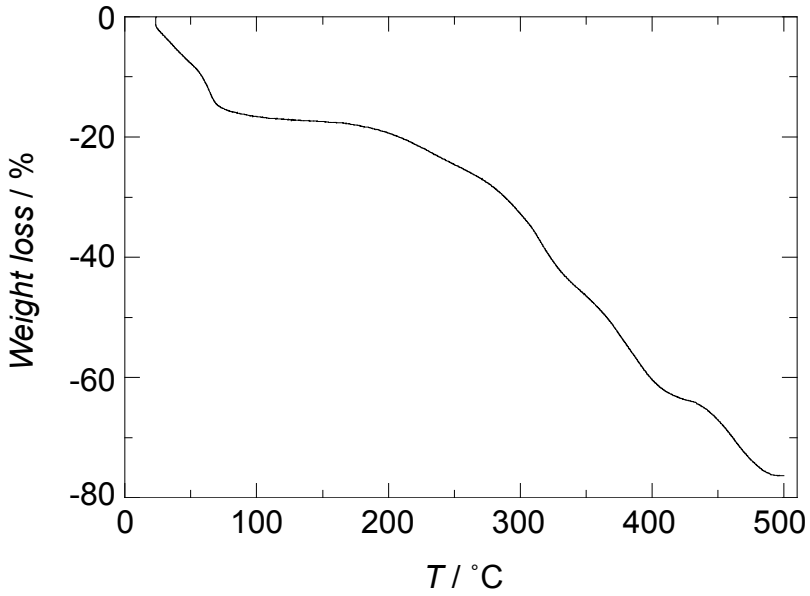

Fig. 7. TGA traces of the rehydrated form **1B'**, $[Ni(dipn)]_2[Ni(dipn)(H_2O)][Fe(CN)_6]_2 \cdot 11H_2O$. The weight loss of 17.4 % until 150 ˚C agrees with the calculated value of 17.8 % for twelve water molecules per formula unit.

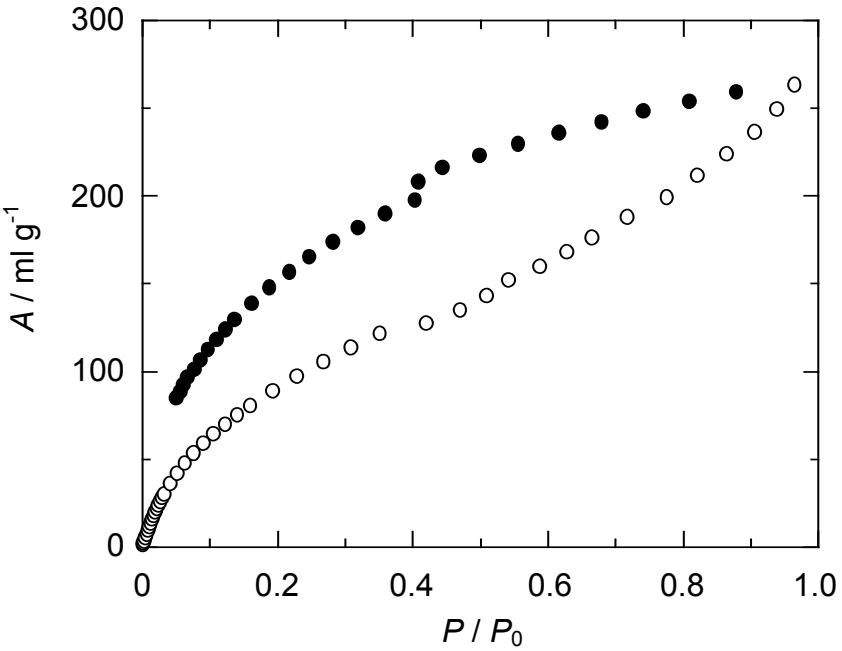

Fig. 8. Water sorption isotherms for **1B** at 298 K. Adsorption and desorption are indicated by open and filled circles, respectively. The ratio of gas pressure to saturation pressure, P/P_0, was obtained with $P_0 = 23.75$ mmHg.

Magnetic properties

χ_M *vs.* T plots of **1A**, **1B**, **1C** and **1B'** are shown in Fig. 9. The measurements were made in the temperature range 2 – 50 K because **1A** readily effloresces in a helium atmosphere (under low relative humidity). The χ_M value of **1A** gradually increased upon cooling to 20 K and rapidly increased below 10 K, up to a maximum value of 35.49 emu·mol^{-1} (23.83 μ_B) at 2.0 K. This behavior suggests the operation of a ferromagnetic interaction between the adjacent Ni^{II} and low-spin Fe^{III} ions through cyano bridges because of the strict orthogonality of the magnetic orbitals. A long-range ferromagnetic ordering (T_c = 8.5 K) was confirmed by a dM/dT plot, weak-field magnetization measurements, temperature dependences of ac susceptibility and magnetic hysteresis loop (H_c = 350 Oe) (Figs. 10 – 12). For the dehydrated form **1B**, the curve showed a quite different shape with a small maximum (12.44 emu mol^{-1}) at 3.0 K. The χ_M' *vs.* T plots of **1B** showed two broad peaks around 6.0 and 3.5 K. The magnetic hysteresis loop of **1B** showed an almost paramagnetic behavior with H_c = 50 Oe. These results indicate that the ferromagnetic interaction is weakened and the magnetic domain is moderately fragmented while keeping short-range order by dehydration in **1B**. The dc and ac magnetic results of **1B'** completely reproduced those of the original form **1A**. The magnetic hysteresis loop of **1B'** showed a similar shape to **1A** with larger remnant magnetization, which suggests larger magnetic domains are generated by rehydration. The dehydrated form **1B** and the rehydrated form **1B'** demonstrate that a complete regeneration of the long-range ferromagnetic ordering accompanied the structural recovery. The anhydrous form **1C** did not show ferromagnetic ordering because of the disorder of the bridging structure.

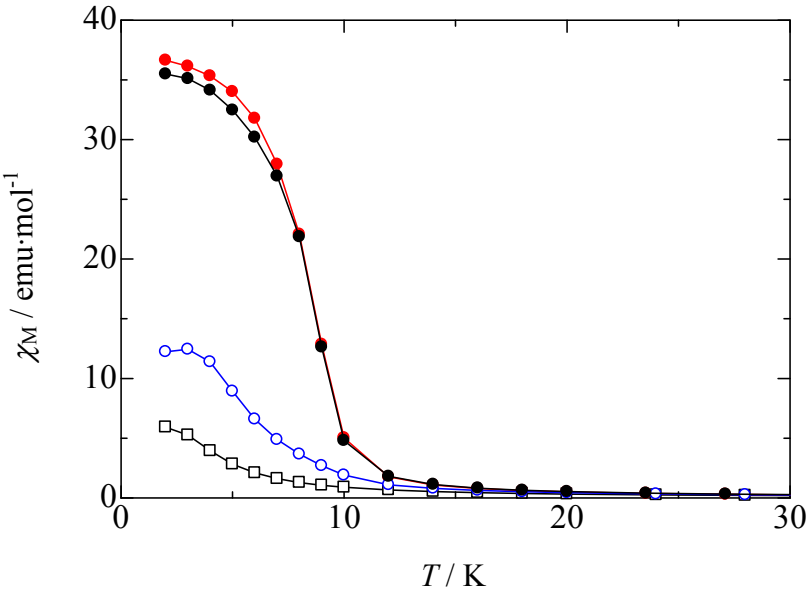

Fig. 9. Temperature dependences of χ_M in an applied dc field of 500 Oe for **1A** (●), **1B** (○), **1B'** (●) and **1C** (□).

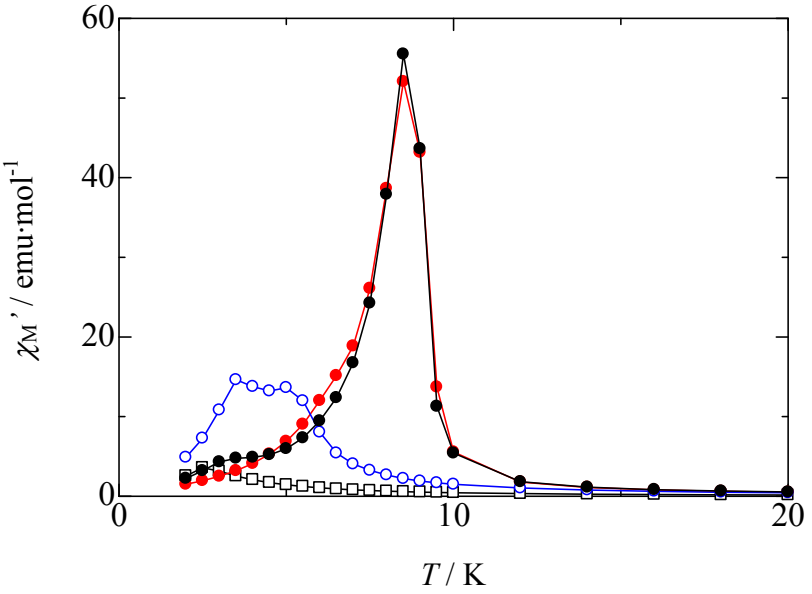

Fig. 10. Temperature dependences of the in-phase ac magnetization, χ_M', in an applied dc field of 3 Oe oscillating at 100 Hz for **1A** (●), **1B** (○), **1B'** (●) and **1C** (□).

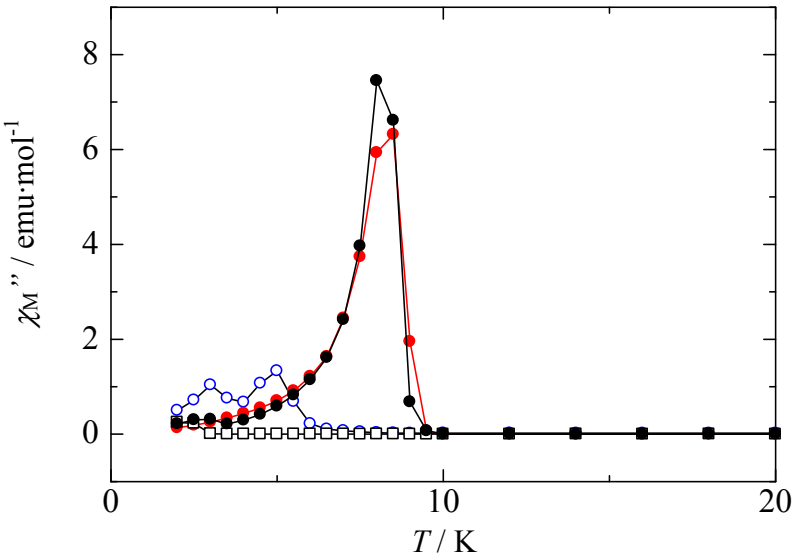

Fig. 11. Temperature dependences of the out-of-phase ac magnetization, χ_M'', in an applied dc field of 3 Oe oscillating at 100 Hz for **1A** (●), **1B** (○), **1B'** (●) and **1C** (□).

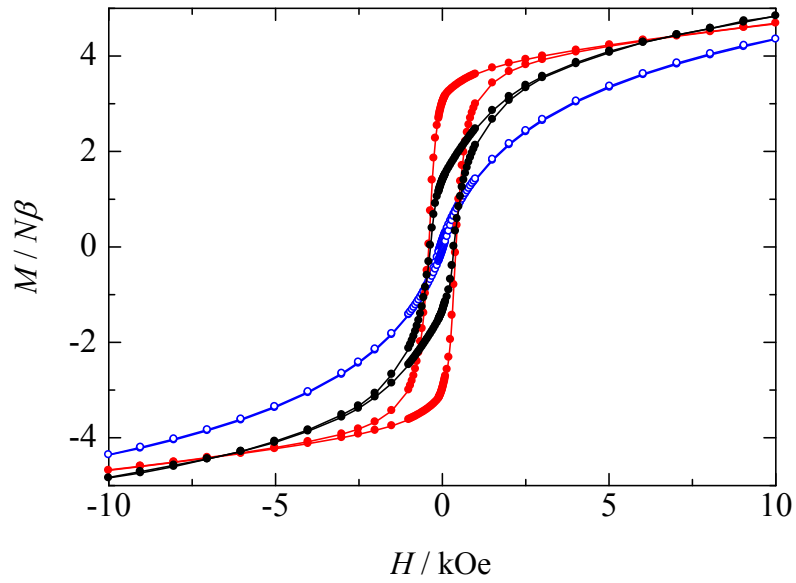

Fig. 12. Magnetic hysteresis loops for **1A** (●), **1B** (○) and **1B'** (●) at 2 K.

Conclusion

The 3-D porous ferromagnet, $[Ni(dipn)]_2[Ni(dipn)(H_2O)][Fe(CN)_6]_2 \cdot 11H_2O$, demonstrated a remarkable magnetic change between ferromagnet and paramagnet associated with the reversible crystal-to-amorphous-like phase transformation in response to water desorption/adsorption. These results prove that the synthetic strategy based on cyanide-bridged bimetallic assemblies is advantageous for the formation of flexible microporous magnets providing interlocked guest-induced magnetic and structural conversion. The dehydrated form **1B** also adsorbs other guests, such as methanol, so further work will focus on magnetic conversion by organic guests or paramagnetic gases such as O_2 or NO.

Experimental

Materials

All chemicals and solvents, obtained from Tokyo Kasei Co., Ltd., and Wako Pure Chemical Industries, Ltd., were reagent grade. They were used without further purification.

Synthesis of $[Ni(dipn)]_2[Ni(dipn)(H_2O)][Fe(CN)_6]_2 \cdot 11H_2O$ (1A)

To a solution of $NiCl_2 \cdot 6H_2O$ (71 mg, 0.3 mmol) in DMF-water (1:1 in volume, 10 ml) was successively added dipn (39 mg, 0.3 mmol) and an aqueous solution of $K_3[Fe(CN)_6]$ (66 mg, 0.2 mmol). The resulting brown mixture was allowed to stand to form dark brown crystals **1A**. They were collected by suction filtration, washed with water and dried in the air.

Yield: 58 %. Elemental analysis (%) for **1A**. Anal. Found: C, 30.18; H, 5.72; N, 23.93 %. Calcd. for $C_{30}H_{75}N_{21}Fe_2Ni_3O_{12}$: C, 29.78; H, 6.25; N, 24.31.

Caution; Cyanide-containing compounds are potentially toxic and should only be handled in small quantities.

The dehydrated form, $[Ni(dipn)]_2[Ni(dipn)(H_2O)][Fe(CN)_6]_2 \cdot H_2O$ (**1B**), and anhydrous form, $[Ni(dipn)]_3[Fe(CN)_6]_2$ (**1C**), were prepared in vacuum at 298 K and 373 K, respectively.

Crystallographic Data Collection and Refinement of the Structure

All measurements were carried out at 243 K on a Rigaku Mercury CCD system with graphite-monochromated Mo-Kα radiation (λ = 0.71070 Å). The structure was solved by direct methods (SIR 97) and followed successive Fourier and difference Fourier syntheses and refined by full-matrix least squares on F^2. All nonhydrogen atoms except for disordered lattice water oxygen atoms were refined anisotropically. All hydrogen atoms were added geometrically and refined by using a riding model. All calculations were performed using the SHELX 97[30] program.

Physical Measurements

Magnetic susceptibilities of polycrystalline **1A, 1B, 1C**, and **1B'** were measured on a Quantum Design MPMS-XL5R SQUID susceptometer in the temperature range of 1.8 – 300 K with an applied field of 500 Oe. Samples were put into a gelatin capsule, mounted inside straw, and then fixed to the end of the sample transport rod.

Diamagnetic correction was made with the Pascal's constants. Infrared spectra (4000 – 400 cm^{-1}) were taken using a Perkin-Elmer system 2000 Ft-IR, where KBr was used as the dispersal medium. Thermogravimetric analyses were recorded on a Rigaku Thermo plus TG 8120 apparatus in the temperature range between 30 and 500 °C under a nitrogen atmosphere at a heating rate of 5 °C min^{-1}. The adsorption/desorption isotherms for H_2O at 298 K were measured with BELSORP-18 volumetric adsorption equipment from BEL Japan, Inc. The dehydrated sample $[Ni(dipn)]_2[Ni(dipn)(H_2O)]$-$[Fe(CN)_6]_2 \cdot H_2O$ (**1B**) was obtained by treatment under reduced pressure (< 10^{-2} Pa) at 298 K.

References

1. K. Yamada, H. Tanaka, S. Yagishita, K. Adachi, T. Uemura, S. Kitagawa, S. Kawata, *Inorg. Chem.*, **2006**, *45*, 4322.
2. S. Kitagawa, K. Uemura, *Chem. Soc. Rev.*, **2005**, *34*, 109.
3. S. Bourrelly, P. L. Llewellyn, C. Serre, F. Millange, T. Loiseau, G. Férey, *J. Am. Chem. Soc.*, **2005**, *127*, 13519.
4. S. Kitagawa, R. Kitaura, S.-i. Noro, *Angew. Chem., Int. Ed.,* **2004**, *43*, 2334.
5. M. J. Rosseinsky, *Microporous Mesoporous Mater.*, **2004**, *73*, 15.
6. J. L. C. Rowsell, O. M. Yaghi, *Microporous Mesoporous Mater.*, **2004**, *73*, 3.
7. D. N. Dybtsev, H. Chun K., Kim, *Angew. Chem., Int. Ed.*, **2004**, *43*, 5033.
8. K. Biradha, Y. Hongo, M. Fujita, *Angew. Chem., Int. Ed.,* **2002**, *41*, 3395.
9. K. S. Min, M. P. Suh, *Chem.-Eur. J.,* **2001**, *7*, 303.
10. C. J. Kepert, *Chem. Commun.*, **2006**, 695.
11. H. -B. Cui, K. Takahashi, Y. Okano, H. Kobayashi, Z. Wang, A. Kobayashi, *Angew. Chem., Int. Ed.,* **2005**, *44*, 6508.
12. A. L. Goodwin, K. W. Chapman, C. J. Kepert, *J. Am. Chem. Soc.*, **2005**, *127*, 17980.
13. V. Niel, A. L. Thompson, M. C. Muñoz, A. Galet, A. S. E. Goeta, J. A. Real, *Angew. Chem., Int. Ed.*, **2003**, *42*, 3760.
14. G. J. Halder, C. J. Kepert, B. Moubaraki, K. S. Murray, J. D. Cashion, *Science,* **2002**, *298*, 1762.
15. S. Ohkoshi, K. Arai, Y. Sato, K. Hashimoto, *Nature Mat.,* **2004**, *3*, 857.
16. D. Maspoch, D. Ruiz-Molina, K. Wurst, N. Domingo, M. Cavallini, F. Biscarini, J. Tejada, C. Rovira, J. Veciana, *Nat. Mater.,* **2003**, *2*, 190.
17. N. Usuki, M. Ohba, H. Ōkawa, *Bull. Chem. Soc. Jpn.,* **2002**, *75*, 1693.
18. H. Miyasaka, H. Ieda, N. Matsumoto, N. Re, R. Crescenzi, C. Floriani, *Inorg. Chem.*, **1998**, *37*, 255.
19. M. Kurmoo, H.Kumagai, K. W. Chapman, C. J. Kepert, *Chem. Commun.,* **2005**, 3012.
20. D. Maspoch, D. Ruiz-Molina, J. Veciana, *J. Mater. Chem.,* **2004**, *14*, 2713.
21. Z. Wang, B. Zhang, B. Fujiwara, H. Kobayashi, M. Kurmoo, *Chem. Commun.,* **2004**, 416.
22. N. Guillou, C. Livage, M. Drillon, G. Férey, *Angew. Chem., Int. Ed.,* **2003**, *42*, 5314.
23. Y. -Q. Tian, C. -X. Cai, X. -M. Ren, C. -Y. Duan, Y. Xu, S. Gao, X. -Z. You, *Chem.*

-*Eur. J.,* **2003**, *9*, 5673.
24. B. Moulton, J. Lu, R. Hajndl, S. Hariharan, M. J. Zaworotko, *Angew. Chem. Int. Ed.*, **2002**, *41*, 2821.
25. L. G. Beauvais, J. R. Long, *J. Am. Chem. Soc.,* **2002**, *124*, 12096.
26. J. Larionova, S. A. Chavan, J. V. Yakhmi, A. G. Frøystein, J. Sletten, C. Sourisseau, O. Kahn, *Inorg. Chem.,* **1997**, *36*, 6374.
27. M. Ohba, H. Ōkawa, *Coord. Chem. Rev.*, **2000**, *198*, 313.
28. M. Ohba, M. Yamada, N. Usuki, H. Ōkawa, *Mol. Cryst. Liq. Cryst.*, **2002**, *379*, 241.
29. L. Spek, *PLATON, A Multipurpose Crystallographic Tool*; Utrecht University: Utrecht, The Netherlands, **2001**.
30. G. M. Sheldrick, *SHELXL97*, University of Göttingen, Germany, **1997**.

Chapter 5

Bidirectional Chemo-switching of Spin State in a Microporous Fe(II)Pt(II) Coordination Polymer

Abstract

Here we report bidirectional magnetic chemo-switching at room temperature using the microporous coordination polymer {Fe(pz)[Pt(CN)$_4$]} (**1**, pz = pyrazine), incorporating a spin-crossover (SCO) subunits and rotary pz bridges. The simultaneous guest adsorption and bidirectional spin transition were elucidated by *in situ* magnetic measurements following guest vapor injection. Most guest molecules transform **1** from the low-spin (LS) state to the high-spin (HS) state, whereas CS_2 exceptionally causes the reverse HS-to-LS transition. Theoretical calculations clarified the preference for CS_2 in the framework and stabilization of the induced LS state due to the entropy loss resulting from immobilization of the pz bridges. A new concept for creation of responsive functional materials is presented using PCPs utilizing (1) elastic and rotatable coordination bonds, (2) the inner space which allows for guest clathration and freedom in motion, and (3) SCO subunits.

Introduction

Porous coordination polymers (PCPs) have appeared in the past decade as a new class of porous materials providing permanent and designable regular microporosity through flexible coordination bonds.[1–19] Compared with existing inorganic porous materials, PCPs provide significant enhancement in flexibility and in the dynamics of their frameworks.[18,19] This versatility has created prospects for technological applications in gas storage, gas separation and heterogeneous catalysis. The next generation of PCPs is being conceived to switch various solid-state properties (*e.g.*, optics, conductivity or magnetism) through guest adsorption processes, which resembles a simplified form of the conversion process from chemical stimulus to information signal in the chemosensory organs for taste and smell. Here, the chemical response of the framework would be crucial for producing drastic physicochemical changes. To implement such chemoresponsive switching at ordinary temperatures we focused on coupling of the porous properties and the spin-crossover (SCO) phenomenon. SCO is well known in iron(II) coordination compounds, whose electron configurations can move between high-spin (HS) and low-spin (LS) states under external perturbations (temperature, pressure and light irradiation), producing changes in magnetic, optical, dielectric and structural properties.[20–36] In special cases, this switch can be performed within the hysteresis loop based on the first-order spin transition (ST). Although several compounds have already been reported as PCPs incorporating SCO subunits (SCO–PCPs), these materials do not display a room temperature first-order hysteretic ST,[34–36] the guest adsorption and SCO being essentially disconnected events. In these SCO–PCPs, adsorption of guest molecules induces an incomplete and gradual ST at low temperature. Even now, strategies for direct coupling of porous properties and magnetic switching are still underdeveloped.

To establish a new approach to guest-responsive SCO, we adopted Hofmann-type three-dimensional (3-D) SCO–PCPs, $\{Fe(pz)[M^{II}(CN)_4]\}$ (pz = pyrazine; M^{II} = Ni, Pd, Pt)[24] as a platform. These compounds display cooperative magnetic and chromatic thermal- and light-induced ST in the region of room temperature.[25–28] In particular, $\{Fe(pz)[Pt(CN)_4]\}$(**1**) displays a first-order ST with *ca*. 25 K wide hysteresis (critical temperatures: $T_{c\downarrow}$ = 285 K and $T_{c\uparrow}$ = 309 K), and its SCO properties are retained in a thin film[26,27] or nanocrystals.[29,30] Based on *ab initio* X-ray powder diffraction results of dihydrated **1 (1·2H$_2$O)**, we found that the framework provides two guest-interactive sites, one between the pz-bridges (site A) and another between the four-coordinated Pt centers (site B). Furthermore, the pz-bridges are provided with rotational freedom in

the framework. These features should be *a priori* important for the chemical response of the framework.

Here we report chemoresponsive bidirectional spin-state switching in **1** in the room temperature bistability region. Compound **1** can allow reversible control of the magnetic and optical outputs through the chemical response of the framework, as one of a new generation of functional materials responding to their environment. The key factors for the guest-responsive ST were highlighted by theoretical calculations.

Results and Discussions

Crystal structure

Crystal parameters and selected bond distances and angles are listed in Tables 1 – 3. Representative structures are given in Figs. 1 and 2.

*{Fe(pz)[Pt(CN)$_4$]} (**1**)*

Compound **1** is found in its dihydrate form **1·2H$_2$O**. The structures of **1·2H$_2$O** in the HS and LS states were determined using the same single crystal at 293 K, where the HS and LS states were stabilized by cooling from 340 K to 293 K and by heating from 240 K to 293 K, respectively. In both states, each square-planar $[Pt(CN)_4]^{2-}$ anion connects four adjacent axially distorted octahedral Fe(II) atoms (Figs 1A – E). The equatorial positions of Fe are occupied by the four cyano nitrogen atoms of the $[Pt(CN)_4]^{2-}$ anions. In the lattice, a two-dimensional $\{Fe[Pt(CN)_4]\}_\infty$ grid is formed by the Pt – CN – Fe linkages on the (001) plane with Fe_2Pt_2 square windows. The pyrazine ligand bridges the axial positions of the Fe with two arrangements around the C_4 axis as a pillar connecting consecutive layers along the (001) direction (Fig. 1), and it forms channels with a gate size of 3.92 × 4.22 Å^2 for the HS state and 3.43 × 3.94 Å^2 for the LS state, parallel to the (100) and (010) directions (Fig. 1B, C). The equatorial and axial Fe – N bond distances at 293 K are 2.148(6) and 2.215(15) Å for the HS state and 1.941(7) and 1.985(16) Å for the LS state. Upon the ST, the unit cell volume changes by 53.5(5) Å^3 per Fe atom. The solvent-accessible voids of the LS state and HS state were estimated to be 18.1 and 22.4 %, respectively. *Ab initio* X-ray powder diffraction studies suggested that the two crystallographically independent water molecules were localized in the center of the tetragonal prism defined by two consecutive Fe_2Pt_2 square windows (site A) and halfway between two consecutive Pt atoms (site B), respectively.[24]

*{Fe(pz)[Pt(CN)$_4$]·pz} (**1·pz**), {Fe(pz)[Pt(CN)$_4$]·CS$_2$} (**1·CS$_2$**)*

The guest-free framework of **1** adsorbs various guest molecules in the gas phase or solution and forms their clathrates. X-ray diffraction measurements of the CS_2 clathrate (**1·CS$_2$**) were performed at 93 K to minimize thermal vibration (Fig. 2A and B). The equatorial and axial Fe – N bond distances are typical of the LS state, at 1.927(7) and 1.971(9) Å, respectively. The CS_2 molecules lie in the middle of the channels running along the (010) direction, and there is no direct contact between the CS_2 molecule and the Fe center (Fe···S1 = 4.921 Å and Fe···S2 = 5.797 Å). The S1 atom

interposes between the pz rings (site A) with a separation from the center of the pz ring of 3.588 Å. The S2 atom sits over the Pt atoms (site B) with a separation of 3.405 Å. The S1 atom is located on the mirror plane, and the S2 atom lies on two sites with an occupancy of 0.5. Hence, there are two distinct interactive spaces partitioned by pyrazine pillars along the (001) direction (site A) and by Pt atoms along the (100) direction (site B).

In the case of the pyrazine clathrate (**1·pz**), the guest pyrazine molecule lies in site A and leans toward the pz pillars with three-point π···π contacts (3.425 – 3.546 Å) (Figs. 2C and D). The Fe – N bond distances correspond well with those of the HS state (equatorial, 2.128(12) Å; axial, 2.252(14) Å). When the crystals of **1·CS_2** and **1·pz** are heated, the guest-free framework **1** results from a single-crystal-to-single-crystal transformation. The prepared structures of **1** in the LS and HS states determined at 293 K display the original ST behavior observed in **1**.

Table 1. Crystallographic parameters for {Fe(pz)[Pt(CN)$_4$]·2H$_2$O} (**1·2H$_2$O**) in the HS and LS states

Compound	**1·2H$_2$O** (HS)	**1·2H$_2$O** (LS)
Formula	$C_8H_8N_6O_2FePt$	$C_8H_8N_6O_2FePt$
Formula Weight	471.12	471.12
Temperature / K	293	293
Crystal Color	yellow	red
Crystal System	tetragonal	tetragonal
Space Group	*P*4/mmm (#123)	*P*4/mmm (#123)
a / Å	7.457(4)	7.184(6)
b / Å	7.457(4)	7.184(6)
c / Å	7.259(4)	6.783(5)
α / deg	90	90
β / deg	90	90
γ / deg	90	90
V / Å^3	403.6(4)	350.1(5)
Z value	1	1
D_{calc} / g·cm^{-3}	1.790	2.064
μ / mm^{-1}	9.503	10.957
R	0.0472	0.0494
Rw	0.0844	0.0737
Goodness of Fit	1.000	1.022

Table 2 Crystallographic parameters for CS_2 and pyrazine clathrates (**1·CS₂** and **1·pz**)

Compound	**1·CS₂**	**1·pz**
Formula	$C_8H_4N_6S_2FePt$	$C_{12}H_8N_8FePt$
Formula Weight	511.23	515.17
Temperature / K	93	200
Crystal Color	red	yellow
Crystal System	orthorhombic	monoclinic
Space Group	*P*mmm (#47)	*P*2/m (#10)
a / Å	6.737(5)	7.2810(7)
b / Å	7.122(5)	7.460(1)
c / Å	7.175(6)	7.441(1)
α / deg	90	90
β / deg	90	95.814(8)
γ / deg	90	90
V / Å^3	344.3(5)	402.09(9)
Z value	1	1
D_{calc} / g·cm^{-3}	2.466	2.128
μ / mm^{-1}	11.455	9.597
R	0.0224	0.0719
Rw	0.0599	0.1816
Goodness of Fit	1.143	1.095

Table 3. Selected bond distances for **1**-HS, **1**-LS, **1·CS₂** and **1·pz**

Compound	**1**-HS	**1**-LS	**1·CS₂**	**1·pz**
Fe – N1 / Å	2.148(6)	1.941(7)	1.971(9)	2.12(1)
Fe – N2 / Å	2.21(1)	1.98(1)	1.927(7)	2.25(1)
Pt – C1 / Å	2.004(8)	2.011(9)	1.979(8)	1.99(1)
site A···S1 / Å	–	–	3.587	–
site B···S2 / Å	–	–	3.405	–
site A···pz (center) / Å	–	–	–	3.720
site A···site A / Å	7.457(4)	7.184(6)	7.175(6)	7.441(1)
site B···site B / Å	7.259(4)	6.783(5)	6.737(5)	7.2810(7)

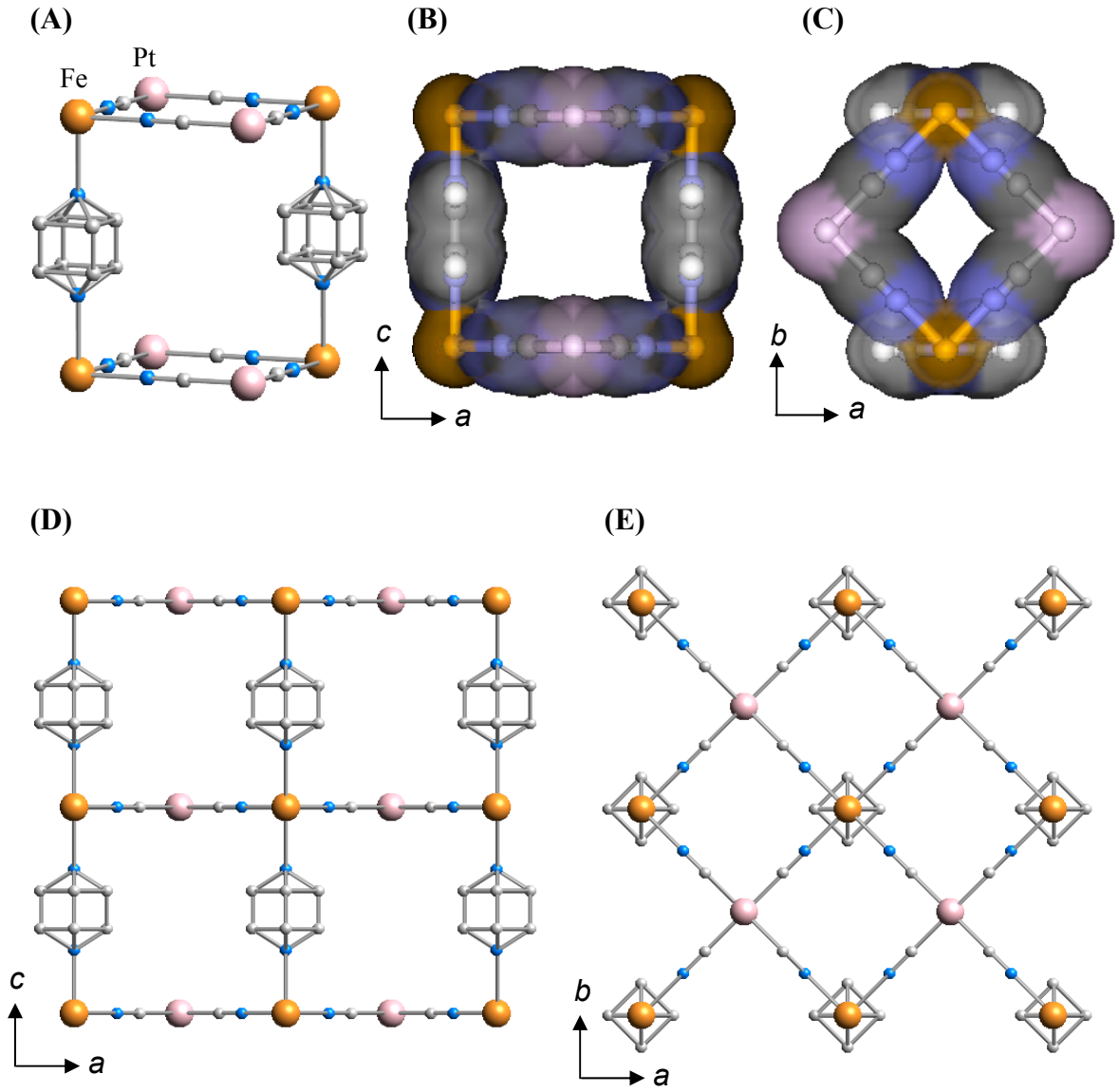

Fig. 1. Crystal structures of {Fe(pz)[Pt(CN)$_4$]·2H$_2$O} (**1·2H$_2$O**). **(A)** The basic cavity structure of **1·2H$_2$O**. **(B** and **C)** The pore gates of **1·2H$_2$O** along the (100) and (010) directions and along the (001) direction. **(D** and **E)** Projections of the 3D porous framework on to the *ac* and the *ab* planes**)**. Color code: Fe (orange), Pt (pink), N (blue), C (gray), S (yellow).

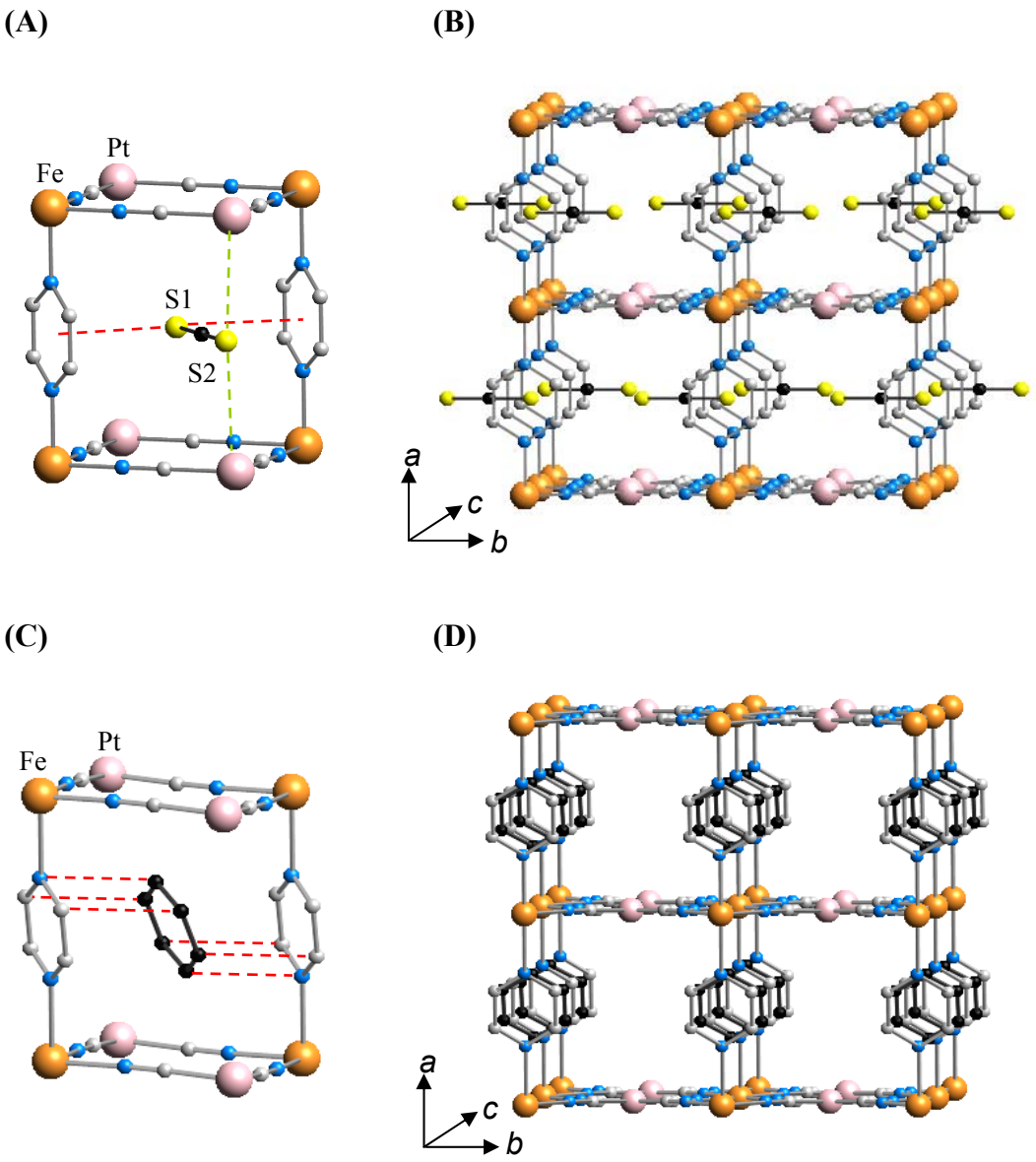

Fig. 2. Crystal structures of CS_2 and pyrazine clathrates (**1·CS$_2$** and **1·pz**). **(A)** The basic cavity structure of **1·CS$_2$**. The S2 atom is disordered through the mirror plane on the S1 atom, and one S2 atom is omitted for clarifying. **(B)** Projection of the 3-D porous framework of **1·CS$_2$**. **(C)** The basic cavity structure of **1·pz**. **(D)** Projection of the 3-D porous framework of **1·pz**. Color code: Fe (orange), Pt (pink), N (blue), C (gray), C2 (balck in C and D), S (yellow), guest molecules are depicted in black except for S atoms.

Guest adsorption

Sorption-desorption isotherms of CO_2, O_2 and N_2 at 298 K were carried out using the completely dehydrated **1** (Scheme 1). Only the CO_2 adsorption profile shows a gradual increase with uptake of *ca*. 1.0 mol per Fe at $P/P_0 = 0.95$. The amount of O_2 and N_2 adsorption was negligible over the time scale (equilibrium time = 120 s) at 298 K. The LS state is retained after adsorption of CO_2. There is no significant difference between the isotherms using **1**-LS and **1**-HS, in spite of the difference in the pore volume. At low temperature, type 1 adsorption isotherms of CO_2 (at 195 K), O_2 (at 77 K) and N_2 (at 77 K) were observed with rapid saturation and uptake of *ca*. 1.6, 1.9 and 2.2 mol/mol at $P/P_0 = 0.95$, respectively, in which **1**-LS retains the LS state after guest adsorption at that temperature.

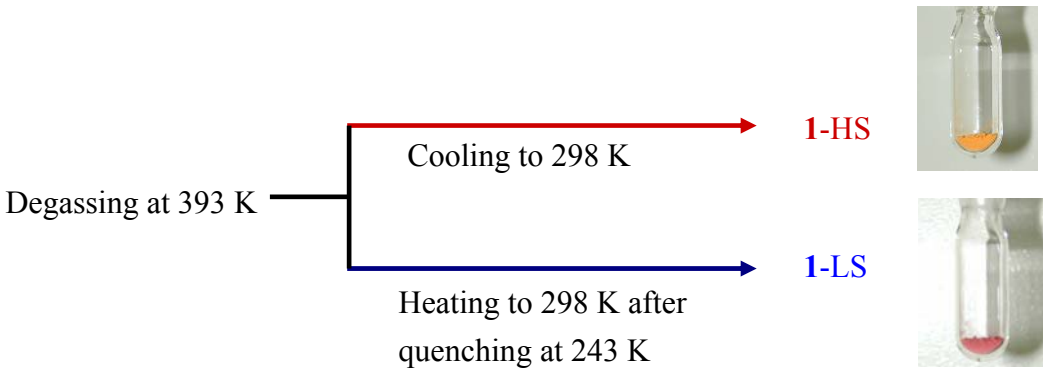

Scheme 1. Preprocessing schemes of **1**-HS and **1**-LS.

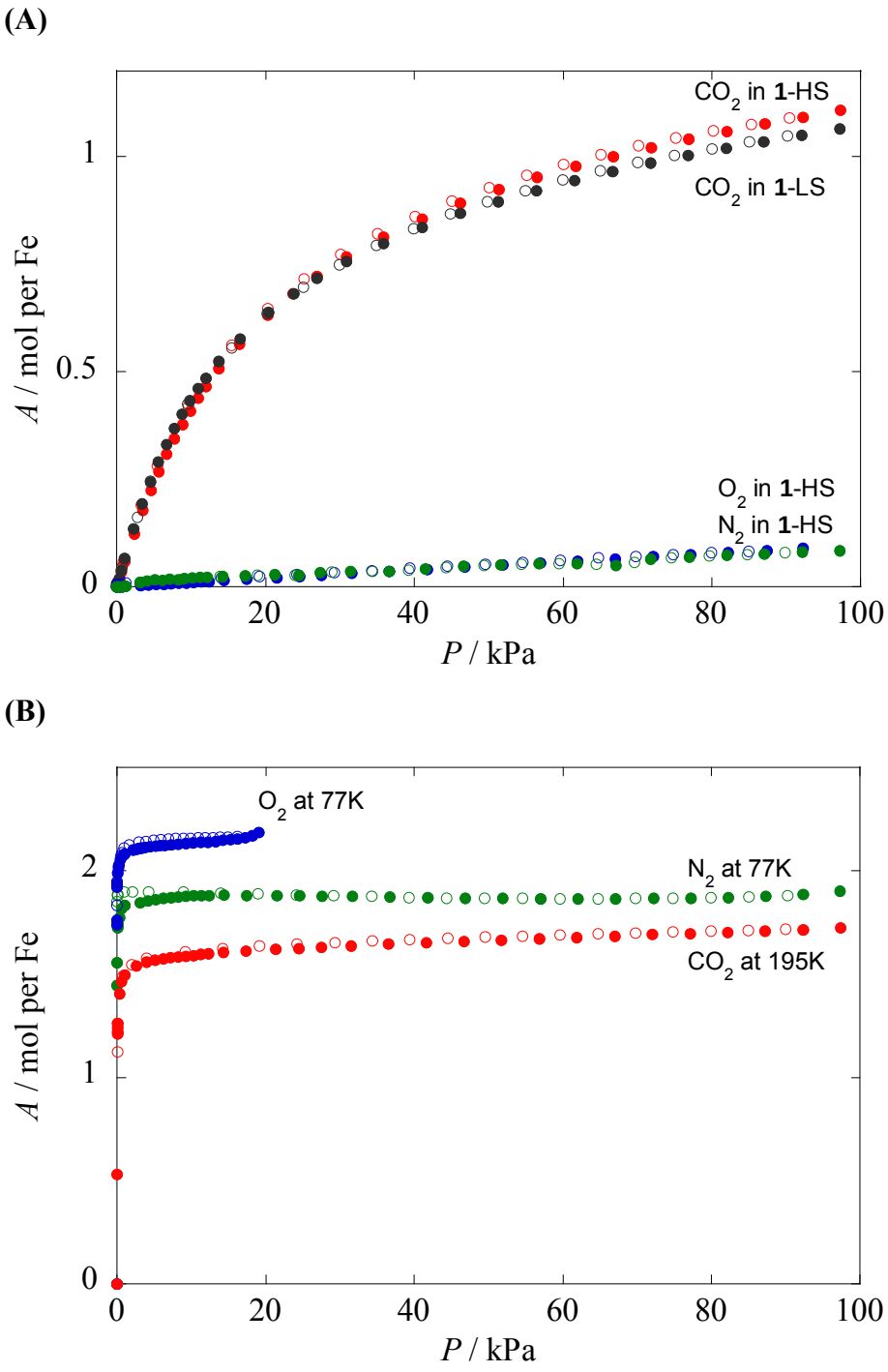

Fig. 3. Sorption and desorption isotherms for gases: **(A)** CO_2 in **1**-LS (black), CO_2 in **1**-HS (red), N_2 in **1**-LS (green) and O_2 in **1**-LS (blue) at 298 K in the pressure range from 10^{-6} to 100 kPa and equilibrium time of 120 sec., and **(B)** CO_2, N_2 and O_2 in **1**-LS (at low temperature): CO_2 (red), N_2 (green), O_2 (blue) in the pressure range from 10^{-6} to 100 kPa and equilibrium time of 120 sec. Filled and open circles express adsorption and desorption processes, respectively.

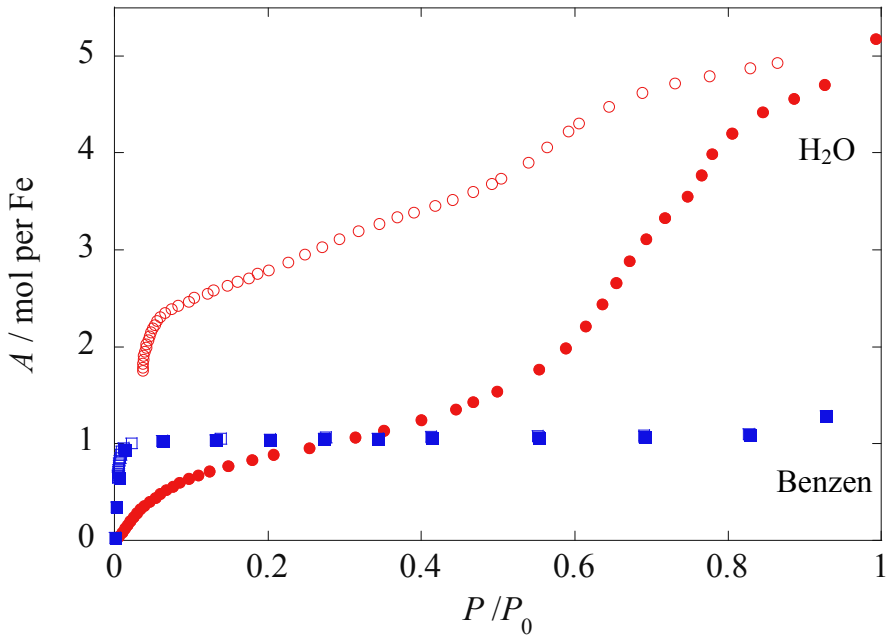

Fig. 4. Sorption and desorption isotherms for H_2O (red) and benzene (blue) in **1** (filled and open circles indicate the adsorption and desorption processes, respectively). P/P_0 is the relative pressure, where equilibrium time is 600 sec. and saturated vapor pressures, P_0, at 298 K are 3.17 kPa for H_2O and 13.44 kPa for benzene.

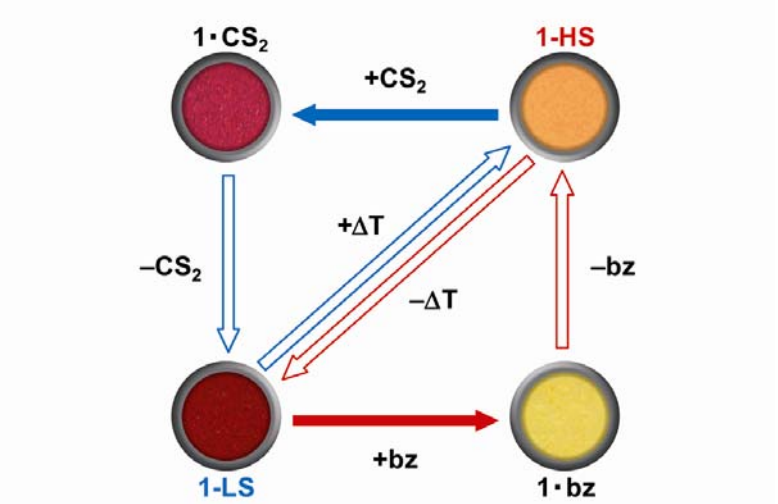

Scheme 2. Schematic chemical and thermal memory process. The color circles are photos of samples. Adsorption of benzene induces the HS state from **1**-LS (red solid arrow). The recorded HS state is retained after desorption of benzene under vacuum and then returned to the initial LS state by cooling (red outlined arrows). Conversely, CS_2 produces the LS state from **1**-HS with contraction of the framework as a recorded state (blue solid arrow). The recorded LS state is initialized by successive desorption of CS_2 under vacuum and heating (blue outlined arrows).

The adsorption isotherm of benzene using **1**-LS shows a step rise at a very low P/P_0 value (*ca*. 0.05) with saturation accompanied by a color change (Fig. 4). The benzene clathrate (**1·bz**) is paramagnetic at all temperatures (Fig. 5a). *In situ* observation of the benzene-induced ST at 293 K was monitored directly using a sample holder specially designed to introduce vapor into the SQUID magnetometer. As shown in Fig. 5b, a complete and relatively rapid conversion from the LS state to the HS state is observed for P/P_0 = 0.19. Desorption of benzene by vacuuming produces the unclathrated framework **1**-HS. The system does not recover the initial LS state over a period of months after releasing benzene within the bistable temperature region. This memory function retains information about adsorption of the guest molecules in the form of the spin state—magnetism, color and structure—that can be erased by desorption and cooling (Scheme 2). X-ray powder diffraction of **1·bz** suggested essentially the same structure as for **1·pz**, which shows the same magnetic behavior as **1·bz**. Other six- or five-membered aromatic molecules such as pyrazine, pyridine, thiophene, pyrrole and furan, or solvents such as methanol, ethanol, propanol and tetrahydrofuran, display a similar behavior to that shown by benzene at room temperature (Table 4). In all of the preceding examples, **1**-HS is stabilized after inclusion of the guests within the hysteresis loop of **1**.

In contrast, **1**-HS promptly adsorbs one molecule of CS_2 for $P/P_0 < 0.1$ and simultaneously changes to the LS state leading to **1·CS₂** (Fig. 5b). The magnetic change rate is faster than that of **1·bz**, which means a higher affinity of CS_2 for the framework than that of benzene. Indeed, injection of CS_2 vapor onto **1·bz** induces a gradual and complete replacement of benzene by CS_2 even under a saturated benzene vapor atmosphere. **1·CS₂** maintains the LS state without ST in the temperature range 2 – 330 K (Fig. 5a); above 330 K the $\chi_M T$ value increases because of the release of CS_2. When the CS_2 molecule is removed at 298 K, the framework retains the LS state as a result of the memory effect described above (Scheme 2). Benzene adsorption resulted in expansion (softening) of the framework with an LS-to-HS transition; in stark contrast, CS_2 adsorption contracted (hardened) the framework accompanying an HS-to-LS transition (Fig. 6 and Table 5). The analogs of $\{Fe(pz)[M(CN)_4]\}$ (M = Ni, Pd) demonstrate similar guest-responsive spin-state switching. In the case of the gas molecules, CO_2, O_2 and N_2, only CO_2 is adsorbed without spin state change at 298 K.

Table 4. Summary of the guest induced spin state of **1** at 293 K.

Class	Guest molecule	Effect	Relative size
I	CO_2	No	Small
	N_2		Small
	O_2		Small
II	H_2O	HS stabilized	Small
	D_2O		Small
	MeOH		Small
	EtOH		Medium
	2-PrOH		Medium
	Acetone		Medium
	Benzene		Large
	Pyrazine		Large
	Toluene		Large
	Thiophene		Large
	Pyrrole		Large
	Pyridine		Large
	Furan		Large
	THF		Large
III	CS_2	LS stabilized	Small

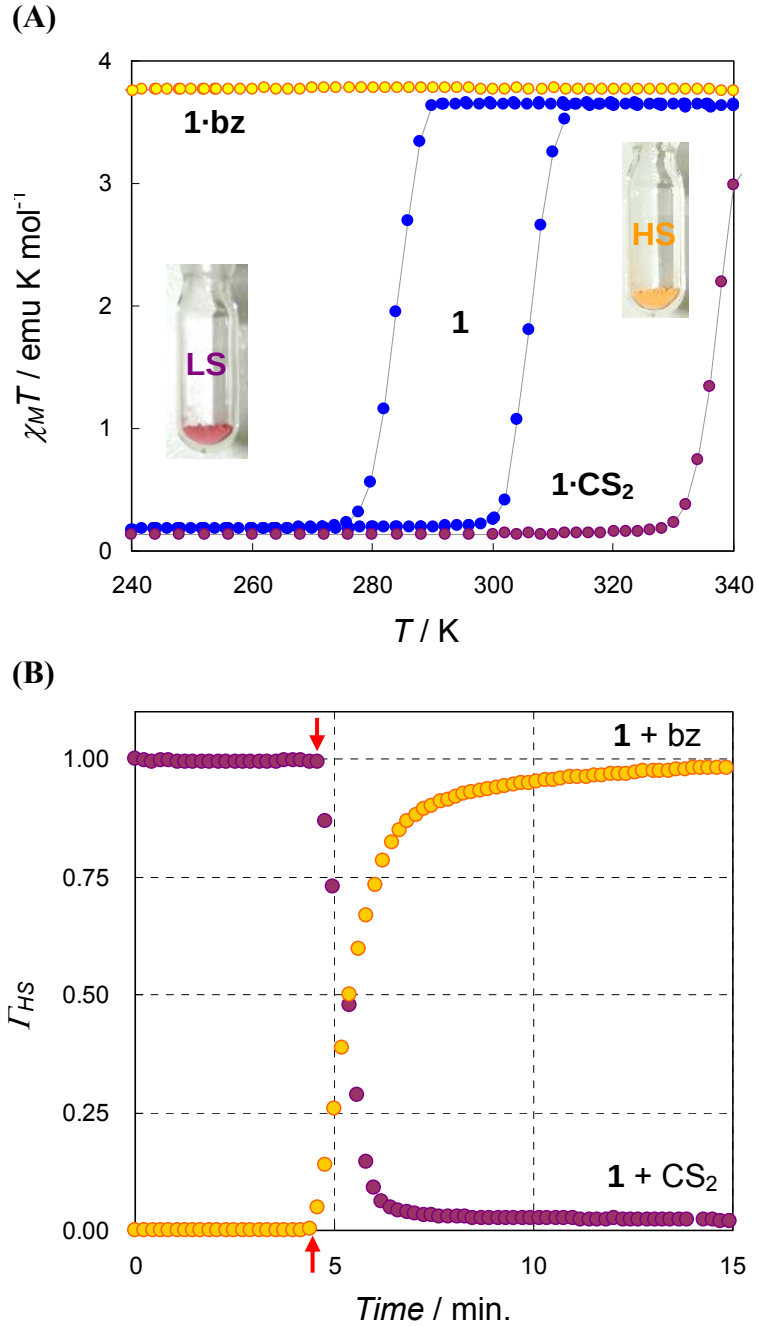

Fig. 5. Magnetic behaviors of **1** and its clathrates, and *in-situ* observation of the guest-induced ST. **(A)** Temperature dependences of $\chi_M T$ for guest-free **1** (blue), benzene clathrate (**1·bz**: yellow) and CS_2 clathrate (**1·CS₂**: purple) in the temperature range 240 – 340 K. The sample color changed between deep red (LS) and yellow-orange (HS) depending on the temperature and guest molecules. **(B)** Time dependence of the fraction of the HS state under a benzene (yellow) and CS_2 (purple) atmosphere at 293 K. Red arrows indicate the starting points of guest injection (valve opening).

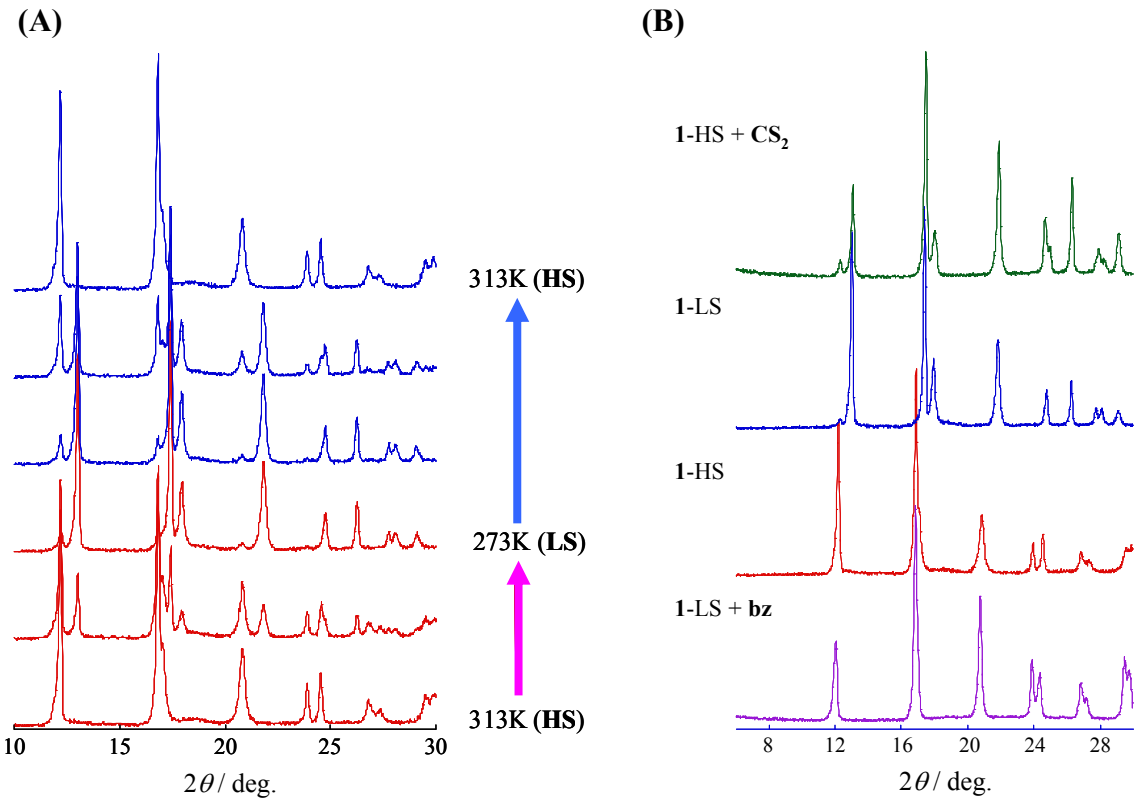

Fig. 6. **(A)** Temperature dependence of the X-ray powder diffraction (XRPD) patterns for **1·2H$_2$O**. Crystalline **1·2H$_2$O** was cooled from 313 K to 273 K and then heated to 313 K. **(B)** XRPD patterns for **1·bz**, **1**-HS, **1**-LS and **1·CS$_2$**.

Table 5. Distances of capital indexes and cell volumes estimated by each XRPD patterns. ΔV means difference in volume from that of **1**-HS.

	1-HS	**1-LS**	**1·bz**	**1·CS$_2$**
(001) / Å	7.25	6.79	7.34	6.77
(1 1 0) / Å	5.25	5.09	5.26	5.06
(1 0 1) / Å	5.19	4.94	5.23	4.91
V / Å^3	399.9	351.8	406.2	346.7
ΔV / %	---	-12.0	+ 1.6	-13.3

The studied guest molecules (G) can be grouped into three major classes according to their effect on the spin state (Table 4). Class I (gas molecules: N_2, O_2 and CO_2) showed no effect on the spin state; class II (H_2O, alcohols, acetone and five- or six-membered ring molecules) stabilized the HS state; and class III (CS_2) stabilized the LS state. The structural characteristics of the clathrates are as follows: (i) the CS_2 molecules are located at sites A and B; and (ii) the pz guest molecules are located exclusively at site A with preventing further contraction of the framework to the LS state. These structural results, together with guest classification, point to four key factors as the origins of the relative stabilities of the HS and LS states: (1) the size and shape of G; (2) the G···pz interaction at site A; and (3) the G···Pt interaction at site B.

To corroborate the exceptional response of the framework to CS_2, binding energies between CS_2 and each site (A and B) were estimated (Fig. 7 and Schemes 3 – 5). Although potential energy surfaces calculated with the DFT and the Hartree-Fock methods showed no binding between S and each site, the highly accurate CCSD(T) method with the counterpoise correction[11] gave binding energies of ca. 4.2 kcal/mol at site A (Fig. 7A) and ca. 5.5 kcal/mol at site B (Fig. 7B), indicating that van der Waals interactions rather than charge-transfer interactions mainly contribute. The van der Waals interactions make the guest molecule take the midpoint between two pz bridges. In the case of isomorphic CO_2 molecules (class I), they indicate a weak interaction (*ca*. 2.9 kcal/mol at site A; *ca*. 4.2 kcal/mol at site B). These computational results highlight the significant interaction of CS_2 at sites A and B. In the next stage, the rotation of pyrazine bridges, the change of crystallographic symmetry and the change of π-acceptor character of the cyanide groups will be verified as potential factors for stabilization of the LS state. In contrast, for class II, the number of guests per iron atom, guest size and shape determine the stabilization of the HS state. Steric hindrance prevents further contraction of the clathrates' framework, resulting in an inhibition of the HS-to-LS transition or a notable displacement of $T_{c\downarrow}$ to lower temperatures.

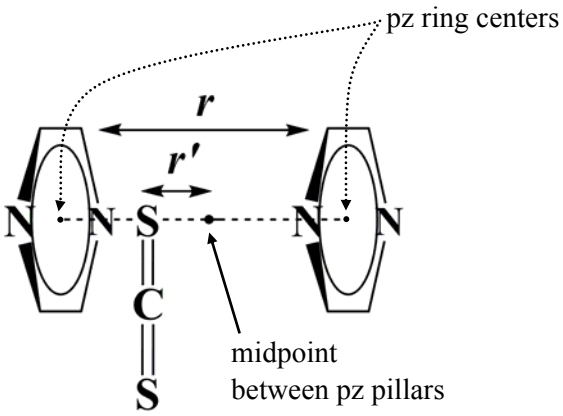

Scheme 3. Model system for calculation of the interaction at site A. A model system which consists of two pz bridges and one CS_2 (or CO_2) molecule was theoretically examined to elucidate the van der Waals interaction between guest molecule and framework at the site A. In this model, all molecules are arranged parallel with one another and one of the S (or O) atoms is placed just between the two pz bridges like in the experimental structure, **1·CS$_2$**.

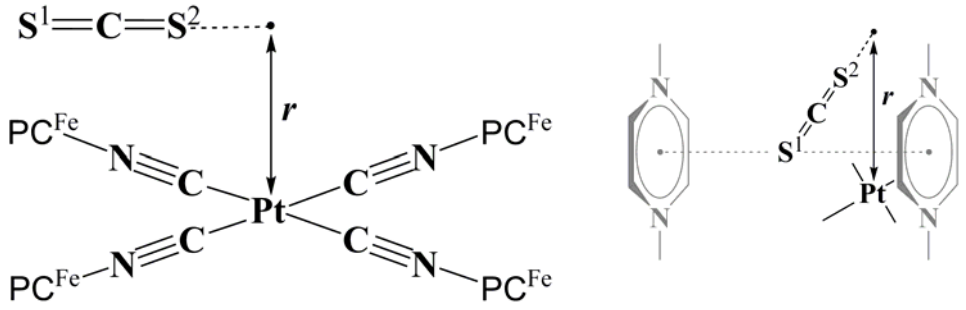

Scheme 4. Model system employed to investigate the interaction at site B. PC^{Fe} represents a point charge (+0.5), to model a Fe atom. The S^1 (O^1) atom is placed at the midpoint between two pz-bridges. A model system which consists of a square-planar $[Pt(CN)_4]^{2-}$ anion and one CS_2 (or CO_2) molecule were theoretically investigated (Fig. 7B). In this model, one of the S (or O) atoms is placed at the midpoint between two pz bridges.

(A) CS_2 adsorption

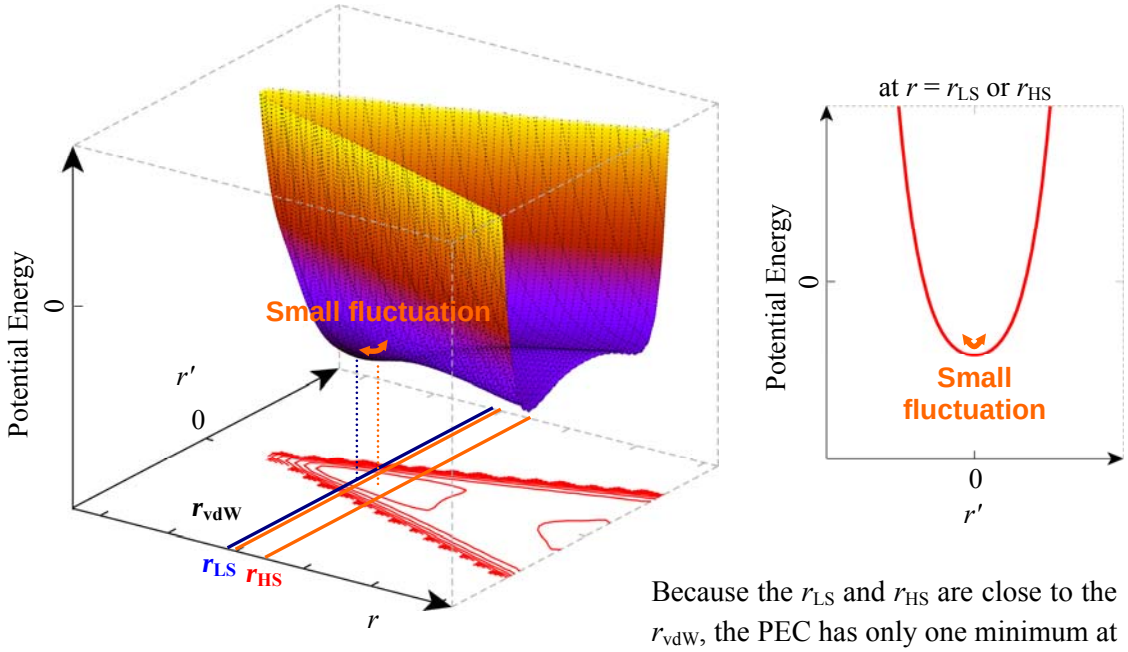

Because the r_{LS} and r_{HS} are close to the r_{vdW}, the PEC has only one minimum at $r = r_{LS}$ and r_{HS}.

(B) CO_2 adsorption

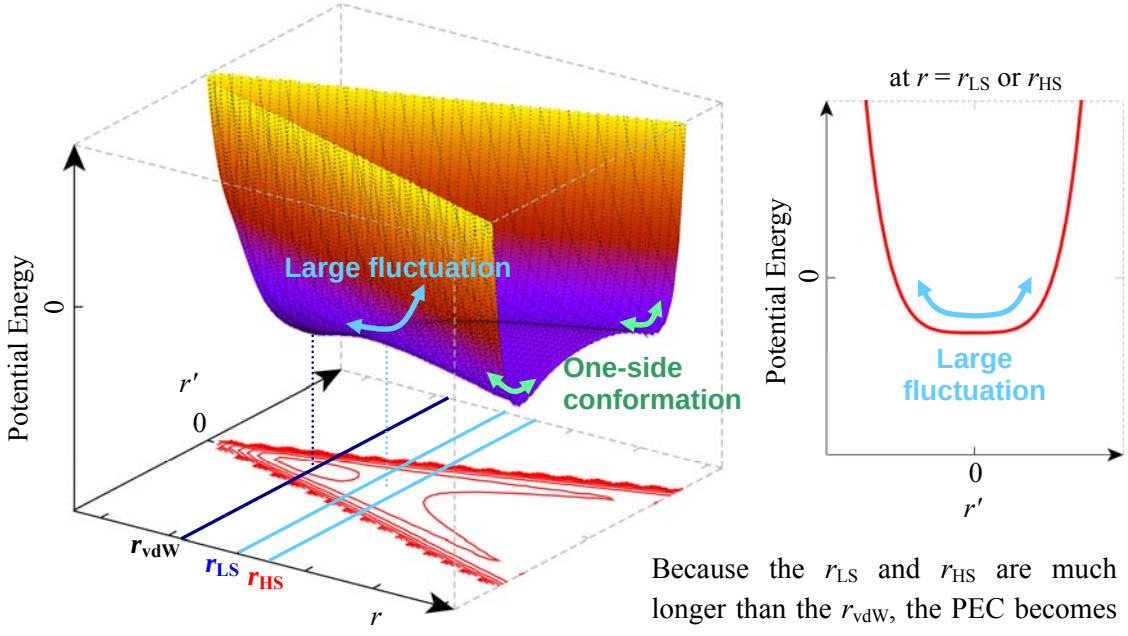

Because the r_{LS} and r_{HS} are much longer than the r_{vdW}, the PEC becomes flat at $r = r_{LS}$ and r_{HS}.

Scheme 5. Schematic potential energy surfaces along the r and r' axes: **(A)** CS_2 and **(B)** CO_2 adsorptions. The one-side conformation means the structure in which the guest molecule interacts with only one pz pillar. The r_{vdW} is the distance at which the van der Waals interaction becomes maximum.

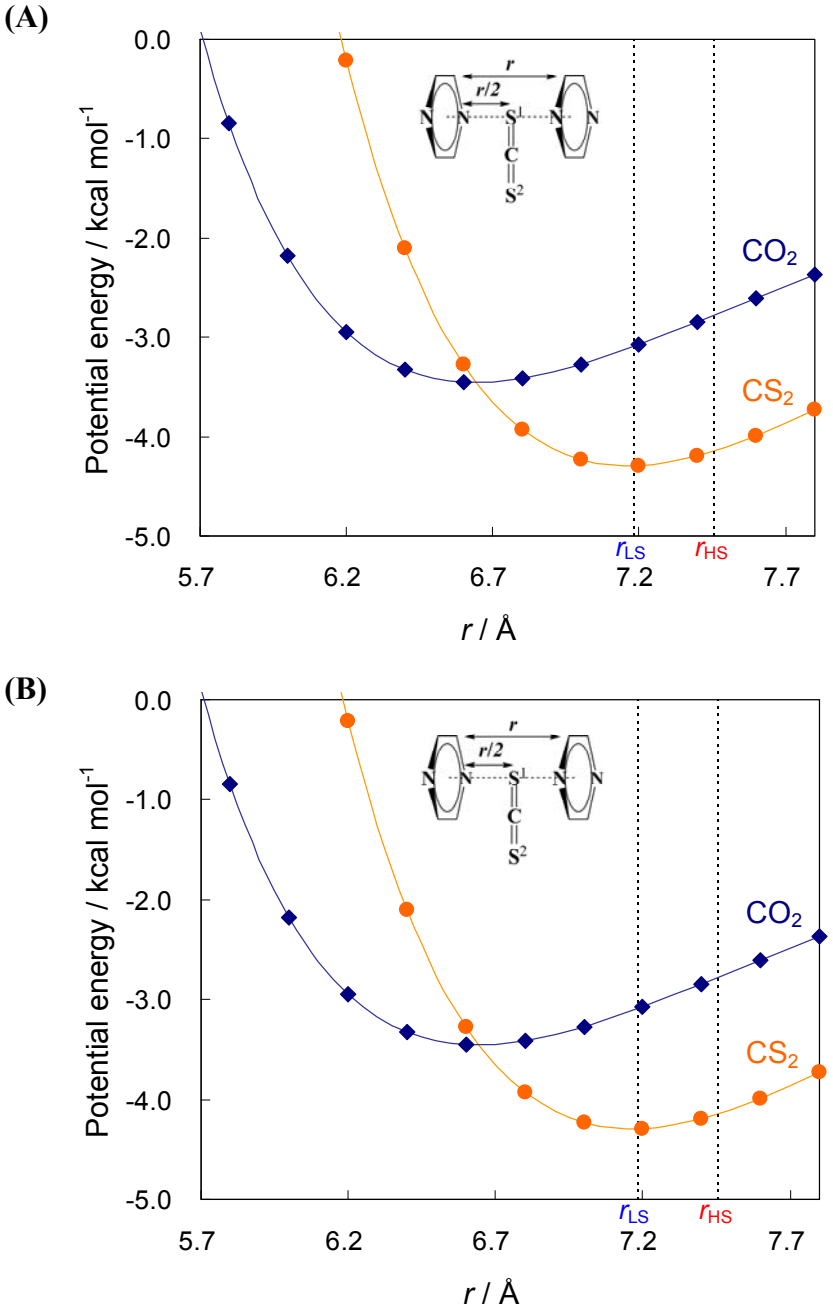

Fig. 7. Potential energy curves for the interaction of CS_2 and CO_2 at **(A)** site A and **(B)** site B. r_{LS} and r_{HS} represent the corresponding distances in the experimental **1·2H$_2$O** (LS) and **1·2H$_2$O** (HS) frameworks, respectively. The binding energies of CS_2 and CO_2 at site B discussed in the text are estimated as double value in Fig. 7B.

Conclusion

An unprecedented bidirectional chemo-switching is delivered using the dynamic microporous SCO–PCP {Fe(pz)[Pt(CN)$_4$]} (**1**) at room temperature. The HS and LS states are reversibly induced with coupling of guest adsorption (Scheme 2). The space inside the framework of **1** allows a chemical response for sites A and B. The CS_2 molecule suitably interacts with sites A and B like a key molecule for the framework, and exceptionally stabilizes the LS state. The singularity of the framework response for CS_2 is corroborated by theoretical calculations. The SCO–PCP **1** presents bidirectional chemo-switching of spin state and memory effect at room temperature, which will open a route for evolving the PCPs to environmentally responsive materials; *e.g.*, nano-size chemical memory and chemical sensors.

Experimental

Materials

All chemicals and solvents, obtained from Tokyo Kasei Co., Ltd., and Wako Pure Chemical Industries, Ltd., were reagent grade. They were used without further purification.

Synthesis of {Fe(pz)[Pt(CN)$_4$]·2H$_2$O} (1·2H$_2$O)

An aqueous solution (2 mL) of [Fe(SO$_4$)$_2$(NH$_4$)$_2$]·6H$_2$O (3.03 mg, 7.73×10^{-3}mmol) and pyrazine (1.24 mg, 1.55×10^{-2} mmol) were transferred to a glass tube containing a small amount of ascorbic acid, and then a methanolic solution (2 mL) of K$_2$[Pt(CN)$_4$] (3.33 mg, 7.73×10^{-3} mmol) was poured into the glass tube under N$_2$ without mixing the solutions at 318 K. The resulting mixture was allowed to stand over two weeks to obtain yellow-orange cubic crystals of **1**-HS. IR (KBr): υ (cm^{-1}) = 3424 m, 2168 l, 2147 l, 1613 w, 1490 w, 1419 m, 1156 w, 1126 w, 1110 w, 1086 w, 1053 l, 804 m.

Synthesis of {Fe(pz)[Pt(CN)$_4$]·pz} (1·pz)

The pyrazine clathrate (1·pz) was prepared by slow diffusion in an H-shaped vessel (volume ca. 10 mL). An aqueous solution (1 mL) containing [Fe(SO$_4$)$_2$(NH$_4$)$_2$]·6H$_2$O (40 mg, 1×10^{-4} mol) and pz (16 mg, 2×10^{-4} mol) was placed in one side of the H vessel while the other side contained 38 mg (1×10^{-4} mol) of K$_2$[Pt(CN)$_4$] dissolved in 0.5 mL of water. Then the H-tube was filled with water. Yellow single crystals of **1·pz** were formed in two weeks.

Synthesis of {Fe(pz)[Pt(CN)$_4$]·CS$_2$} (1·CS$_2$) and the other guest clathrates

The CS$_2$ clathrate (**1·CS$_2$**) and the other clathrates were prepared by exposing **1·2H$_2$O** to saturated guest vapor for 1 day.

Crystallographic Data Collection and Refinement of the Structure

X-ray diffraction data of **1·2H$_2$O**(HS), **1·2H$_2$O**(LS), **1·CS$_2$**, **1**-HS and **1**-LS were collected on a Rigaku Varimax CCD system while **1·pz** was collected with a Nonius Kappa-CCD single crystal diffractometer. In all cases, graphite-monochromated Mo-Kα radiation (λ = 0.71070 Å) was used. A single crystal was mounted on a fiber loop with liquid paraffin and the temperature kept constant under flowing N$_2$. All of the structures were solved by a standard direct method (Crystal Clear 1.4. crystallographic software package of the Molecular Structure Corp. and Rigaku) and

expanded using Fourier techniques. Full-matrix least-squares refinements were carried out with anisotropic thermal parameters for all non-hydrogen atoms. All of the hydrogen atoms were placed in the calculated positions and refined using a riding model.

Physical Measurements

Variable-temperature X-ray powder diffraction was carried out on a Rigaku RINT-2000 Ultima diffractometer with Cu-Kα radiation. Thermogravimetric analyses were recorded on a Rigaku Thermo plus TG 8120 apparatus in the temperature range between 300 and 773 K under a nitrogen atmosphere at a heating rate of 5 K min^{-1}. The adsorption isotherms of CO_2, O_2 and N_2 were measured with Quantachrome AUTOSORB-1 and adsorption/desorption isotherms for H_2O and benzene at 298 K were measured with BELSORP-18 volumetric adsorption equipment from BEL Japan, Inc. The anhydrous sample **1** was obtained by treatment under reduced pressure (< 10^{-2} Pa) at 400 K for more than 2 h.

Magnetic susceptibilities of all samples were measured on a Quantum Design MPMS−XL5R SQUID susceptometer in the temperature range 2 − 400 K in an applied dc field of 500 Oe. The samples were placed in a glass tube and fixed to the end of the sample transport rod. Guest-free sample was prepared by vacuuming for 2 h in the SQUID sample chamber at 293 K. The guest molecules were injected through the long metallic rod of the sample holder ending in a hermetically closed cylindric chamber with controlling its vapor pressure at 293 K. The molar magnetic susceptibility, χ_M, was corrected for the diamagnetism of the constituent atoms.

References

1. G. Férey, C. Mellot-Draznieks, C. Serre, F. Millange, *Acc. Chem. Res.*, **2005**, *38*, 217.
2. N. W. Ockwig, O. Delgado-Friedrichs, M. O'keeffe, O. M. Yaghi, *Acc. Chem. Res*., **2005**, *38*, 176.
3. S. Kitagawa, R. Kitaura, S. Noro, *Angew. Chem. Int. Ed.,* **2004**, *43*, 2334.
4. M. J. Rosseinsky, *Microporous Mesoporous Mater.*, **2004**, *73*, 15.
5. C. Janiak, *Dalton Trans,* **2003***,* 2781.
6. G. S. Papaefstathiou, L. R. MacGillivary, *Coord. Chem. Rev.,* **2003**, *246*, 169.
7. B. Moulton, M. J. Zaworotko, *Chem. Rev.,* **2001**, *101*, 1629.
8. G. Férey, C. Mellot-Dranznieks, C. Serre, F. Millange, J. Dutour, S. Surblé, I. Margiolaki, *Science*, **2005**, *309***,** 2040.
9. R. Matsuda, R. Kitaura, S. Kitagawa, Y. Kubota, R. V. Belosludov, T. C. Kobayashi, H. Sakamoto, T. Chiba, M. Takata, Y. Kawazoe, Y. Mita, *Nature*, **2005**, *436*, 238.
10. O. M. Yaghi, M. O'Keeffe, N. W. Ockwig, H. K. Chae, M. Eddaoudi, J. Kim, *Nature*, **2003**, *423*, 705.
11. M. Eddaudi, J. Kim, N. Rosi, D. Vodak, J. Wachter, M. O'keeffe, O. M. Yaghi, *Science*, **2002**, *295*, 469.
12. J. S. Seo, D. Whang, H. Lee, S. I. Jun, J. Oh, Y. J. Jeon, K. Kim, *Nature*, **2000**, *404*, 982.
13. D. Maspoch, S. R. Molina, J. Veciana, *Chem. Soc. Rev.*, **2007**, *36*, 770.
14. N. Yanai, W. Kaneko, K. Yoneda, M. Ohba, S. Kitagawa, *J. Am. Chem. Soc.*, **2007**, *129*, 3496.
15. C. J. Kepert, *Chem. Commun.* **2006**, 696.
16. S. Ohkoshi, K. Arai, Y. Sato, K. Hashimoto, *Nature Mater*., **2004**, *3*, 857.
17. D. Maspoch, D. R. Molina, K. Wurst, N. Domingo, M. Cavallini, F. Biscarini, J. Tejada, C. Rovira, J. Veciana, J. *Nature Mater*., **2003**, *2*, 190.
18. S. Kitagawa, R. Matsuda, *Coord. Chem. Rev.*, **2007**, *251*, 2490.
19. S. Horike, R. Matsuda, D. Tanaka, S. Matsubara, M. Mizuno, K. Endo, S. Kitagawa, *Angew. Chem. Int. Ed.*, **2006**, *45*, 7226.
20. P. Gütlich, H. A. Goodwin (Eds.), *Spin Crossover in Transition Metal Compounds*, *Top. Curr. Chem.*, **2004**, *233-235*, Springer.
21. O. Kahn, C. J. Martines, *Science*, **1998**, *279*, 44.
22. J. A. Real, A. B. Gaspar, M. C. Muñoz, *Dalton Trans*, **2005**, 2062.
23. J. A. Real, A. B. Gaspar, V. Niel, M. C. Muñoz, *Coord. Chem. Rev.*, **2003**, *236*, 121.

24. V. Niel, J. M. Martinez-Agudo, M. C. Muñoz, A. B. Gaspar, J. A. Real, *Inorg. Chem.,* **2001**, *40*, 3838.
25. S. Cobo, D. Ostrovskii, S. Bonhommeau, L. Vendier, G. Molnár, L. Salmon, K. Tanaka, A. Bousseksou, *J. Am. Chem. Soc.*, **2008**, *130*, 9019.
26. G. Molnár, S. Cobo, J. A. Real, F. Carcenac, E. Daran, C. Vieu, A. Bousseksou, *Adv. Mat*., **2007**, *19*, 2163.
27. S. Bonhommeau, G. Molnár, A. Galet, A. Zwick, J. A. Real, J. J. McGarvey, A. Bousseksou, *Angew. Chem., Int. Ed.*, **2005**, *44*, 4069.
28. T. Tayagaki, A. Galet, G. Molnár, M. C. Muñoz, A. Zwick, K. Tanaka, J. A. Real, A. Bousseksou, *J. Phys. Chem. B*, **2005,** *109,* 14859.
29. I. Boldog, A. B. Gaspar, V. Martínez, P. Pardo-Ibáñez, V. Ksenofontov, A. Bhattacharjee, P. Gütlich, J. A. Real, *Angew. Chem. Int. Ed.,* **2008**, *47*, 6443.
30. F. Volatron, L. Catala, E. RivieÌre, A. Gloter, O. Steìphan, T. Mallah, *Inorg. Chem.* **2008**, 47, 6584.
31. P. Gütlich, A. Hauser, H. Spiering, *Angew. Chem. Int. Ed.*, **2004**, *33*, 2024.
32. A. Hauser, J. Jeftic, H. Romstedt, R. Hinek, H. Spiering, *Coord. Chem. Rev.*, **1999**, *190-192*, 471.
33. S. Decurtins, P. Gütlich, C. P. Köhler, H. Spiering, A. Hauser, *Chem. Phys. Lett.*, **1984**, *105*, 1.
34. J. A. Real, E. Andrés, M. C. Muñoz, M. Julve, T. Granier, A. Bousseksou, F. Varret, *Science*, **1995**, *268*, 265.
35. G. J. Halder, C. J. Kepert, B. Moubaraki, K. S. Murray, J. D. Cashion, *Science*, **2002**, *298*, 1762.
36. S. M. Neville, G. J. Halder, K. W. Chapman, M. B. Duriska, P. D. Southon, J. D. Cashion, J. F. Létard, B. Moubaraki, K. S. Murray, C. J. Kepert, *J. Am. Chem. Soc*., **2008**, *130*, 2869.
37. S. F. Boys, F. Bernardi, *Mol. Phys*. **1970**, *19*, 553.

Chapter 6

Guest-responsive Porous Magnetic Frameworks Using Polycyanometallates

Abstract

Three types of cyanide-bridged porous magnetic frameworks based on polycyanometallates exhibited reversible magnetic conversions associated with different guest-responsive structural transformation, *i.e.*: (1) reversible magnetic and structural conversion of $[Ni(dipn)]_2[Ni(dipn)(H_2O)][Fe(CN)_6]_2 \cdot 11H_2O$ (**1**: dipn = *N*,*N*-di(3-aminopropyl)amine) triggered by water desorption/adsorption; (2) reversible topochemical transformation of a ferrimagnet, $[Mn(HL)(H_2O)][Cr(CN)_6] \cdot H_2O$ (**2**: L = *N,N*-dimethylethylenediamine); and (3) bidirectional magnetic chemo-switching of $\{Fe(pz)[Pt(CN)_4] \cdot 2H_2O\}$ (**3**: pz = pyrazine). In compound **1**, the flexible Fe – CN – Ni linkage, bidirectional hydrogen bonds between lattice water molecules and non-bridging cyano nitrogen atoms play crucial roles in the reversible structural and magnetic conversion. Compound **2** provides a flexible magnetic framework incorporating removable solvent co-ligands, and deliver structural and magnetic transformations in response to solvation/desolvation. Compound **3** incorporating spin-crossover sites in the porous framework successfully delivers an objective reversible magnetic switching in response to guest molecules at room temperature. These results highlight the viable strategy using a polycyanometallate for constructing the guest-responsive magnetic frameworks.

Introduction

Molecular-based magnets (MMs) have been studied extensively since the end of the 1980s[1–6]. These studies started with the challenge to achieve long-range magnetic ordering with control over magnetic interactions and the arrangement of magnetic centers. Several functionalized MMs, *e.g.*, magnetic switches in response to light,[7–12] pressure,[13–18] solvent[19–34] *etc*., have been developed through various trials. These efforts paved the way towards new magnetic materials, and developed into a new active research area.[35] The basic molecular design for MMs with infinite structures has aspects in common with that of coordination polymers (CPs) that have frameworks extended by coordination bonds[36,37]. Thus, MMs and CPs providing magnetic properties can be identified as coordination polymer magnets (CPMs). As is obvious, CPMs inherit characteristics of CPs, such as high regularity, diversity, and flexibility in combining various components, *e.g.*, bridging ligands, metal ions, co-ligands, *etc.*, with elaborately designed frameworks. In particular, the flexible frameworks have potential to respond to external physical and chemical stimuli. Herein, we focus on the design of CPMs to implement guest-responsive magnetic switching.

The porous framework is one noteworthy functionalized architecture derived from CPs. In the past decade, porous coordination polymers (PCPs) have emerged as a new class of porous materials, representing an advanced version of CPs.[36,38–43] Flexible PCPs' pores allow expansion or shrinkage of their framework in association with guest adsorption or desorption.[44,45] Therefore, PCPs are expected to be multifunctional platforms exhibiting porous properties with specific chemical and physical properties. From this perspective, porous coordination polymer magnets (PCPMs) incorporating magnetic properties into the porous framework would be ideal multifunctional materials, particularly as chemoresponsive materials.[46,47] Kahn *et al*. first introduced the concept of a "magnetic sponge'' in molecular magnets that can reversibly release and reabsorb both non-coordinated and coordinated solvent molecules, accompanied by a drastic change of magnetic properties.[19,22] Although this concept restricts the intended guest molecules to solvents in non-porous systems, it expresses the essence of guest-responsivity in PCPMs. Here we use "guest-responsive magnets" as an umbrella term instead of magnetic sponges.

To couple the magnetic and porous properties, we need a more sophisticated design strategy. Magnetic ordering requires short bridging structures to mediate strong magnetic interactions between magnetic centers, while porous frameworks generally consist of relatively long bridging ligands forming a large inner space. One rational

design for PCPMs is based on using large paramagnetic compounds (linkers) to combine magnetic centers. From this viewpoint, a polycyanometallate anion, $[M_A(CN)_n]^{m-}$ (n = 2 – 8), is a suitable linker because it gives a relatively long M_B – NC – M_A – CN – M_B linkage (*ca.* 1 nm) for the inner pore and mediates effective magnetic interaction between M_A and M_B (Scheme 1). Prussian blue, $Fe^{III}_4[Fe^{II}(CN)_6]_3 \cdot nH_2O$, is representative of magnetic compounds using a polycyanometallate linker. A number of Prussian blue analogues (PBAs) have been reported so far.[48–50] Several PBAs exhibit magnetic and porous properties, but the cyanide bridges do not have sufficient structural flexibility except for structural defects because of their close-packed structures.[47,51–53] A convertible structure responsive to chemical stimuli is a significant function to implement in guest-responsive magnets. The key to creating such a flexible but durable framework is to utilize weak molecular interactions in addition to strong coordination bonds. From this perspective, we have extensively studied cyanide-bridged CPMs by the use of $[M_A(CN)_n]^{m-}$ and secondary building units (SBU) consisting of metal ions M_B^{n+} and auxiliary ligands (co-ligands).[17,18,29,30,54–62] The co-ligands play a significant role in avoiding the formation of a PB-type structure and deriving the desired frameworks based on rational molecular designs by limiting the available coordination sites on the SBU. In addition, the incorporation of co-ligands prevents formation of close-packed structures and results in non-bridging cyano groups in the framework. The non-bridging cyano groups act as guest-interactive sites by forming hydrogen bonds, which is of considerable importance for reversible structural conversion.

Here we highlight our strategy for building guest-responsive magnets based on the utility component, polycyanometallate, with three types of guest-responsive cyanide-bridged PCPMs, *i.e.*: (1) reversible magnetic and structural conversion of $[Ni(dipn)]_2[Ni(dipn)(H_2O)][Fe(CN)_6]_2 \cdot 11H_2O$ (**1**: dipn = *N*,*N*-di(3-aminopropyl)-amine)[29] triggered by water desorption/adsorption; (2) reversible topochemical transformation of a ferrimagnet, $[Mn(HL)(H_2O)][Cr(CN)_6] \cdot H_2O$ (**2**: L = *N,N*-dimethyl-ethylenediamine)[30]; and (3) bidirectional magnetic chemo-switching of $\{Fe(pz)[Pt(CN)_4] \cdot 2H_2O\}$ (**3**: pz = pyrazine).[63]

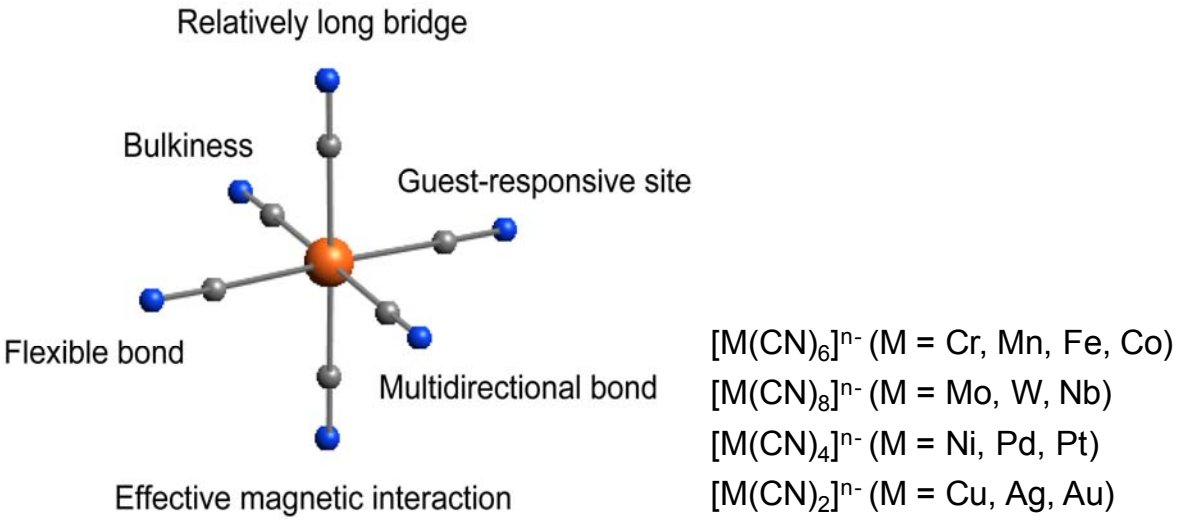

Scheme 1 Major characteristics of polycyanometallate

Results and Discussions

$[Ni(dipn)]_2[Ni(dipn)(H_2O)][Fe(CN)_6]_2 \cdot 11H_2O$ (1)

Compound **1** was obtained as black crystals by reaction of $NiCl_2 \cdot 6H_2O$, dipn and $K_3[Fe(CN)_6]$ in 3:3:2 mole ratio in DMF-water solution.[29] The asymmetric unit of **1** consists of one $[Fe(CN)_6]^{3-}$ anion, one $[Ni(dipn)]^{2+}$ and one half $[Ni(dipn)(H_2O)]^{2+}$ cations and 5.5 water molecules. In the lattice, this compound forms a 3-D porous framework consisting of 2-D layers extended by alternating array of $[Ni(dipn)]^{2+}$ and $[Fe(CN)_6]^{3-}$, and $[Ni(dipn)(H_2O)]^{2+}$ units linking the 2-D layers (Fig. 1). The porous framework has a honeycomb-type channel structure with a solvent-accessible void of 29.0 %. The tridentate co-ligand, dipn, coordinates to Ni^{2+} in meridional positions and gives three coordinatable sites on the SBU. Four cyano groups of $[Fe(CN)_6]^{3-}$ coordinate to the adjacent Ni^{2+} ions, and the other two in *cis* positions are non-bridging and face the pore. Most of the lattice water is disordered and resides in the pore. In the asymmetric unit, only one lattice water molecule is immobilized by forming bidirectional hydrogen bonds with two non-bridging cyano groups (Fig. 2). The as-synthesized compound **1** exhibited ferromagnetic ordering at 8.5 K based on the strict orthogonality of magnetic orbitals of Ni^{2+} and low-spin Fe^{3+}. After vacuum treatment at room temperature, a dehydrated form, $[Ni(dipn)]_2[Ni(dipn)(H_2O)][Fe(CN)_6]_2 \cdot H_2O$ (**1a**), was obtained and this form showed amorphous-like XRPD patterns and paramagnetic behaviour (Fig. 3). The dehydrated form **1a** adsorbed water at room temperature with a high maximum uptake of 9.93 mol/mol. The rehydrated form (**1b**) showed the same XRPD pattern and magnetic behaviour of the initial form **1** (Fig. 3). The reversible crystal-to-amorphous-like phase transformation could be performed repeatedly by water desorption/adsorption. In contrast, the anhydrous form, $[Ni(dipn)]_3[Fe(CN)_6]_2$ (**1c**), was an amorphous paramagnet and did not recover the initial crystallinity and ferromagnetic phase upon exposure to gaseous water or immersion in water.

The flexible Fe – CN – Ni linkage, bidirectional hydrogen bonds between lattice water molecules and non-bridging cyano nitrogen atoms play crucial roles in the reversible structural and magnetic conversion. Other porous cyanide-bridged magnetic frameworks, *e.g.* $Cu_3[W(CN)_8](pym)_2 \cdot 8H_2O$ (pym = pyrimidine),[31] $\{[Mn(HL)(H_2O)]_2Mn[Mo(CN)_7]_2\} \cdot 2H_2O$ (L = *N,N*-dimethylalaninol)[33] and $\{[Ni(cyclam)]_3[W(CN)_8]_2\} \cdot 16H_2O$ (cyclam = 1,4,8,11-tetraazacyclotetradecane)[34] have been reported, and showed both porous and magnetic properties. These results demonstrate the viability of our strategy of using a polycyanometallate and co-ligands for the construction of porous magnetic frameworks.

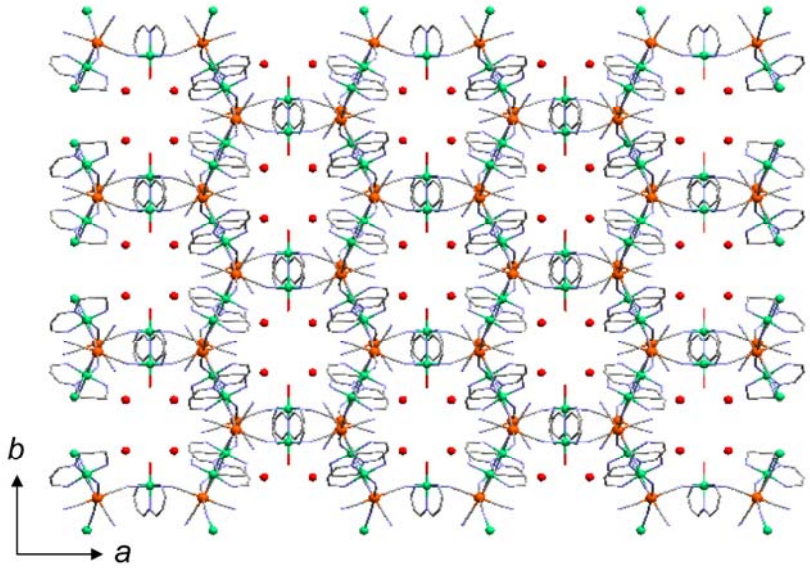

Fig. 1. Projection of **1** onto the *ab* plane. Disordered lattice water molecules are omitted. Atoms: Fe (orange), Ni (green), O (red), N (light blue), C (gray).

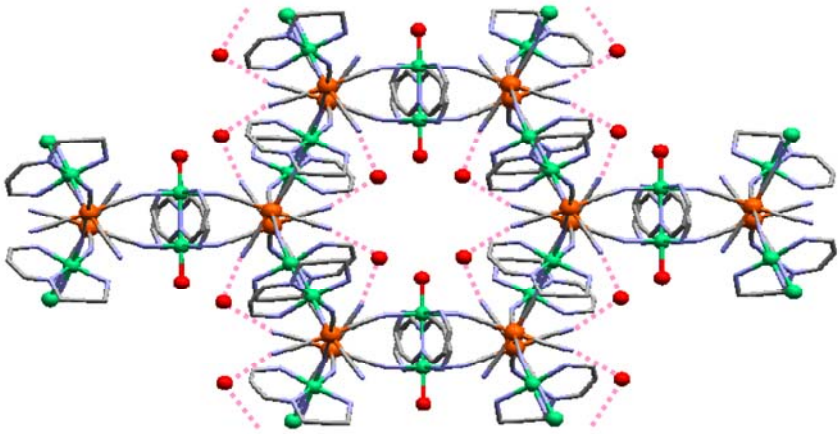

Fig. 2. Bidirectional hydrogen bonds (pink dotted lines) between lattice water molecules and non-bridging cyano groups.

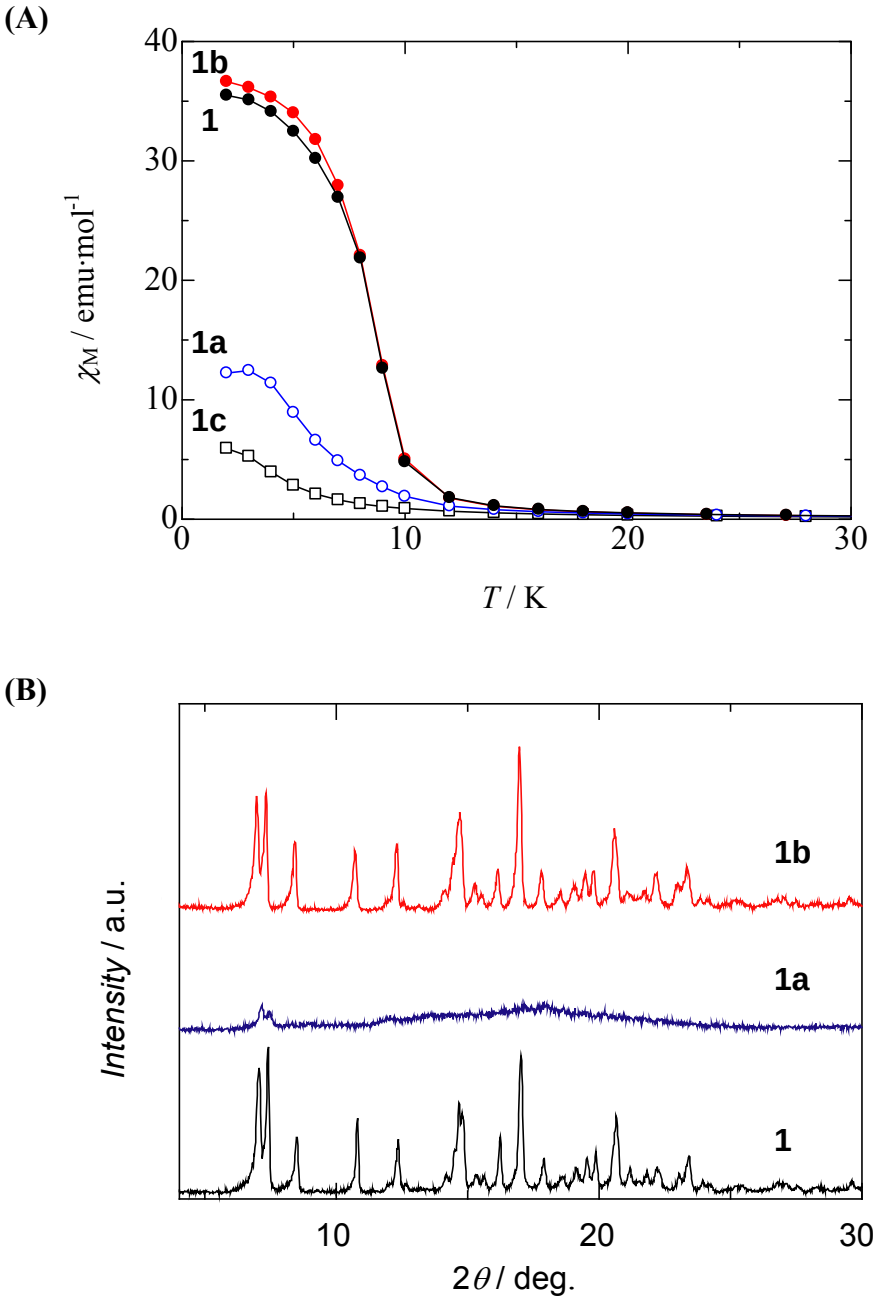

Fig. 3. Temperature dependences of χ_M for the initial form **1** (●), the dehydrated form **1a** (○), the rehydrated form **1b** (●) and the anhydrous form **1c** (□) in an applied dc field of 500 Oe **(A)** and the corresponding XRPD patterns **(B)**.

$[Mn(HL)(H_2O)][Cr(CN)_6]H_2O$ (2)

Compound **2** was prepared as pale-green crystals by reaction of $K_3[Cr(CN)_6]$, $MnCl_2{\cdot}4H_2O$ and co-ligand L (NNdmen) in a deoxygenated aqueous solution at room temperature.[30] The asymmetric unit of **2** consists of $[Mn(HL)(H_2O)]^{3+}$ cation, $[Cr(CN)_6]^{3-}$ anion and a lattice water molecule. In the lattice the compound forms a 2-D layer structure extended by Cr – CN – Mn linkages (Fig. 4a). Four cyano nitrogen atoms in the equatorial positions of $[Cr(CN)_6]^{3-}$ coordinate to adjacent Mn^{2+} ions, and the other two in axial positions, are non-bridging. One protonated co-ligand and one water molecule are located at the axial positions of the Mn^{2+} ion as monodentate ligands. The coordinated water molecules form Mn – OH_2···NC – Cr hydrogen bonds with non-bridging cyano groups in the next layer (Fig. 5a). The hydrogen bonds adjust the topology between layers. A dehydrated form, $[Mn(HL)][Cr(CN)_6]$ (**2a**), was obtained as a single crystal by careful heating of **2** at 343 K. After dehydration, the 2-D structure was changed to a 3-D framework, in which the coordinated water molecules were eliminated and extra Cr – CN – Mn bridges were generated between neighbouring sheets through topochemical solid-state reactions (Figs. 4b and 5b). The dehydrated form has a very narrow 1-D channel based on a highly distorted Mn_2Cr_2 quadrangular gate (0.8 × 1.6 $Å^2$ based on van der Waals radii). The initial form exhibited ferrimagnetic ordering with a T_c of 35.2 K, and the T_c was shifted to 60.2 K by dehydration because of increments in the magnetic interaction pathways and correlation dimensions (Fig. 6). Upon exposure to air or water vapour at 303 K, **2a** immediately reproduced the same XRPD pattern as **2**. The dehydrated form smoothly adsorbed water (2.3 mol/mol) with a large hysteresis because of the restoration of the 2-D structure, including replacement of the extra cyanide bridges to water molecules. In addition, **2a** showed size-selective solvent adsorption, linking chemi- and physisorption processes. The rehydrated form, **2b**, recovered the initial structure and magnetic behaviour of **2**. The structure and magnetic characteristics could be converted repeatedly by dehydration/rehydration processes and topochemical reactions.

Analogues using other co-ligands, 1,2-propanediamine (pn)[60,64] and ethylenediamine (en),[65,66] also show similar 2-D/3-D conversion with shifting T_c. In addition, conversions between the 0-D paramagnet and 2-D ferromagnet of $[K(18\text{-crown-}6)(MeOH)_2][Mn(L)(H_2O)(MeOH)]_2[Fe(CN)_6]{\cdot}MeOH$ (L = *N*,*N*'-ethylene-di(5-chlorosalicylideneaminate)[21] and between the 1-D metamagnet and 2-D ferromagnet of $[Ni(dmen)_2][Ni(dmen)_2(H_2O)][Fe(CN)_6](bpds)_{0.5}{\cdot}3H_2O$ (dmen = 1,1-dimethylethylenediamine, $bpds^{2-}$ = 4,4'-biphenyldisulfonate)[23] have been reported, based on the same strategy using hexacyanometallates. These compounds provide a

flexible magnetic framework incorporating removable solvent co-ligands, and deliver structural and magnetic transformations in response to solvation/desolvation. The initial structures are stabilized thermodynamically using solvent co-ligands to avoid forming closed-packed structures. Each independent framework is interlinked to adjacent framework(s) through hydrogen bonds formed between solvent co-ligands and non-bridging cyano groups. The metastable desolvated form is obtained by topochemical solid-state reaction directed by the hydrogen bonds, and cannot retain its structure under the solvent vapour. Steric repulsion in the desolvated form would be a key driving force to recover the initial structure. From this perspective, the primary building units, $[M_A(CN)_n]^{m-}$, are advantageous for constructing guest-responsive (solvato-responsive) magnetic systems, because they: (1) contain extendable and flexible cyanide bridges; (2) are good magnetic mediators; (3) are able to form hydrogen bond with protonic solvent molecules; and (4) are moderately bulky for generating steric repulsion with co-ligands in adjacent SBUs.

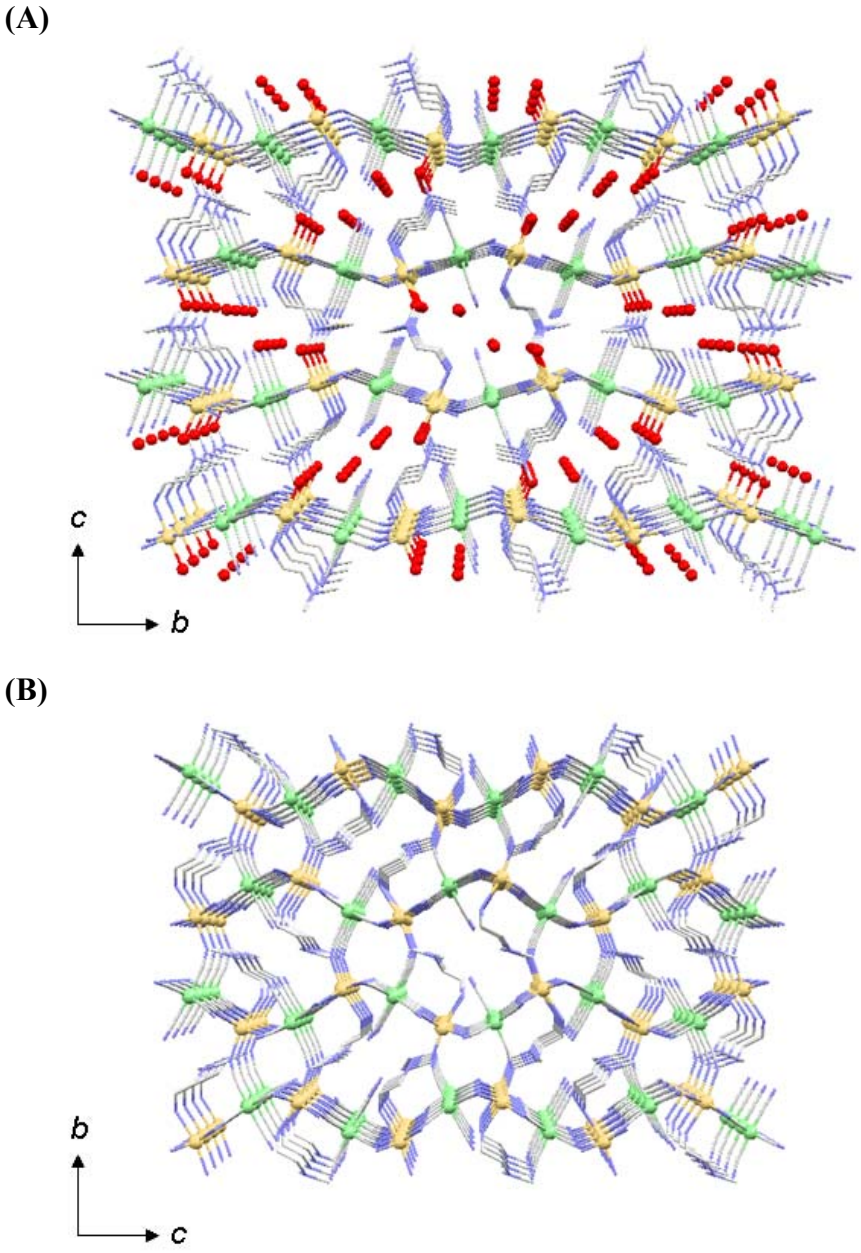

Fig. 4. Projections of the initial form **2** onto the *bc* plane **(A)** and of the dehydrated form **2a** onto the *bc* plane **(B)**. Atoms: Cr (green), Mn (yellow), O (red), N (light blue), C (gray).

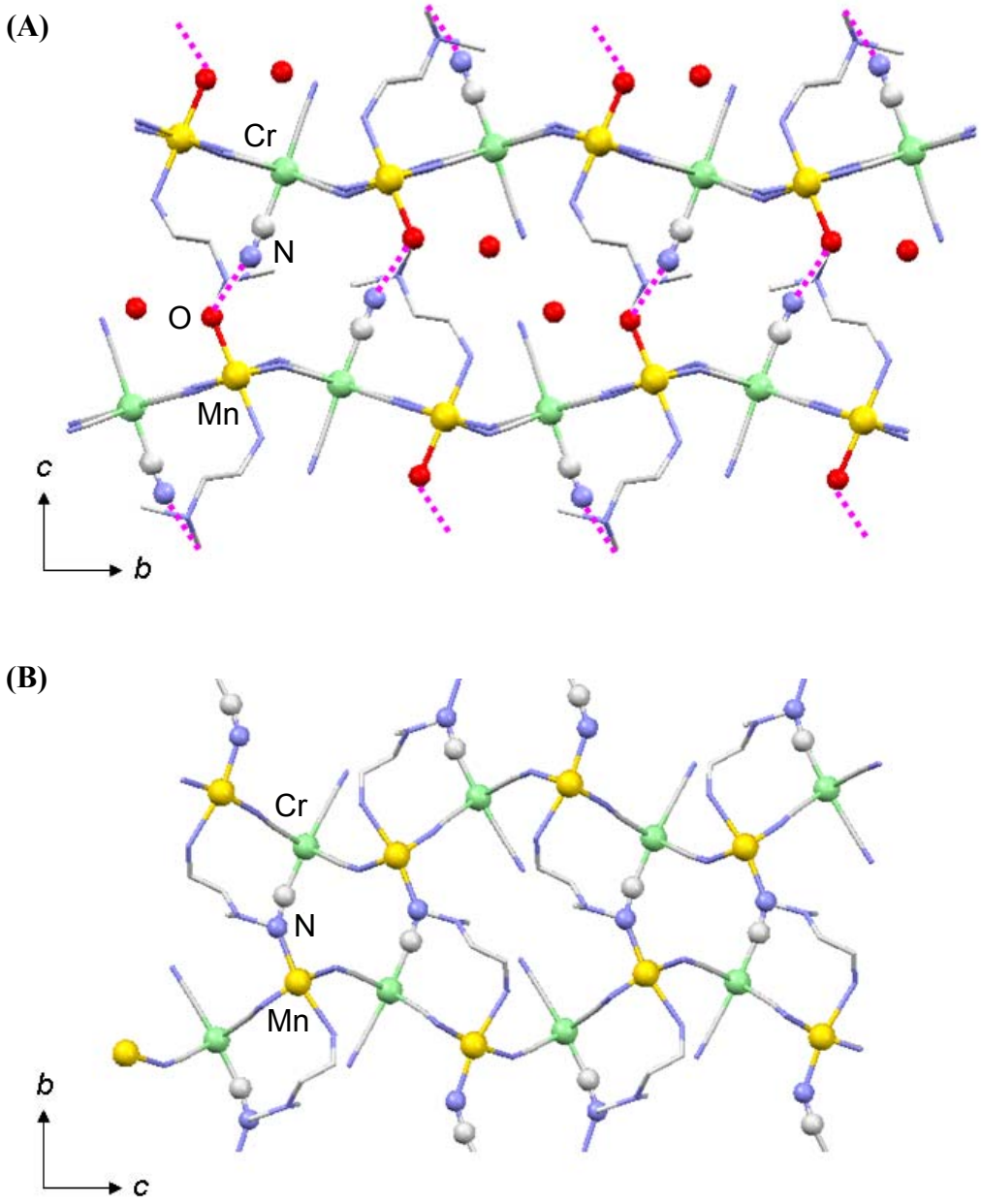

Fig. 5. Reversible topochemical structural transformation between **2 (A)** and **2a (B)**. Hydrogen bonds are denoted by pink dotted lines.

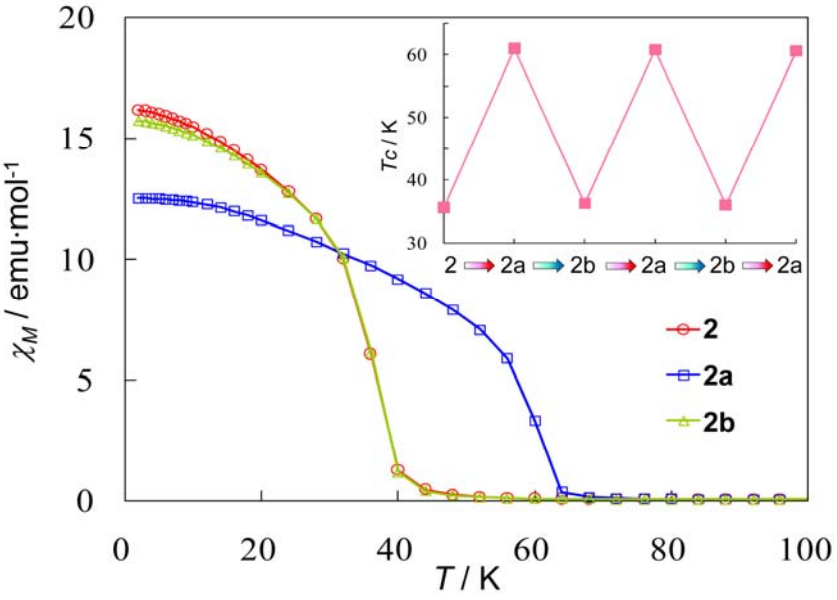

Fig. 6. Temperature dependences of χ_M for the initial form **2** (○), the dehydrated form **2a** (□) and the rehydrated form **2b** (Δ) in an applied dc field of 500 Oe. The insert shows the reversible T_c switching by dehydration/hydration treatments (red/blue arrows, respectively).

{Fe(pz)[Pt(CN)$_4$]}2H$_2$O (3)

Spin crossover (SCO) is a well-known phenomenon in which electron configurations can be switched between high-spin (HS) and low-spin (LS) states in response to external stimuli (temperature, pressure and light irradiation), producing changes in magnetism, colour and structure.[1,12,67–74] A number of SCO compounds have been elaborated, with control of their spin states in molecules and molecular assemblies, and some have successfully exhibited bistable states around room temperature.[75,76]

As mentioned above, guest-responsive magnetic conversion in PCPMs and CPMs has been reported but there is a large gap in working temperature between guest adsorption/desorption and the magnetic ordering temperature T_c. The SCO phenomenon would be one solution to overcome this temperature problem instead of ordered magnetism. PCPs incorporating SCO centres (SCO–PCP) may propagate the SCO cooperatively to the whole framework. Such SCO–PCPs may raise T_c and undergo first- order hysteretic spin transition (ST) producing a bistable state in the framework, which is expected to exhibit a guest-responsive SCO. Two representative SCO–PCPs, [Fe^{II}L$_2$(NCS)$_2$]·*n*S (L = 1,2-bis(4-pyridyl)ethylene,[77,78] *trans*-4,4'-azopyridine,[79] *DL*-1,2-bis(4-pyridyl)-1,2-ethanediol;[80] S = alcohol molecule), and {Fe(pym)(H$_2$O)[M^{I}(CN)$_2$]$_2$}H$_2$O,[81] have been reported by Real *et al*. and Kepert *et al*. These examples clearly display guest-responsive SCO, however, the SCO and guest adsorption-desorption are still not simultaneous. One of the ideal SCO–PCP, {Fe(pz)[Pt(CN)$_4$]·2H$_2$O} (**3**), using [Pt(CN)$_4$]$^{2-}$ and pyrazine (pz) co-ligand has been reported by Real et al.[63,76,82–87] Compound **3** forms a 3-D Hofmann-like framework, in which pz forms rigid bridges between Fe ions as pillars linking the 2-D layers extended by Pt – CN – Fe linkages and forms channels with square Fe$_2$Pt$_2$ windows (Fig. 7A). Note that this framework provides two guest-interactive sites: one between the pz bridges (site A) and another between the Pt centres (site B) (Fig. 7B). These features should be important *a priori* for the chemical response of the framework. This compound displays a first-order ST with *ca*. 25 K-wide hysteresis, with $T_{c\downarrow}$ of 285 K and $T_{c\uparrow}$ of 309 K. The solvent-accessible voids of the LS and HS states were estimated to be 18.1 % and 22.4 %, respectively. The guest-free form **3a** adsorbs various guest molecules in the gas phase or solution, and forms their clathrates. The spin state changes, depending on the guest molecules. *In situ* magnetic measurements following guest vapour injection elucidates the simultaneous guest adsorption and bidirectional spin transition (Fig. 8). Most guest molecules transform **3a** from the low-spin (LS) state to the high-spin (HS) state, whereas CS$_2$ stabilizes the LS state exceptionally.

The induced spin states are retained after removing guest molecules, and both spin states are interchangeable by exchanging guest molecules with controlled vapour pressure. The guest molecules studied can be grouped into three major classes (Table 2), where class I shows no effect on the spin state; class II stabilizes the HS state; and class III stabilizes the LS state. Structures of pz and CS_2 clathrates reveal that: (i) the pz guest molecules are located exclusively at site A; and (ii) the CS_2 molecules are located at sites A and B. These systematic structural and magnetic results point to three key factors for stabilizing the spin states: (1) the size and shape of the guest (G); (2) the G···pz interaction at site A; and (3) the G···Pt interaction at site B. Theoretical calculation of binding energies between CS_2 and each site suggests that the CS_2 molecule interacts suitably with both sites, like a key molecule for the framework.[63] Compound **3** successfully delivers a desired magnetic switch in response to guest molecules at room temperature. The porous SCO framework is constructed by three functional components; (1) SCO Fe(II) ions as framework joints; (2) flat tetracyanometallate, $[M(CN)_4]^{2-}$ (M^{II} = Pt, Pd, Ni), providing guest-accessible sites (site B) and forming flexible M – CN – Fe linkages; and (3) pyrazine co-ligands as rigid pillars and guest-interactive sites (site A) (Fig. 7). A well-designed simple framework gives appropriate interactive pores and allows the spin transition coupled to guest adsorption/desorption while retaining its cooperativity.

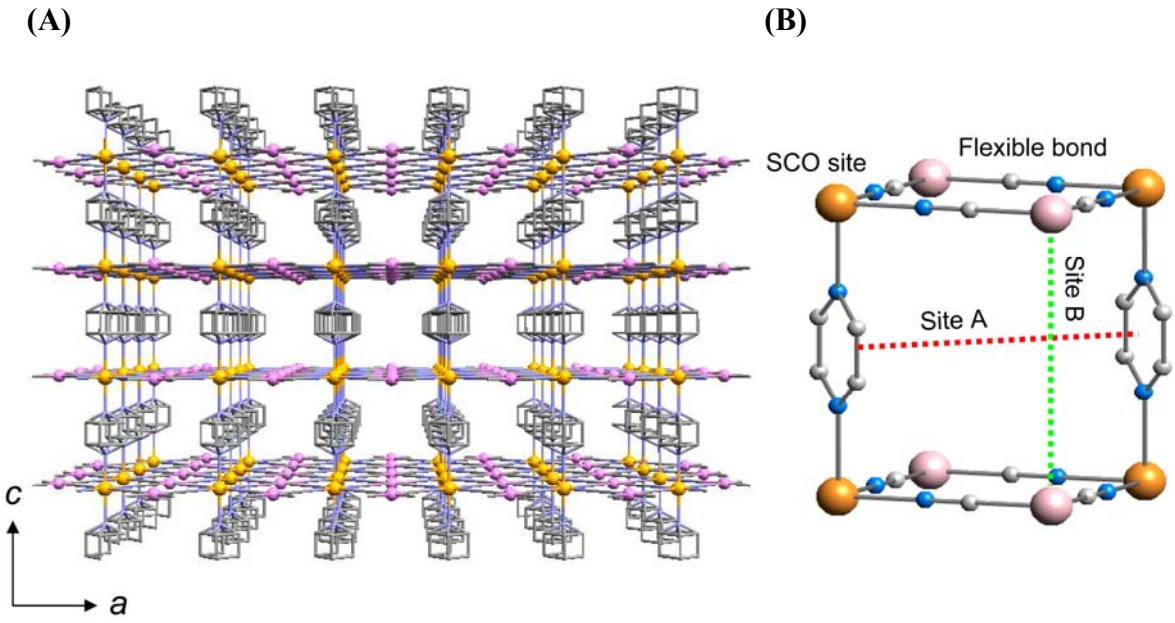

Fig. 7. Projection of **3** onto the *ac* plane **(A)** and the functional cavity structure of **3 (B)**. Lattice water molecules are omitted. Atoms: Fe (orange), Pt (pink), N (light blue), C (gray).

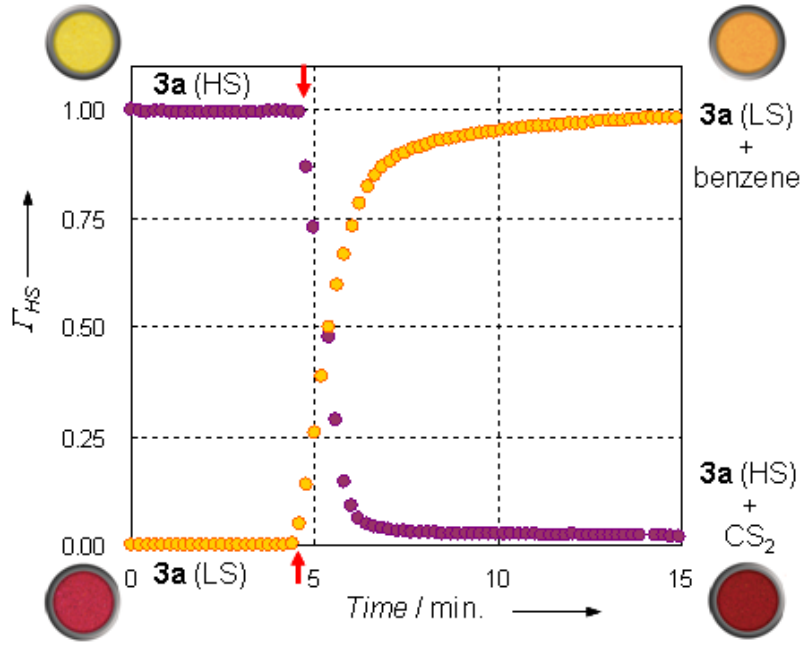

Fig. 9. Time dependence of the HS fraction of **3a** under a benzene (yellow) and CS_2 (purple) atmosphere at 293 K. Red arrows indicate the starting points of guest injection (valve opening). The color circles are photos of samples.

Table 1. Crystal parameters of compounds **1**, **2**, **2a**, **3**(HS) and **3**(LS)

Compound	**1**	**2**	**2**
Formula	$C_{30}H_{75}N_{21}Fe_2Ni_3O_{12}$	$C_{10}H_{17}N_8CrMnO_2$	$C_{10}H_{13}N_8CrMn$
Formula Weight	1209.82	388.23	352.20
No. of water	12	2	0
Crystal System	monoclinic	monoclinic	monoclinic
Space Group	*C*2/c (#15)	$P2_1$/n (#11)	$P2_1$/c (#13)
a / Å	24.044(8)	7.681(3)	7.85(1)
b / Å	14.343(4)	14.498(5)	14.31(3)
c / Å	16.688(5)	16.598(6)	12.97(2)
β / deg	100.552(4)	97.326(5)	90.10(3)
V / Å^3	5657(3)	1833.0(10)	1456.2(4)
R	0.0630	0.0612	0.0957
Rw	0.2050	0.792	0.1146
D_{calc} / g·cm^{-3}	1.421	1.407	1.606
D_{calc} / g·cm^{-3} (without lattice water)	1.188	1.341	1.606
Solvent-accessible Void /%	28.2	5.2	0

Compound	**3**(HS)	**3**(LS)
Formula	$C_8H_8N_6FePtO_2$	$C_8H_8N_6FePtO_2$
Formula Weight	471.11	471.11
No. of water	2	2
Crystal System	tetragonal	tetragonal
Space Group	*P*4/mmm (#123)	*P*4/mmm (#123)
a = *b* / Å	7.457(4)	7.184(6)
c / Å	7.259(4)	6.783(5)
V / Å^3	403.6(4)	350.1(5)
R	0.0472	0.0494
Rw	0.0844	0.737
D_{calc} / g·cm^{-3}	1.938	2.234
D_{calc} / g·cm^{-3} (without lattice water)	1.790	2.064
Solvent-accessible Void /%	22.4	18.1

Conclusion

As shown above, the triad of polycyanometallate, SBU and co-ligand demonstrates the viability of our approach for guest-responsive magnetic frameworks. In the case of PCPMs **1** and **2**, hexacyanometallates work as good linkers and magnetic mediators, but the low T_c remains an issue even now. Guest adsorption and magnetic ordering are not simultaneous events in these compounds. It is necessary to shift the coexistence phase of magnetic and porous properties to a cooperative phase. A more elaborate porous magnetic framework that transcribes a backbone of PBAs with high T_c, *e.g.,* $M^{II}_3[Cr(CN)_6]nH_2O$ (T_c = 240 K for M = Cr, 315 K for M = V),[48,50] would overcome the temperature problem. Recently, Sutter et al. reported a PCPM, $\{[Mn(HL)(H_2O)]_2Mn[Mo(CN)_7]_2\}2H_2O$ (L = *N,N*-dimethylalaninol),[33] which provides ring-shaped channels with potential void of 9.2% and exhibits ferrimagnetic ordering at 106 K in a dehydrated form. This compound presents high potential as a polycyanometallate PCPM constituent. Such PCPMs with high T_c would exhibit a unique synergy between the magnetic properties and guest molecules, *e.g.,* paramagnetic, chiral or polar guests. On the other hand, the SCO–PCP $\{Fe(pz)[Pt(CN)_4]\}$ (**3**) successfully delivered magnetic chemo-switching at room temperature that will open a route to evolve into new environmentally responsive PCP materials. Control of the interactions between the SCO framework and guest molecules will allow precise and universal magnetic switching. As the next step, more advanced functions, *e.g.*, selective guest adsorption and separation, or externally controlled uptake and release of guest molecules, may be implemented using SCO–PCPs with shape-, volume- and chirality-changeable pores depending on the spin state.

Experimental

Crystallographic Data Collection and Refinement of the Structure

X-ray diffraction data of **1**, **2** and **2a** were colleted on on a Rigaku Mercury CCD system, while **3**(HS) and **3**(LS) were collected on a Rigaku Varimax CCD system. In all cases, graphite-monochromated Mo-Kα radiation (λ = 0.71070 Å) was used. A single crystal was mounted on a fiber loop with liquid paraffin and the temperature kept constant under flowing N_2. Crystal parameters are listed in Table 1. All the structures were solved by a standard direct method and expanded using Fourier techniques. Full-matrix least-squares refinements were carried out using Crystal Clear 1.4. (crystallographic software package of the Molecular Structure Corp. and Rigaku) for **1**, **3**(HS) and **3**(LS) and teXsan (crystal structure analysis package of the Molecular Structure Corp.) for **2** and **2a**, with anisotropic thermal parameters for all non-hydrogen atoms. All of the hydrogen atoms were placed in the calculated positions and refined using a riding model.

Physical Measurements

Variable-temperature X-ray powder diffraction was carried out on a Rigaku RINT-2000 Ultima diffractometer with Cu-Kα radiation. Thermogravimetric analyses were recorded on a Rigaku Thermo plus TG 8120 apparatus in the temperature range between 300 and 700 K under a nitrogen atmosphere at a heating rate of 1 K min^{-1}. Magnetic susceptibilities of all samples were measured on a Quantum Design MPMS-XL5R SQUID susceptometer in the temperature range 2 − 300 K in an applied dc field of 500 Oe. The samples were placed in a glass tube and fixed to the end of the sample transport rod. Dehydrated samples were prepared by vacuuming for 2 h in the SQUID sample chamber at 400 K. The guest molecules were injected into the glass tube through the sample transport rod with controlling its vapor pressure at 293 K. The molar magnetic susceptibility, χ_M, was corrected for the diamagnetism of the constituent atoms.

References

1. O. Kahn, *Molecular Magnetism*, **1993**.
2. J. S. Miller, M. Drillon, *Magnetism: Molecules to Materials*, **2001**.
3. D. Gatteschi, R. Sessoli, *Angew. Chem. Int. Ed*., **2003**, *42*, 268.
4. Y. Pei, M. Verdaguer, O. Kahn, J. Sletten, J. P. Renard, *J. Am. Chem. Soc*., **1986**, *108*, 7428.
5. J. S. Miller, J. C. Calabrese, H. Rommelmann, S. R. Chittipeddi, J. H. Zhang, W. M. Reiff, A. J. Epstein, *J. Am. Chem. Soc*., **1987**, *109*, 769.
6. A. Caneschi, D. Gatteschi, R. Sessoli, P. Rey, *Acc. Chem. Res*., **1988**, *22*, 392.
7. O. Sato, T. Iyoda, A. Fujishima, K. Hashimoto, *Science*, **1996**, *272*, 704.
8. M. Verdaguer, *Science*, **1996**, *272*, 698.
9. S. I. Ohkoshi, K. Hashimoto, *J. Am. Chem. Soc*., **1999***, 121*, 10591.
10. Y. Arimoto, S. I. Ohkoshi, Z. J. Zhong, H. Seino, Y. Mizobe, K. Hashimoto, *J. Am. Chem. Soc*., **2003**, *125*, 9240.
11. S. I. Ohkoshi, H. Tokoro, K. Hashimoto, *Coord. Chem, Rev*., **2005**, *249*, 1830.
12. O. Sato, J. Tao, Y. Z. Zhang, *Angew. Chem. Int. Ed*., **2007**, *46*, 2152.
13. K. Awaga, T. Sekine, M. Ōkawa, W. Fujita, S. M. Holmes, G. S. Girolami, *Chem. Phys. Lett*., **1998**, *293*, 352.
14. M. Mito, T. Kawae, K. Takeda, S. Takagi, Y. Matsushita, H. Deguchi, J. M. Rawson, F. Palacio, *Polyhedron*, **2001**, *20*, 1509.
15. V. Ksenofontov, G. Levchenko, S. Reiman, P. Gütlich, A. Bleuzen, V. Escax, M. Verdaguer, *Physical Review B - Condensed Matter and Materials Physics*, **2003**, *68*, 244151.
16. E. Coronado, M. C. Giménez-López, G. Levchenko, F. M. Romero, V. García-Baonza, A. Milner, M. Paz-Pasternak, *J. Am. Chem. Soc*., **2005**, *127*, 4580.
17. W. Kaneko, M. Mito, S. Kitagawa, M. Ohba, *Chem.-Eur. J*., **2008**, *14*, 3481.
18. M. Ohba, W. Kaneko, S. Kitagawa, T. Maeda, M. Mito, *J. Am. Chem. Soc*., **2008**, *130*, 4475.
19. J. Larionova, S. A. Chavan, J. V. Yakhmi, A. G. Frøystein, J. Sletten, C. Sourisseau, O. Kahn, *Inorg. Chem*., **1997**, *36*, 6374.
20. H. Miyasaka, N. Matsumoto, N. Re, E. Gallo, C. Floriani, *Inorg. Chem*., **1997**, *36*, 670.
21. H. Miyasaka, H. Ieda, N. Matsumoto, N. Re, R. Crescenzi, C. Floriani, *Inorg. Chem*., **1998**, *37*, 255.
22. O. Kahn, J. Larionova, J. V. Yakhmi, *Chem.-Eur. J.*, **1999**, *5*, 3443.

23. N. Usuki, M. Ohba, H. Ōkawa, *Bull. Chem. Soc. Jpn*., **2002**, *75*, 1693.
24. D. Maspoch, D. Ruiz-Molina, K. Wurst, N. Domingo, M. Cavallini, F. Biscarini, J. Tejada, C. Rovira, J. Veciana, *Nature Mater.*, **2003**, *2*, 190.
25. S. I. Ohkoshi, K. I. Arai, Y. Sato, K. Hashimoto, *Nature Mater.*, **2004**, *3*, 857.
26. Z. Wang, B. Zhang, H. Fujiwara, H. Kobayashi, M. Kurmoo, *Chem. Commun*., **2004**, *10*, 416.
27. M. Kurmoo, H. Kumagai, K. W. Chapman, C. J. Kepert, *Chem. Commun*., **2005**, 3012.
28. H. B. Cui, K. Takahashi, Y. Okano, H. Kobayashi, Z. Wang, A. Kobayashi, *Angew. Chem. Int. Ed.*, **2005**, *44*, 6508.
29. N. Yanai, W. Kaneko, K. Yoneda, M. Ohba, S. Kitagawa, *J. Am. Chem. Soc*., **2007**, *129*, 3496.
30. W. Kaneko, M. Ohba, S. Kitagawa, *J. Am. Chem. Soc*., **2007**, *129*, 13706.
31. S. I. Ohkoshi, Y. Tsunobuchi, H. Takahashi, T. Hozumi, M. Shiro, K. Hashimoto, *J. Am. Chem. Soc*., **2007**, *129*, 3084.
32. Z. Wang, Y. Zhang, T. Liu, M. Kurmoo, S. Cao, *Adv. Funct. Mater.*, **2007**, *17*, 1523.
33. J. Milon, M. C. Daniel, A. Kaiba, P. Guionneau, S. Brandés, J. P. Sutter, *J. Am. Chem. Soc.*, **2007**, *129*, 13872.
34. B. Nowicka, M. Rams, K. Stadnicka, B. Sieklucka, *Inorg. Chem*., **2007**, *46*, 8123.
35. E. Coronado, D. Gatteschi, *J. Mater. Chem.*, **2006**, *16*, 2513.
36. S. Kitagawa, R. Kitaura, S. -I. Noro, *Angew. Chem. Int. Ed.*, **2004**, *43*, 2334.
37. N. R. Champness, *Dalton Transactions*, **2006**, 877.
38. M. Yaghi, M. O'Keeffe, N. W. Ockwig, H. K. Chae, M. Eddaoudi, J. Kim, *Nature*, **2003**, *423*, 705.
39. J. L. C. Rowsell, O. M. Yaghi, *Microporous Mesoporous Mater*., **2004**, *73*, 3.
40. M. J. Rosseinsky, *Microporous Mesoporous Mater.*, **2004**, *73*, 15.
41. G. Férey, C. Mellot-Draznieks, C. Serre, F. Millange, J. Dutour, S. Surblé, I. Margiolaki, *Science*, **2005**, *309*, 2040.
42. J. F. Eubank, V. C. Kravtsov, M. Eddaoudi, *J. Am. Chem. Soc.*, **2007**, *129*, 5820.
43. G. Férey, *Chem. Soc. Rev*., **2008**, *37*, 191.
44. K. Uemura, S. Kitagawa, M. Kondo, K. Fukui, R. Kitaura, H. C. Chang, T. Mizutani, *Chem.-Eur. J*., **2002**, *8*, 3586.
45. R. Matsuda, R. Kitaura, S. Kitagawa, Y. Kubota, T. C. Kobayashi, S. Horike, M. Takata, *J. Am. Chem. Soc*., **2004**, *126*, 14063.
46. J. Kepert, *Chem. Commun*., **2006**, 695.
47. D. Maspoch, D. Ruiz-Molina, J. Veciana, *Chem. Soc. Rev*., **2007**, *36*, 770.

48. T. Mallah, S. Thiebaut, M. Verdaguer, P. Veillet, *Science*, **1993**, *262*, 1554.
49. M. Verdaguer, A. Bleuzen, V. Marvaud, J. Vaissermann, M. Seuleiman, C. Desplanches, A. Scuiller, C. Train, R. Garde, G. Gelly, C. Lomenech, I. Rosenman, P. Veillet, C. Cartier, F. Villain, *Coord. Chem. Rev.*, **1999**, *190-192*, 1023.
50. S. Ferlay, T. Mallah, R. Ouahés, P. Veillet, M. Verdaguer, *Nature*, **1995**, *378*, 701.
51. S. S. Kaye, H. J. Choi, J. R. Long, *J. Am. Chem. Soc*., **2009**, *130*, 16921.
52. S. S. Kaye, J. R. Long, *J. Am. Chem. Soc*., **2005**, *127*, 6506.
53. K. W. Chapman, P. D. Southon, C. L. Weeks, C. J. Kepert, *Chem. Commun*., **2005**, 3322.
54. M. Ohba, H. Ōkawa, *Coord. Chem. Rev.*, **2000**, *198*, 313.
55. H. Ōkawa, M. Ohba, *Bull. Chem. Soc. Jpn*., **2002**, *75*, 1191.
56. M. Ohba, N. Maruono, H. Ōkawa, T. Enoki, J. M. Latour, *J. Am. Chem. Soc*., **1994**, *116*, 11566.
57. M. Ohba, H. Ōkawa, N. Fukita, Y. Hashimoto, *J. Am. Chem. Soc*., **1997**, *119*, 1011.
58. M. Ohba, N. Usuki, N. Fukita, H. Ōkawa, *Angew. Chem. Int. Ed*., **1999**, *38*, 1795.
59. K. Inoue, H. Imai, P. S. Ghalsasi, K. Kikuchi, M. Ohba, H. Kawa, J. V. Yakhmi, *Angew. Chem. Int. Ed*., **2001**, *40*, 4242.
60. K. Inoue, K. Kikuchi, M. Ohba, H. Ōkawa, *Angew. Chem. Int. Ed*., **2003**, *42*, 4810.
61. T. Shiga, H. Ōkawa, S. Kitagawa, M. Ohba, *J. Am. Chem. Soc*., **2006**, *128*, 16426.
62. W. Kaneko, S. Kitagawa, M. Ohba, *J. Am. Chem. So*c., **2007**, *129*, 248.
63. M. Ohba, K. Yoneda, G. Agustí, M. C. Muñoz, A. B. Gaspar, J. A. Real, M. Yamasaki, H. Ando, Y. Nakao, S. Sakaki, S. Kitagawa, *Angew. Chem. Int. Ed*., **2009**, *48*, 4767.
64. Y. Yoshida, K. Inoue, M. Kurmoo, *Chem. Let*t., **2008**, *37*, 586.
65. Y. Yoshida, K. Inoue, M. Kurmoo, *Chem. Lett*., **2008**, *37*, 504.
66. Y. Yoshida, K. Inoue, M. Kurmoo, *Inorg. Chem*., **2009**, *48*, 267.
67. "Spin Crossover in Transition Metal Compounds" (Eds: P. Gütlich, H. A. Goodwin), Top. Curr. Chem., **2004**, *233-235*.
68. J. A. Real, A. B. Gaspar, M. Carmen Muñoz, *Dalton Transactions*, **2005**, 2062.
69. H. Spiering, T. Kohlhaas, H. Romstedt, A. Hauser, C. Bruns-Yilmaz, J. Kusz, P. Gütlich, *Coord. Chem. Rev.*, **1999**, *629*, 190.
70. S. Hayami, R. Kawajiri, G. Juhász, T. Kawahara, K. Hashiguchi, O. Sato, K. Inoue, Y. Maeda, *Bull. Chem. Soc. Jpn*., **2003**, *76*, 1207.
71. P. Gütlich, A. Hauser, H. Spiering, *Angew. Chem. Int. Ed*., **1994**, *33*, 2024.
72. P. Gütlich, Y. Garcia, T. Woike, *Coord. Chem. Rev.*, **2001**, *219-221*, 839.
73. J. A. Real, A. B. Gaspar, V. Niel, M. C. Muñoz, *Coord. Chem. Rev*., **2003**, *236*, 121.

74. A. Hauser, J. Jeftic, H. Romstedt, R. Hinek, H. Spiering, *Coord. Chem. Rev*., **1999**, *190-192*, 471.
75. O. Kahn, C. J. Martinez, *Science*, **1998**, *279*, 44.
76. V. Niel, J. M. Martinez-Agudo, M. C. Muñoz, A. B. Gaspar, J. A. Real, *Inorg. Chem*., **2001**, *40*, 3838.
77. J. A. Real, E. Andrés, M. C. Muñoz, M. Julve, T. Granier, A. Bousseksou, F. Varret, *Science*, **1995**, *268*, 265.
78. J. Halder, K. W. Chapman, S. M. Neville, B. Moubaraki, K. S. Murray, J.-F. Létard, C. J. Kepert, *J. Am. Chem. Soc*., **2008**, *130*, 17552.
79. J. Halder, C. J. Kepert, B. Moubaraki, K. S. Murray, J. D. Cashion, *Science*, **2002**, *298*, 1762.
80. S. M. Neville, G. J. Halder, K. W. Chapman, M. B. Duriska, P. D. Southon, J. D. Cashion, J.-F. Létard, B. Moubaraki, K. S. Murray, C. J. Kepert, *J. Am. Chem. Soc*., **2008**, *130*, 2869.
81. V. Niel, A. L. Thompson, M. C. Muñoz, A. Galet, A. E. Goeta, J. A. Real, *Angew. Chem. Int. Ed*., **2003**, *42*, 3760.
82. S. Cobo, D. Ostrovskii, S. Bonhommeau, L. Vendier, G. Molnár, L. Salmon, K. Tanaka, A. Bousseksou, *J. Am. Chem. Soc.*, **2008**, *130,* 9019.
83. Molnár, S. Cobo, J. A. Real, F. Carcenac, E. Daran, C. Vieu, A. Bousseksou, *Adv. Mater*., **2007**, *19*, 2163.
84. S. Bonhommeau, G. Molnár, A. Galet, A. Zwick, J. A. Real, J. J. McGarvey, A. Bousseksou, *Angew. Chem. Int. Ed*., **2005**, *44*, 4069.
85. T. Tayagaki, A. Galet, G. Molnár, M. C. Muñoz, A. Zwick, K. Tanaka, J. A. Real, A. Bousseksou, *J. Phys. Chem. B*, **2005**, *109*, 14859.
86. I. Boldog, A. B. Gaspar, V. Martínez, P. Pardo-Ibáñez, V. Ksenofontov, A. Bhattacharjee, P. Gütlich, J. A. Real, *Angew. Chem. Int. Ed.*, **2008**, *47*, 6433.
87. F. Volatron, L. Catala, E. Rivière, A. Gloter, O. Stéphan, T. Mallah, *Inorg. Chem*., **2008**, *47*, 6584.

List of Publications

Chapter 1

Three-dimensional Ferromagnetic Frameworks of *Syn-Anti*-type Carboxylate-bridged Ni^{II} and Co^{II} Coordination Polymers

Ko Yoneda, Masaaki Ohba, Takuya Shiga, Hiroki Oshio, Susumu Kitagawa

Chem. *Lett*. **2007**, *36*, 1184–1185.

Chapter 2

A Homometallic Ferrimagnet Based on Mixed Antiferromagnetic and Ferromagnetic Interactions through Oxamato and Carboxylato Bridges

Ko Yoneda, Yukari Hori, Masaaki Ohba, Susumu Kitagawa

Chem. *Lett*. **2008**, *37*, 64–65.

Chapter 3

A steep one-step [HS–HS] to [LS–LS] spin transition in a 4,4'-bipyridine linked one-dimensional coordination polymer constructed from a pyrazolato bridged Fe(II) dimmer

Ko Yoneda, Keiichi Adachi, Shinya Hayami, Yonezo Maeda, Motomi Katada, Akira Fuyuhiro, Satoshi Kawata, Sumio Kaizaki

Chem. Commun. **2006**, 45–47.

Chapter 4

Reversible Water-Induced Magnetic and Structural Conversion of a Flexible Microporous Ni(II)Fe(III) Ferromagnet

Nobuhiro Yanai, Wakako Kaneko, Ko Yoneda, Masaaki Ohba, Susumu Kitagawa

J. *Am*. *Chem*. *Soc*. **2007**, *129*, 3496–3497.

Chapter 5

Bidirectional Chemo-Switching of Spin State in a Microporous Framework

Masaaki Ohba, Ko Yoneda, Gloria Agustí, M. Carmen Muñoz, Ana B. Gaspar, José A. Real, Mikio Yamasaki, Hideo Ando, Yoshihide Nakao, Shigeyoshi Sakaki, Susumu Kitagawa

Angew. Chem. Int. Ed. **2009**, *48*, 4767–4771.

Chapter 6

Guest-responsive Porous Magnetic Frameworks Using Polycyanometallates

Masaaki Ohba, Ko Yoneda, Susumu Kitagawa

CrystEngComm. accepted.

Other Publications

Polymorph-Dependent Molecular Valence Tautomerism Synchronized with Crystal-Melt Phase Transitions
Ho-Chol Chang, Daisuke Kiriya, Kohei Nakamura, Daisuke Tanaka, Ko Yoneda; Susumu Kitagawa
Chem. Mater. **2009**, *21* 1980–1988.

An $[Fe^{II}_3O]^{4+}$ Core Wrapped by Two $[Fe^{II}L_3]^{-}$ Units
Ko Yoneda, Keiichi Adachi, Kyonosuke Nishio, Mikio Yamasaki, Akira Fuyuhiro, Motomi Katada, Sumio Kaizaki, Satoshi Kawata
Angew. *Chem*. *Int*. *Ed*. **2006**, *45*, 5459–5461.

Synthesis, structure and magnetic properties of pyrazolate-bridged dinuclear complexes $[\{M(NCS)(4\text{-Phpy})\}_2(\mu\text{-bpypz})_2]$ ($M = Co^{2+}$ and Fe^{2+})
Ko Yoneda, Keisaku Nakano, Junji Fujioka, Koichi Yamada, Takayoshi Suzuki, Akira Fuyuhiro, Satoshi Kawata, Sumio Kaizaki
Polyhedron **2005**, *24*, 2437–2442.

Triple Hydrogen Bonds Direct Crystal Engineering of Metal-Assembled Complexes: The Effect of a Novel Organic-Inorganic Module on Supramolecular Structure
Keiichi Adachi, Yuichi Sugiyama, Ko Yoneda, Koichi Yamada, Koichi Nozaki, AkiraFuyuhiro, Satoshi Kawata
Chem. *Eur*. *J*. **2005**, *11*, 6616–6628.

Substituent effect of the coordinated pyridine in a series of pyrazolato bridged dinuclear diiron(II) complexes on the spin-crossover behavior
Keisaku Nakano, Naohiko Suemura, Ko Yoneda, Satoshi Kawata, Sumio Kaizaki
Dalton Transactions **2005**, 740–743.